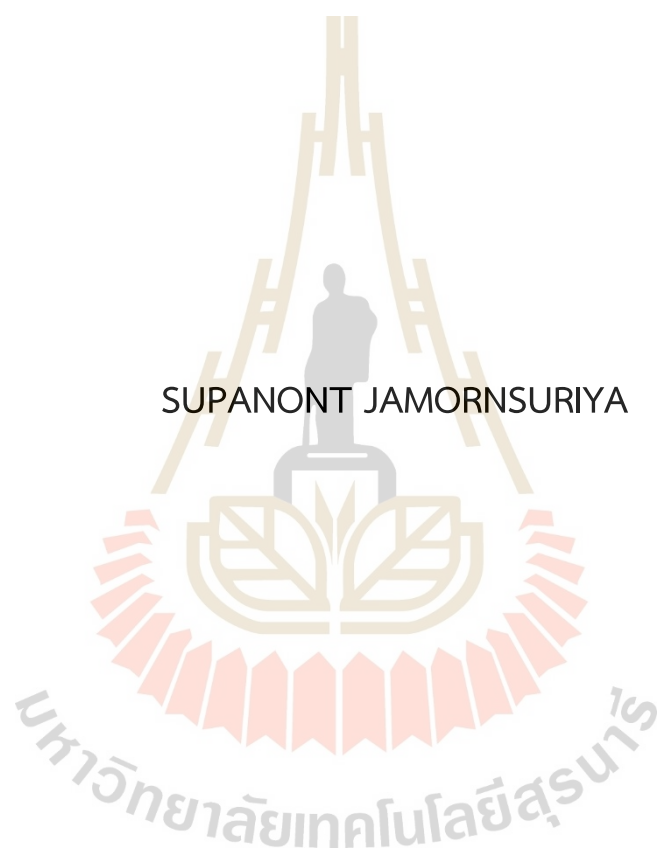# STRUCTURES, DYNAMICS, SURFACE AND CRYSTALLIZATION CHARACTERISTICS OF SOME MODIFIED POLYOLEFINS

SUPANONT JAMORNSURIYA

A Thesis Submitted in Partial Fulfillment of the Requirements for the

Degree of Master of Science in Chemistry

Suranaree University of Technology

Academic Year 2021

ลักษณะเชิงโครงสร้าง พลวัต พื้นผิว และการตกผลึกของพอลิโอเลฟินที่ดัดแปรบางชนิด

นายศุภนนท์ จามรสุริยา
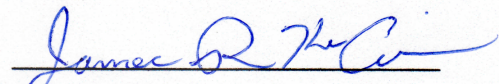
STRUCTURES, DYNAMICS, SURFACE AND CRYSTALLIZATION
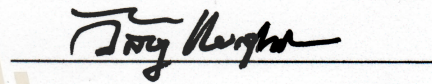# CHARACTERISTICS OF SOME MODIFIED POLYOLEFINS

Suranaree University of Technology has approved this thesis submitted in partial fulfillment of the requirements for a Master's Degree.

Thesis Examining Committee

_____
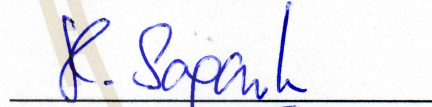
(Prof. Dr. James R. Ketudat-Cairns)

Chairperson

_____
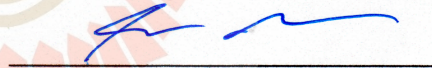
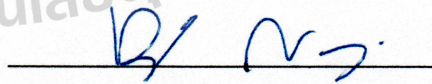(Assoc. Prof. Dr. Visit Vao-soongnern)

Member (Thesis Advisor)

_____

(Prof. Dr. Kritsana Sagarik)

Member

_____
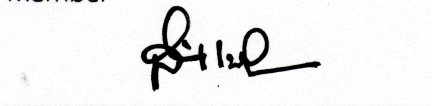
(Assoc. Prof. Dr. Chaiwat Ruksakulpiwat)
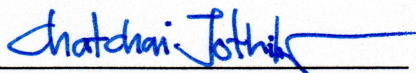
Member

_____

(Assoc. Prof. Dr. Piyarat Nimmanpipug)

Member

_____

(Assoc. Prof. Dr. Chatchai Jothityangkoon)

Vice Rector for Academic Affairs and

Quality Assurance

_____

(Prof. Dr. Santi Maensiri)

Dean of Institute of Science

ศุภนนท์ จามรสุริยา : ลักษณะเชิงโครงสร้าง พลวัต พื้นผิว และ การตกผลึกของพอลิโอเลฟิน
ที่มีการดัดแปรบางชนิด (STRUCTURES, DYNAMICS, SURFACE AND CRYSTALLIZATION
CHARACTERISTICS OF SOME MODIFIED POLYOLEFINS) อาจารย์ที่ปรึกษา:
รองศาสตราจารย์ ดร.วิสิษฐ์ แววสูงเนิน, 147 หน้า.

คำสำคัญ: การจำลองระดับโมเลกุล, พื้นผิวพอลิเมอร์, การตกผลึก, การกระเจิงรังสีเอ็กซ์มุมแคบด้วย
แสงซินโครตรอน, พอลิเอทิลีน, พอลิโพรพิลีนเอทิลีนโคพอลิเมอร์แบบสุ่ม

การดัดแปรพอลิเมอร์ระดับโมเลกุลทางเคมีและทางกายภาพทำได้วัสดุพอลิเมอร์ที่มีสมบัติ
ใหม่และดีขึ้น งานวิจัยนี้จะใช้เทคนิคการจำลองโมเลกุลและการทดลองเพื่อศึกษาให้เกิดความเข้าใจ
ความสัมพันธ์ระหว่างโครงสร้างและสมบัติของพอลิเมอร์ดัดแปรนี้ วิทยานิพนธ์จะมีสี่หัวข้อหลักเพื่อ
ศึกษาสมบัติวัสดุ พื้นผิว และการตกผลึกของพอลิเมอร์ดัดแปรโดยการจำลองระดับโมเลกุล และการ
ทดลอง สำหรับหัวข้อแรกได้ศึกษาคุณสมบัติเชิงโมเลกุลและพื้นผิวของฟิล์มบางโพลิเอทิลีน-โพรพิลีน
เมื่อสัดส่วนเอทิลีนเพิ่มขึ้นจะทำให้โครงสร้างฟิล์มมีความหนาแน่นมากขึ้น ส่วนปลายโซ่มีมากขึ้น
บริเวณพื้นผิว พันธะจัดเรียงในทิศทางขนานกับพื้นผิวมากขึ้น และมีการเปลี่ยนแปลงรูปร่างและขนาด
โมเลกุลตามปริมาณเอทิลีน แกนโมเลกุลที่ใหญ่สุดจัดวางในทิศทางขนานกับพื้นผิวฟิล์มและแบบสุ่ม
เมื่อปริมาณเอทิลีนลดลง หัวข้อที่สองคือการศึกษาผลของมอนอเมอร์และลำดับเฉพาะต่อโครงสร้าง
และพลวัตของโคพอลิเมอร์เอทิลีน-โพรพิลีนแบบสุ่ม ผลที่ได้ชี้ให้เห็นถึงแนวโน้มของสมบัติการแพร่ที่
เร็วขึ้นสำหรับรูปแบบที่คล้ายบล็อกมากกว่าลำดับอื่น ๆ ที่ปริมาณเอทิลีนระดับต่ำถึงระดับปานกลาง
อันเนื่องมาจากอันตรกิริยาระหว่างสายโซ่ สำหรับปริมาณเอทิลีนที่สูง อันตรกิริยาภายในสายโซ่มี
แนวโน้มที่จะมีอิทธิพลต่อการเคลื่อนที่ของโซ่มากกว่า ส่วนที่สามคือการศึกษาผลกระทบของเอทิลีน
จำนวนเล็กน้อยต่อลักษณะการตกผลึกของพอลิไอโซแทคติกพอลิโพรพิลีนโดยการทดลอง การศึกษา
จลนพลศาสตร์และสัณฐานวิทยาของผลึกแบบอุณหภูมิเสมอด้วยการกระเจิงรังสีเอ็กซ์มุมแคบ (SAXS)
ระยะเวลาการเหนี่ยวนำในการตกผลึกของโพลิโพรพิลีนไอโซแทคติกใช้เวลาประมาณ 10 นาที
สำหรับตัวอย่างที่มีเอทิลีนอยู่ จะลดระยะเวลาการเหนี่ยวนำเป็น 3 นาที การวิเคราะห์ข้อมูลทำโดยใช้
แบบจำลองพาราคริสตัลและฟังก์ชันสหสัมพันธ์ความหนาแน่นอิเล็กตรอน 1 มิติ สำหรับตัวอย่างที่มี
ปริมาณเอทิลีนสูง (PE 0.59%) ระยะห่างเฉลี่ยของความหนาระหว่างชั้นผลึก (L_p) และความหนาของ
ผลึกเฉลี่ย (L_c) เท่ากับ 18.36 และ 6.35 นาโนเมตร เมื่อเทียบกับตัวอย่างที่มีเอทิลีนต่ำกว่า (0.09%
PE) พารามิเตอร์เหล่านี้จะมีขนาดมากขึ้น คือ L_p = 18.46 และ L_c = 6.76 นาโนเมตร ผลเหล่านี้
ชี้ให้เห็นว่าแผ่นผลึกมีขนาดเล็กลงเมื่อมีเอทิลีนมากขึ้น หัวข้อสุดท้ายคือการศึกษาการตกผลึกของ
แบบจำลองพอลิเอทิลีนโครงสร้างแบบวงแหวนเปรียบเทียบกับแบบเชิงเส้น สมบัติบางอย่างที่

วิเคราะห์ได้จากการจำลองเพื่อบ่งชี้การตกผลึกได้แก่ สัดส่วนของโครงรูปแบบทรานส์ ฟังก์ชัน สหสัมพันธ์ของการจัดเรียง และการโตขึ้นของเส้นกราฟโครงสร้างการกระเจิง ผลการศึกษาพอว่าพอลิ เมอร์แบบบวงแหวนจะเกิดโครงสร้างเป็นระเบียบยากกว่าเมื่อพิจารณาจากฟังก์ชันสหสัมพันธ์ระหว่าง โมเลกุล (S_G) แม้ว่าเศษส่วนโครงรูปแบบทรานส์จะค่อนข้างสูง ถึงแม้ค่า S_G จะแตกต่างกันอย่างมี นัยสำคัญประมาณ 0.7 และน้อยกว่า 0.1 สำหรับพอลิเมอร์เชิงเส้นและแบบบวงแหวนตามลำดับ เมื่อ พิจารณาอย่างละเอียดพบว่าพอลิเมอร์วงแหวนอาจก่อตัวเป็นผลึกได้โดยจะมีหลายโดเมนที่จัดเรียงใน ทิศทางที่แตกต่างกัน

สาขาวิชาเคมี

ปีการศึกษา 2564

ลายมือชื่อนักศึกษา _____

ลายมือชื่ออาจารย์ที่ปรึกษา _____

SUPANONT JAMORNSURIYA : STRUCTURES, DYNAMICS, SURFACE AND CRYSTALLIZATION CHARACTERISTICS OF SOME MODIFIED POLYOLEFINS. THESIS ADVISOR : ASSOC.PROF. VISIT VAO-SOONGNERN, 147 PP.
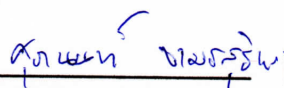
Keyword: Molecular simulation, polymer surface, crystallization, synchrotron SAXS, polyethylene, poly(propylene-ran-ethylene)

Chemical and physical modification of polymer chains at the molecular level can give new and better properties of polymeric materials. In this work, molecular simulation and experimental techniques were employed to gain more understanding of the correlation between structure and property relationships of modified polymers. There are four main parts in the thesis to investigate the bulk, surface and crystallization properties of modified polymer by means of molecular simulation and experiment. For the first part, molecular and surface properties of poly(ethylene-ran-propylene) free-standing thin films were studied. When the ethylene fraction was increased, it led to denser film structures, chain ends became more abundant in the surface region, the bonds oriented in a direction more parallel to the surface and significant changes in molecular shape and size were observed as a function of ethylene content. The largest molecular axis was oriented in a parallel direction to the film surface, and changed toward random orientation when the ethylene content was decreased. The second topic is to study the effect of comonomer composition and specific sequences on structure and dynamics of bulk ethylene propylene random copolymer melts. The results suggest the tendency of faster diffusion for block-like pattern than other sequences at low to intermediate ethylene content, due to the interchain interaction. For high ethylene content, the intra-chain interaction likely to have more influence on the chain mobility. The third part is to study the effect of few ethylene defects on the crystallization characteristics of isotactic poly(propylene) by experiments. Investigation of the kinetics and crystal morphology was performed by *in-situ* isothermal crystallization with simultaneous synchrotron small-angle X-ray

scattering (SAXS). The induction period for the crystallization of isotactic poly(propylene) takes about 10 min. For the sample with ethylene defects, the induction period can be decreased to 3 min. Data was analyzed by the paracrystalline model and 1-D electron density correlation function. For high ethylene content (0.59% PE) sample, the average long period distance (L_P) and the average crystal lamellar thickness (L_C) are 18.36 nm. and 6.35 nm. Compared to the sample with lower ethylene defects (0.09% PE), these parameters become larger $i.e.$ L_P = 18.46 nm and L_C = 6.76 nm. These results suggest that smaller crystal lamellae are formed at higher ethylene defects. The final part is the study of crystallization characteristics of cyclic in comparison to linear polyethylene models. Some properties evaluated from simulation to indicate crystallization are the fraction of $trans$ conformation, orientation correlation function and evolution of the scattering structure factor. It is more difficult for cyclic polymer to form an ordered phase considered by the evolution of intermolecular orientation correlation function, (S_G). Although the $trans$ fraction for both systems are quite high, the S_G values are significantly different $i.e.$, about 0.7 and less than 0.1 for linear and cyclic PE, respectively. By careful inspection for cyclic chain system, it was observed that crystal may be able to form with multiple domains in different orientation.

School of Chemistry

Academic Year 2021

Student's Signature

Advisor's Signature

ACKNOWLEDGEMENTS

CONTENTS

CONTENTS (Continued)

CONTENTS (Continued)

LIST OF TABLES

LIST OF TABLES (Continued)

LIST OF FIGURES

LIST OF FIGURES (Continued)

LIST OF FIGURES (Continued)

LIST OF FIGURES (Continued)

LIST OF ABBREVIATIONS

2nnd	Second Nearest Neighbor Diamond
t_0	Induction period
T_m^0	Equilibrium melting temperature
$<R_e^2>$	Mean Square End-to-End distance
$<R_g^2>$	Mean Square Radius of Gyration
$<m(t).m(0)>$	Orientational autocorrelation function of bond vector
$<R(t).R(0)>$	Chain end-to-end vector orientational autocorrelation
2nnd	The Second Nearest Neighbor Diamond
*a*PP	Atactic polypropylene
Å	Angstroms
β, k_B	Boltzman constant
B_2	Second Virial Coefficient
C_n	Characteristic Ratio
d_{ac}	Long spacing
DSC	Differential Scanning Calorimetry
E	Ethylene unit
EPRC	Ethylene-Propylene Random Copolymer
g	*Gauche state*
h	Planck's constant
I	Intensity
*i*PP	Isotactic polypropylene
k	Crystallization rate constant
K	Kelvin
L	Sample-to-detector distance
L_1 , L_2 , L_3	Primary Axis, Secondary Axis, Tertiary Axis
L_c or L	Average lamellar thickness
LJ	Lennard-Jones

LIST OF ABBREVIATIONS (Continued)

L_p or D	Long period
MC	Monte Carlo
MCS	Monte Carlo Step
mm	millimeter
$M_n(j)$	Intramolecular bond orientation correlation functions
MSD	Mean Square Displacement
Mw	Weight average molecular weight
n	Avrami exponent
nm	nanometer
OCAF	Orientation Autocorrelation Function
P	Propylene unit
P_E	Fraction of ethylene
PCF	Pair Correlation Function
PE	Polyethylene
PP	Polypropylene
q	Scattering vector
R_g	Radius of gyration
RIS	Rotational Isomeric State
SAXS	Small Angle X-ray Scattering
S_G	Global orientation order parameter
S_L	Local intermolecular
$t_{0.5}$	Crystallization half-time
T	Temperature
T_c	Crystallization temperature
T_i	Crystallization onset temperature
T_m	Melting temperature
T_p	Crystallization peak temperature
t	trans state
WAXD	Wide Angle X-ray Diffraction

LIST OF ABBREVIATIONS (Continued)

Z	Partition Function
Z_C	Overall rate constant
ρ	Density
Φ	Cooling rate
λ	Wavelength
$X(T)$	Fraction of temperature
$\gamma(r)$	Correlation function

CHAPTER I

INTRODUCTION

Polymer is a macromolecule which is composed of monomers, numerous of the repeating structural units. Each polymer molecule may comprise hundreds to a million monomers with the possibility to be a linear, branched, or network structure. It is generally known that the length of a polymer chain is a very important factor to determine its material properties. For polyolefin, as the number of carbons increases to several hundred atoms, the materials transform from the liquid state to glassy solid. When the quantity of carbon atoms in the polymer chain excels a thousand, the solid polymeric material with strength, flexibility and toughness properties is obtained, which called polyethylene (PE). Change in the thermodynamic state takes place when the length of the polymer increases along with the total binding forces between molecules.

In this thesis, we are interested in chemical and physical modification of polyethylene by means of (1) **copolymerization** with propylene monomers in the whole composition range (propylene fraction = 0.0 to 1.0) and the change in the structures and dynamics of these polymeric materials, and (2) change in molecular **topology**, such as cyclic structure in comparison to linear structure, of the same ethylene repeating units for the difference in crystallization characteristics.

In the first case, the properties of polymer can be altered by the incorporation of co-monomer to the homopolymer backbone. New polymeric materials can be obtained with new properties, such as lowering its melting and glass transition temperatures, decreasing the crystallinity, being more transparent and having higher impact resistance. In this part, ethylene-propylene copolymers were studied by a molecular simulation method in order to study the influence of the comonomer composition and sequence to their structural, dynamic and surface properties at the melt state.

In the second case, cyclic isomers with the same chemical structure with the linear PE chains were investigated for the crystallization behavior. The molecular

topology is known as the key aspect in various research topics in polymer science due to its influence on the polymer physical properties. Notably, development of various cyclic topologies has recently received high attention. Because of having no chain end group, cyclic polymers possess unique characteristics, including higher glass transition temperatures, less viscosity, and a smaller hydrodynamic radius. Some cyclic polymers have been successfully prepared using two synthetic methods, so-called intramolecular ring closure reactions and ring expansion polymerizations.

Since the melt processing has important role on the application of polymeric materials. It is significant to perceive the crystallization mechanism of polymer from the molten state in which chain folding to the lamella structure has an important role. Chain folding and chain orientation is expected to be different for linear and cyclic polymers during the crystallization process. Due to polymer synthesis being extremely difficult, this issue can be investigated alternatively using computer simulation technique, in which the polymer structure can be controlled precisely, unlike the experimental approach. In this proposal, crystallization characteristics of linear and cyclic PEs will be investigated and compared. Next, general introduction to this proposal will be given as follows: (1) molecular simulation (2) copolymers melts (3) copolymers surface and (4) crystallization of cyclic polymers.

1.1 Molecular simulation

For the past 30 years, modeling and simulation of materials has become an important tool for the research and development in chemical and pharmaceutical industries. Competition in chemical synthesis and separation advancement occur mainly through the development and usage of materials with specific physico-chemical characteristic, *e.g.* metallocene catalysts for polyolefin production, polymer membranes with better permeability and selectivity, and green solvent with specified thermo-physical properties. In addition, product design has been focused more than the process, which is directly related to material behavior. Scientists or engineers play a major role on development of new materials within the range of 0.1-10 nm length scale, to achieve mechanical, electronic, magnetic, optical and other features at this level. Development of the quantitative understanding for structure–property–

processing–performance is very important, which is the main goal of computer simulation and modeling of materials. Using these computational methods along with experimental techniques should be powerful tools to study materials at the fine scale.

At the present, the advancement in computer hardware greatly benefits the polymer modeling and simulation. Development of new methods and algorithms is much more important for simulations, which are based on the physical and chemical science. Each method is used in diverse time and length scales that are appropriate for structures and dynamics occurring in polymeric materials. Currently, multiscale modeling and simulation, involving a consolidation of atomistic (< 10 nm), mesoscopic (10-1000 nm), and macroscopic approaches are generally accepted as successful solutions for materials design. (Kotelyanskii and Theodorou, 2008)

Computer simulation of polymeric materials with coarse-grained lattice models have been taken into account as an efficient simulation method for the time and length scale of these system. High coordination lattice, such as the second-nearest-neighbor diamond (2nnd) lattice simulation has the key advantage because it can keep detailed chemistry of polymer. This method is relevant for the study of large polymer systems with more efficiency, while atomistic simulation cannot equilibrate the large system within the appropriate computation time (Antoniadis et al., 1999; Logotheti and Theodorou, 2007; Antoniadis et al., 1998). The effect of stereochemistry of side chain in vinyl polymer chain on various properties can also be studied using this technique. Unlike enantiomer of small-molecules, computer simulation studies on stereochemical effects on dynamic properties of polymer materials are still not well understood. It is therefore important to have more comprehensive study for the influence of different stereochemical sequences on the dynamics of vinyl polymer chains. For *isotactic* polypropylene (PP), structural modification of this polymer was tried by Thai company to have *i*PP with a small amount of C_2 (ethylene) units in the chain structure which can alter the properties of these plastics. In this proposal, we used dynamic Monte Carlo simulation to investigate the structures and dynamics of *i*PP-PE copolymer with the broader range of ethylene fraction (P_E) of 0.25, 0.50, and 0.75. For each fixed values of ethylene content, the effect of different stereochemical

sequences will be studied to see how each specific PP and PE sequence affects the dynamics of polymer melt states.

1.2 Copolymers melt

- **Polymers with only one monomer type**: These polymers consist of identical repeating units in a long straight chain structure linked with covalent bonds.

- **Polymers with different monomer types/chemical groups**: This type of polymer may contain either branched structure or having functional groups linked to the end unit.

The properties of polymers often reckon on the stereochemical structure. Control of the stereochemistry of homopolymers and copolymers is facilitated by the development of metallocene catalysts (Kaminsky and Arndt, 1997; Soga and Shiono, 1997; Busico and Cipullo, 2001). Using this kind of catalysis can also control the specific sequences of the chains for length scale at the diads *i.e. meso* (M) or *racemo* (R) placement. Atactic chains can be considered as random copolymers, since the stereochemical sequences are random (Flory and Volkenstein, 1969). Atactic polypropylene (*a*PP) has unique conformational partition function in each isomer as a result of a varied fraction of *meso* and *racemo* diads (Mattice, et al., 2007). Changing tacticity can cause high impact on many of its properties, such as thermal, diffusion and crystallization (Soga and Shiono, 1997; Mattice and Waheed, 2006; Chen, Ozisik et al., 2007). For dynamic properties, isotactic polypropylene (*i*PP) with *tg* conformers has a higher diffusion rate than *syndiotactic* polypropylene (*s*PP) chain with *tt* conformers (Antoniadis et al., 1999). From the previous publication, *a*PP chains with random stereochemical sequence and with the fraction of *meso* diad (P_m) in between those of *i*PP and *s*PP chain (Mattice and Waheed, 2006; Mattice et al., 2007; Chen et al., 2007) can diffuse faster (Waheed et al., 2007). In addition, the irregular chain structure of *a*PP can prevent crystallization, which causes *a*PP to have an amorphous rubbery property, while *i*PP and *s*PP are semicrystalline. Both *i*PP and *s*PP usually have some stereochemical defects, which greatly influence their crystallization and the melting point (Chen et al., 2007; Madkour and Mark, 1997).

1.3 Copolymers surface

Even though investigation for the surface and interface of polymeric material has been carried out by numerous experimental techniques, it is still very challenging to characterize polymer thin film at the molecular level. Likewise, many simulation approaches have been employed to inspect the effect of surface confinement on properties of polymeric nano-structured materials. Simulations can be performed using variety of methods, such as the system with discretized lattice (Madden, 1987; Theodorou, 1988; Doruker and Mattice, 1998; Müller and MacDowell, 2000) or continuous space (Mansfield and Theodorou, 1990; Mansfield and Theodorou, 1991), using coarse-grained or fully atomistic detailed model for investigation of either static or dynamic (Doruker and Mattice, 1999) aspects of polymer surface.

1.4 Crystallization of cyclic polymers

Cyclic polymers have unique properties in terms of preserving their old topology. They never change their state of concentration which deliver a supplementary and global constraint for the conformation statics, unlike the linear polymers that take any available conformation under the local constraint of excluded volume. The conformational entropy of polymer melts will be reduced if it is prepared by concentrating a dilute solution of non-concentrated cyclic polymers, which is not the case for linear chains. If the molar mass of the cyclic polymers is larger than the entanglement molecular mass of their linear counterparts, the dynamics at the melted state will be accelerated. This is relevant to the missing of classical reptation dynamics. (Obukhov et al., 1994; Halverson et al., 2011) Since cyclic polymers do not diverge in any other chemical details from their linear counterparts, they offer an intriguing system to study the influence of topology on polymer crystallization.

Structure formation as well as crystallization of polymer chains is an engrossing topic in chemistry, physics and biology (Fujiwara and Sato, 1999). For decades ago, many theoretical and experimental have been developed since chain folding was proposed in polymer science (Keller, 1957). Nevertheless, there is insufficient detail of structure formation mechanism on the molecular level to be fully understood. Small-angle and wide-angle X-ray scattering (SAXS and WAXS) approaches were employed

to examine the crystallization of polymer from melt state throughout the induction period and the spinodal kinetic has been reported in different polymer melt, such as poly(ethylene terephthalate) (PET) (Imai et al, 1994), poly(ether ketone ketone) (PEKK) (Ezquerra et al., 1996), isotactic polypropylene (iPP) (Terrill et al., 1998) ,and polyethylene (PE) (Ryan et al., 1999). The coupling between density and chain conformation (Olmsted et al., 1998) was proposed to be a reason to provoke this process in the coexistence part of the equilibrium liquid and crystalline solid.

Several experimental results on crystallization of cyclic polymers have been gathered to compare with linear topology. Still, partially disputable conclusion has been drawn. (Su et al., 2013). There is a recent comparison review of various experimental studies. (Pérez-Camargo et al., 2015). A general opinion is procured about the fact that there is no influence of the ring topology to the crystalline structure which supports the hypothesis of the same equilibrium heat of fusion, ΔH, regardless of the cyclic topology. So far, the studies of cyclic polymers are usually tended to have higher melting temperature, T_m and higher crystallinity (Schäler et al., 2011) than their linear counterparts under a specified thermal history. Regarding the lamellar thickness contrary trends have been reported. Despite that, a key aspect of the experiments, especially in the melt state, is the purification of the cyclic polymers. A limited number of linear chains can cause a qualitative effect on the state of entanglement and the dynamics of cyclic polymers melts, (Everaers et al., 2004) a fact which potentially clarify some of the contradictory results. (Pérez-Camargo et al., 2015)

In order to disclose the structure formation on molecular level, particularly at the initial stage, some studies based on computer simulation were done for polymer chains. Local structures at a beginning stage and an almost late stage were retrieved from molecular dynamics (MD) simulation and it was found that the global order parameter raised only after the chains were stretched to some extent (Takeuchi, 1998). The folding of long polyethylene chain from solution was studied using MD simulation (Yamamoto, 1997; Martoňák et al., 1996) and Monte Carlo (MC) simulation (Chen and Higgs, 1998). Even so, the structure formation on the molecular level from the dense polymeric system was done with less effort. Hu (Hu, 2000) introduced collinear energy

and parallel energy between two Kuhn segments to simulate structures and melting point of chain polymers on a simple cubic lattice.

1.5 Copolymer crystallization

For the basic of crystallization from liquid substance, adding the second component would strongly alters from the nucleation rate to the overall rate of crystallization at melt state. This cause phase diagrams for two-component systems extent the crystallization region. Therefore, the relative changes for the crystallization process of copolymers, can be expected, and are actually validated by kinetic studies. However, it is the sequence propagation probability rather than the composition of copolymer that is important. (Buzarovska, 2004)

The overall crystallization kinetics and spherulite growth rates of the copolymer composed of *isotactic* polypropylene with small amount of ethylene defect will be analyzed in this thesis, using experimental techniques. It should be reminded from the point of view of polymer chemistry that (1) polyethylene usually contain a lot of branched points so that using PE as the main component is not possible to study by experiments and interpretation at the molecular level is very difficult, (2) polypropylene with large amount of ethylene content is rubbery materials so that it prohibits the crystallization study as the amount of crystallization should be none or very small amount to observe experimentally and (3) *isotactic* polypropylene with small amount of ethylene defect (< 5 mol%) should be an ideal system for investigation as the percent of crystallinity from iPP portion is large enough to be investigated by thermal analysis and X-Ray technique. In addition, real samples can be obtained from the company in Thailand. For this part, the experiments were carried out based on thermal analysis (differential scanning colorimeter, DSC) and synchrotron X-Ray (Small Angle X-ray Scattering, SAXS) techniques to study the crystallization kinetics of *isotactic* polypropylene with small fraction of ethylene monomer from the melt state to shed some light on the effect of monomer defect on structure formation of copolymer.

1.6 Objectives

1. To investigate the effect of comonomer sequence on the structural and dynamic properties of bulk ethylene-propylene copolymer melts.

2. To study the effect of ethylene content on the molecular and surface properties of ethylene-propylene random copolymer thin film.

3. To study the effect of chain topology (linear vs. cyclic) on the crystallization characteristics of polyethylene from the melt state.

4. To investigate the effect of a small amount of ethylene defect on crystallization characteristics of isotactic polypropylene.

1.7 Scope and limitation

This research work has been divided into 2 main parts

1.7.1 Molecular simulation

The simulation technique employed to study molecular, structural, dynamic and surface properties of *i*PP-PE copolymers and the crystallization behavior of linear and cyclic PE homopolymer is based on lattice Monte-Carlo simulation of coarse-grained polymer models. The studies will include:

- Determination of the molecular size (R_g), chain packing (pair correlation function) and dynamics (translational and rotational motion) of bulk melts.

- For polymer thin film, structures and orientation at the molecular and bond level will be investigated.

- For crystallization studies, structural formation and ordering at bond/chain scale will be studied.

1.7.2 Experiments

Crystallization of isotactic polypropylene with a small amount of polyethylene defect (*i*PP-E) will be investigated based on thermal analysis and X-ray scattering. The experimental techniques employed in this section are:

- Differential Scanning Calorimeter (DSC): to determine crystallization behavior of *i*PP-PE for both isothermal and non-isothermal kinetics

- Small Angle X-ray Scattering (SAXS): to determine the crystallization behavior of *i*PP-PE for both isothermal and non-isothermal kinetics

CHAPTER II

LITERATURE REVIEWS

2.1 Introduction

Natta *et al*. firstly synthesize the isotactic polypropylene (*i*PP) In addition to its mechanical performance, lightness, chemical endurance and transparency advantages, *i*PP has become a popular product in the global thermoplastic market. It has a wide range of applications, such as containers, wrappers, medical and laboratory equipment (Utracki, 1998). The outstanding performance is strongly related to its semicrystalline structures controlled by its crystallization kinetics. To improve the properties of *i*PP, placing some comonomer units at random positions within the chain is one of the possible methods to modify material properties. This approach leads to decreased ranges of crystallization and melting temperatures, as well as crystallinity reduction (Flory, 1953; Balbontin, 1992 and Hauser, 1998). Many previous works have been performed to examine the crystallization behavior of random copolymer based on poly(propylene) containing a small fraction of comonomers (Auriemma, À2; Hosoda, 2002; Hosier, 2003; Gou, 2007; Rosa, 2007 and Jeon, 2009).

2.2 Copolymers

Synthesis of the polymer can be conducted with higher potential to control the stereochemical and fractional of homopolymer and copolymer according to the development of metallocene catalysts (Kaminsky, 1997; Soga, 1997 and Busico, 2001). Even for the advancement of catalyst, isotactic polypropylene synthesis still has some raceme defect on the product yield. The modern catalysts can control not only on the polymerization of 100% isotactic and 100% syndiotactic chains, but also to synthesize polymers in which the stereochemical sequence is longer than diads. For PP chains with different tacticity, *atactic* PP (*a*PP) is an amorphous rubbery material as it has an irregular structure that prevent the formation of crystallites while both *isotactic* PP (*i*PP) and *syndiotactic* PP (*s*PP) are semi-crystalline. The crystallization and

the melting temperature of *i*PP and *s*PP are also strongly depended on stereochemical structure (Chen, 2006; Chen, 2007 and Waheed, 2007).

In addition, copolymerization of two different monomers can result in many kinds of structure besides random copolymers (Flory, 1969). We anticipate that new kind of catalyst or synthesis method may be possible in the future to precisely control the sequence of different monomer to arrange in specific position in copolymer chains. The specific sequence of ethylene-propylene copolymer should have some influence on the thermal, diffusion and crystallization properties. In practice, adding ethylene units on polypropylene chain cause the materials become more rubbery behavior.

Theoretical model to describe chain conformational characteristics for copolymer with specific monomer sequence should have the unique conformational partition function (Mattice, 2007). Computer simulation of polymeric materials is still a challenging work due to the nature of long time and length scales involved in the real systems. The simulation with coarse-grained model have been attempted to improve the computational efficiency for polymers system. Simulation of coarse-grained polymer models on the high-coordination second-nearest-neighbor diamond (*2nnd*) lattice (Mattice, 1999; Akten, 2001 and Clancy, 2001) maintain adequate detail to enable the nature of specific chemical details of the simulating polymers, and allows more efficient study for the larger systems which cannot be covered on appropriate length and time scales as done by atomistic simulation (Antoniadis, 1998; Antoniadis, 1999 and Logotheti, 2007). This simulation technique has been used to study various problems including the influence of stereochemistry of polymer chain on structural and dynamic properties. For example of polypropylene case, the stereochemical sequence of *atactic* chain with quenched randomness causes samples with intermediate stereochemical composition at probability of a *meso* diad, P_m (Mattice, 2006; Mattice, 2007 and Chen, 2007), resulting in *meso* and *racemo* sequences in *a*PP chain diffuse faster than *i*PP and *s*PP chain (Waheed, 2007) but each *atactic* chain is composed of different stereochemical pattern of *racemo* and *meso* diads resulting from random sequence on each chain. Despite the stereochemical effect are well studied for mixtures of small organic molecules (Mattice, 2006), the fundamental perspective of the stereochemistry of polymer chain is required to understand the

structural and dynamic properties. Accordingly, more extensive study is vital for abovementioned effect on material properties related to the specific monomer sequences of copolymer chains.

Polymer surface and interface are crucial importance for various technologies such as adhesion, coatings and paints (Feast, 1987 and Stamm, 1992). The substantial understanding of polymer surfaces covers various issues, for example, the contact angle and wettability, surface energy, tribology, interactions/reactions at surfaces, adsorption/adhesion, and surface modification (Mittal, 1983). Molecular level comprehension of polymer surfaces can bestow great chance to modify surface properties to meet specific interests. Several theoretical and experimental approaches have been sought to investigate the research problems of polymer surfaces with infrequent success especially at the molecular level due to their exceptionally small length scale at Angstrom level. Over the years, molecular simulations have been developed to study nanostructure of polymeric materials with free surface. These simulations use various techniques including the lattice (Madden, 1987 and Theodorou, 1988; Doruker, 1998) or of-lattice approaches (Mandsfeld, 1990 and Müller, 2000) of coarse-grained (Doruker, 1998) or fully atomistic models (Mandsfeld, 1990; Mandsfeld, 1991 and Müller, 2000) to study both static and dynamic properties of the surface. One way to modify polymer surface at the molecular level is to use random copolymer with two or more different monomers covalently bonded at statistically random position in the chains which can give new properties compared to the individual homopolymers (Fried, 2014). Molecular simulation is also sturdy to investigate copolymers where different monomer units can affect their physical and chemical properties. In principle, simulation at the fully atomistic level should deliver better details and include the specific characteristics of monomer units in copolymer chain. However, atomistic simulation become rough for structural relaxation and equilibration (Mandsfeld, 1990 and Misra, 1995). The relaxation of copolymer chains should be adequate so that the end-to-end vector of copolymer chain lost any memory with its starting configuration, and the center of mass of copolymer molecule should diffuse at least a distance larger than its radius of gyration.

To prevail this difficulty, Monte Carlo simulation of coarse-grained polymer model on the second nearest neighbor diamond (*2nnd*) coordination lattice has been developed during the past two decades to study polymeric nanostructured materials with free surfaces including thin film, nanofiber and nanoparticle (Doruker, 1998; Vao-soongnern, 1999; Baschnagel, 2000 and Vao-soongnern, 2001). This simulation technique handles homopolymer systems with the Hamiltonian comprised the short-range intramolecular and long-range intermolecular interactions based on the Rotational Isomeric State (RIS) model (Flory, 1969 and Mattice, 1994) and the Lennard–Jones (LJ) potential energy function, respectively. Earlier, this simulation approach combined with the reverse-mapping procedure to the fully atomistic description was employed to study poly(ethylene-*ran*-propylene) thin films (Rane, 2004) and compared results with the sum-frequency generation (SFG) spectroscopy (Opdahl, 2002). Methyl groups become more abundance on the surface than in the bulk region. Nevertheless, structural and surface properties of poly(ethylene-ran-propylene) thin films at all range of comonomer composition had not yet reported

2.3 Polymer crystallization

Crystallization of long chain molecules is an interesting and challenging topic in polymer science. There are many factors that can affect crystallization, such as type and structure of polymer, crystallization temperature, cooling rate and polydispersity. In this thesis, we are interested in the effect of polydispersity, which is used to describe the degree of non-uniformity of a distribution of the polymer, on the degree of crystallinity. There have been many experimental results and theoretical developments in the concept of chain folding proposed in polymer science many decades ago (Keller, 1957 and Wunderich, 1976). In particular, those studies are based on static light scattering, microscopy, and differential scanning calorimetry use to characterize the crystal morphology obtained during the crystallization of polyethylene (PE) which is largely dependent on molecular weight and polydispersity (Mandelkern, 1968; Maxfield, 1977 and Voigt-Martin, 1980). Although many experimental studies have been proceeded on polymer crystallization and nucleus formation, as emphasized by recent reviews (Schick, 2017; Cui, 2018 and Yue, 2018), it

remains challenging for experiments to attain the nanoscale temporal and spatial resolutions required to track the molecular-level evolution of nuclei. Hence, the detailed mechanism of structure formation on the molecular level is not fully understood. In order to expose the formation of structures at the molecular level, especially in the early stages, some works on molecular simulation were needed to perform for polymer crystallization.

Local structures at an early and relatively late stages can be derived from molecular dynamic (MD) simulations and it was realized that the global order parameter only propelled after the chains were stretched to some extent (Sadler, 1986; Takeuchi, 1998 and Fujiwara, 1999). The folding of the long PE chain from solution was also studied through MD (Martonák, 1996 and Yamamoto, 1997) and MC simulation (Chen, 1998). However, less work has investigated the construction of molecular structures from a dense polymer system. Hu (Hu, 2000) simulated the structure and melting point of the polymer chain on a simple cubic lattice through collinear energy and parallel energy between two Kuhn sections. To investigate polymer crystallization based on more realistic polymer model and to reduce computational time compared with fully atomistic MD, MC simulation was performed for coarse-grained PE chains on a high coordination lattice (Xu, 2001). This approach avoided introducing artificial energies, such as collinear energy and parallel energy, which were involved inevitably in other coarse-grained lattice MC simulations. The method was demonstrated for simulation of structure formation in the case of monodisperse PE. In this thesis, the same simulation method will be extended to investigate the crystallization of polymer mixture composed of short and long PE chains.

Recently, cyclic alkanes were also used in polymer crystallization studies, for the onset of chain folding in comparison to linear alkanes (Ozisik, et al., 2002). Investigation for the reptation theory can be carried out by using polymer chain confined in a topological constrained tube and the previous studies founded that all portion along the chain could move except the chain ends (de Gennes, 1979) as in the case of cyclic polymers. In addition, recent experiments found that cyclic poly(dimethyl siloxane) (PDMS) diffuses faster than the linear PDMS (Klein, 1986), which

conflict with the argument that the cyclic chains should have slower motion compared to linear chains.

CHAPTER III

RESHEARCH METHODOLOGY

3.1 Experimental part

3.1.1 Apparatus and materials

- Aluminum sample pans

- PerkinElmer PYRIS (Diamond) Differential Scanning Calorimeters.

- Linkam THMS600 hot stage

- Synchrotron Small X-ray Scattering (SAXS)

- *Isotactic* Polypropylene with small ethylene defect, SCG Chemical

Table 3.1 Data of iPP samples from SCG company.

Sample (*i*PP-*ran*-E)	MHD-RPP1 or MH002 (PPE009)	MHD-RPP2 (PPE016)	MHD-RPP3 (PPE185)	MHD-RPP5 (PPE059)
MI	3.1	2.3	2.34	2.64
mmmm (%)	95.63		96.42	96.05
meso run length			411	188
C2 (%mol)	0.09	0.16	1.85	0.59
Mw			406,383	479,098
Mn			31,452	30,742
MWD			12.92	15.58
Mz			1,858,212	2,135,517

3.1.2 Sample preparation

- For thermal analysis, polymer samples were cut to fit into 3mm diameter of aluminum pan and sample load was about 10 mg. Thermal analysis were performed using PerkinElmer PYRIS (Diamond) Differential Scanning Calorimeters.

- For scattering experiment, all samples were melted and re-shaped into the square sheet with 1 *mm* thickness to suit with the sample holder of temperature programmed SAXS/WAXS. The plastic sheet was cut to 8 x 1.5 - 8 x 2 mm dimension to fit with the sample holder and covered with Kapton tape on both sides of sample holder, which the X-ray can penetrate through the samples at the melt state.

3.1.3 Sample characterization

3.1.3.1 Differential Scanning Calorimeter (DSC)

For thermal analysis, melting temperature (T_m) and the percent of crystallinity of all polymer samples were determined using PerkinElmer PYRIS (Diamond) Differential Scanning Calorimeters (DSC). First, the calibration was done using indium standard material. For the non-isothermal crystallization kinetic studies, The temperature is scanned from 50 °C to 200 °C with the heating rate of 10 °C/min under nitrogen atmosphere. The samples were initially melted at 200 °C for 2 min in order to erase all previous thermal history. Then the samples were cooled down at the different rates of 5, 10, 15, 20, 25 and 30 °C/min. The percentage of crystallinity of all samples were then determined. Finally, DSC thermograms were analyzed quantitatively and fitted with various theoretical models to understand the role of ethylene defect on the non-isothermal crystallization kinetics.

3.1.3.2 Small Angle X-ray Scattering (SAXS)

For SAXS experiment, non-isothermal crystallization of polymer samples was was conducted at BL1.3W beamline, Synchrotron Light Research Institute (SLRI), Nakhon Ratchasima (X-ray wavelength = 1.38 Å and the sample-to-detector = 4.5 m). Silver behenate (d = 3.838 nm) was used to calibrate WAXD scattering angle. The scattering patterns was captured by CCD detector (Mar SX165) with a diameter = 165 mm. An ionization chamber was placed in front of and behind the sample holder with

the photodiode attached in front of a beam stop to monitor the beam intensity. Styrene-ethylene-butadiene-styrene block copolymer (SEBS) with d = 32.8 nm was used as a standard material to calibrate SAXS scattering angle. The sample cell with Kapton windows with 1 mm thickness was used to hold the sample. All specimens were heated to 200 °C and annealed for 5 min to eliminate all the crystalline phases and thermal history. Sample holder was then cooled down to 130 °C which SAXS signals were accumulated at each crystallization temperatures with as exposure time of 60 second. Measurement was made every 5 minutes upto one hour (0, 5, 10, 15, 20, 25, 30, 35, 40, 45, 50, 55, 60 min) with the 120 s.

3.2 Computational method

3.2.1 Monte-Carlo simulation (MC)

3.2.1.1 Coarse-graining of polymer chains

The decision of which method will be used to study the specific phenomenal of each polymer are depending on the length scale and time scale for the properties of interest. The coarse-grained simulation methods will be applied to improve the efficiency of the simulation. Recently, a high coordination lattice (Rapold & Mattice, 1995; Doruker & Mattice, 1999; Baschnagel, et al., 2000) was employed in polymer simulation, in which only two terms of energies (short- and long-range interaction) are included. On this lattice, one occupied site represents two backbone atoms. In the case of polyethylene (PE), one site represents $CH_2=CH_2$ repeating unit as depicted in Figure 3.1. This method can be employed to study much larger systems due to the restriction of bond length and bond angle and the use of discrete space. Furthermore, this model keeps a certain degree of details for chemical bonds. For instance, after the reverse-mapping from coarse-grained into the fully atomistic description, the neglected side methyl groups in polypropylene (PP) can be recovered. At the same time, the stereochemical structure is also retained in this model.
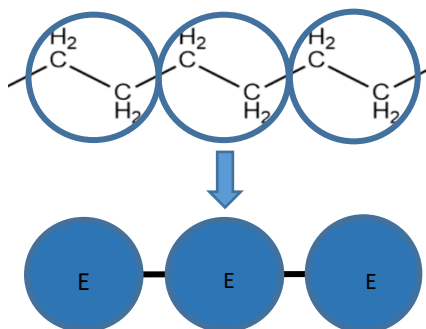
Figure 3.1 Coarse-grained beads of polyethylene with one ethylene repeating unit (two backbone carbons) for each coarse-grained bead.

3.2.1.2 High Coordination lattice

In this study, the simulation will be performed using a coarse-grained Monte Carlo (MC) method on a high coordination lattice. The most natural lattice for polymeric materials is the diamond lattice which gives the tetrahedral structure and the angle between two consecutive bonds and torsion angles (*trans* and *gauche*) are separated by 120°, which is appropriate for polyolefin.

Construction of high coordination lattice, which is called the **2**nd **n**earest **n**eighbor **d**iamond (2nnd) lattice, can be done by eliminating every other site from a diamond lattice. The length of all coarse-grained bonds for both PP and PE are at the same length (2.5Å). This high coordination lattice has the angle between any two axes along the sides of the unit cell equal to 60° (unlike the cubic lattice which has the angle of 90°). The coordination number of the ith shell is $10i^2 + 2$ (12 nearest neighbors in the first shell) which is high enough to provide a flexible definition for rotational state on the lattice. The lattice sites are equivalent to hexagonal packing. Each 2nnd lattice site can be occupied with C_2H_4 (C_3H_6) or C_2H_5 (C_3H_7) repeating unit in the simulation of PE (PP). Therefore, the lattice is partially occupied even when it portrays a dense polymer system with the occupancy for bulk PE and PP around 24% and 12% respectively. Low occupancy has the advantage to improve the simulation efficiency

compared with Molecular Dynamics (MD) simulation. In addition, the coarse-grained chains can be reverse-mapped to fully atomistic model and chain conformation in continuous space can be restored after energy minimization. (Doruker and Mattice, 1997) Furthermore, this high coordination lattice can retain the stereochemical structure which is suitable to study polymers with different stereochemical sequence. Figure 3.2 presents the construction of *2nnd* lattice from a diamond lattice. The 12 nearest neighbors of a center bead are demonstrated in Figure 3.3. The configurations of sub-chains are depended on the position that the third bead occupied, which the relation is shown in Table 3.2.
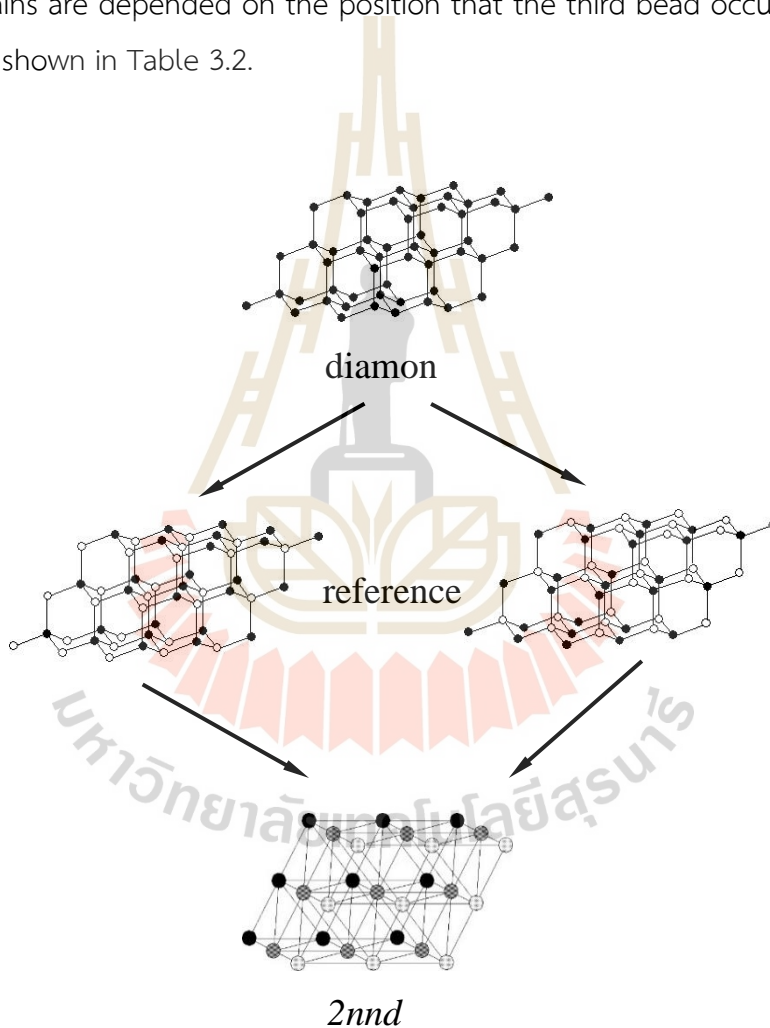
Figure 3.2 Construction of 2nnd lattice from a diamond lattice and two reference lattices.

Table 3.2 Relation of real sub-chain conformations and the distances between every other bead on 2nnd lattice.

Type	Length (Å)	Conformation
A	5.00	tt
B	4.33	tg^+, tg^-, g^+t, g^-t
C	3.53	g^+g^+, g^-g^-
D	2.50	g^+g^-, g^-g^+

A	●	tt
B	●	$tg^\pm$, $g^\pm t$
C	●	$g^\pm g^\mp$
D	○	$g^\pm g^\pm$
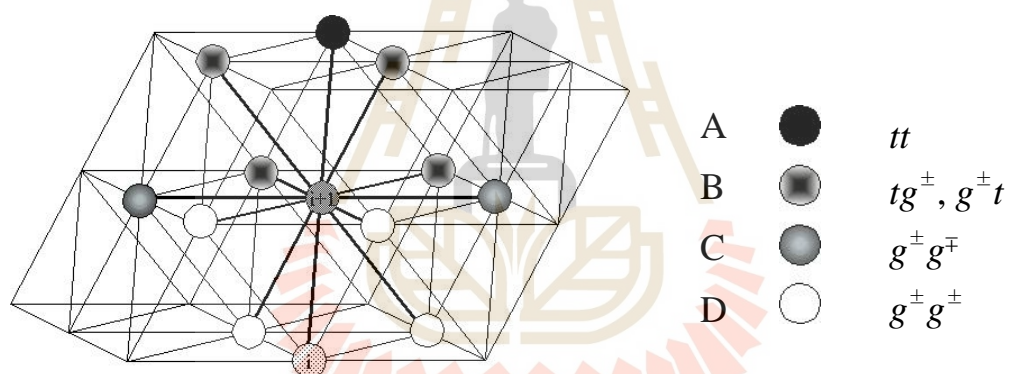
Figure 3.3 Twelve nearest neighbors and chain conformation.
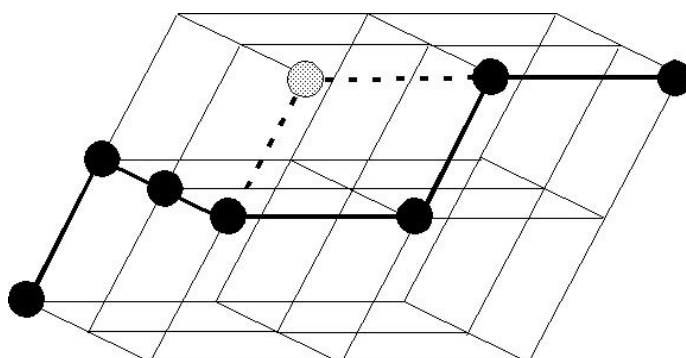
Figure 3.4 Single bead movement on 2nnd lattice.

3.2.1.3 Moves in the simulation

The simulation employs two types of moves. The first one the "single bead moves" (Doruker & Mattice, 1997) where each individual bead is possible to move to its nearest vacant neighbors under the restriction of bond length and energy. The single bead movement on the 2nnd lattice can change the position of either two or three consecutive carbon atoms on the underlying fully atomistic diamond lattice. The movement of a single bead is shown in Figure 3.4.

Another type of move is the multiple beads moves, introduced for the improvement of computational efficiency, called "pivot move", which was proposed by Clancy et al. Figure 8 depicts the example of two-bead pivot move. Using the pivot moves can greatly enhance the rate of equilibration. In every Monte-Carlo Step (MCS), single bead moves and multiple bead pivot moves are occurred arbitrarily. Every bead is tried once, on average. The Metropolis rule (Metropolis et al., 1953) is applied to prevent the movement that cause double occupation and collapses (Carmesin and Kremer, 1998) (Figure 3.5). This formalism criterion is utilized to determine whether the move is made or not.

$$P = \begin{cases} exp(-\Delta E/RT) & \Delta E > 0 \\ 1 & \Delta E \leq 0 \end{cases}. \tag{3.1}$$

For ΔE is the energy difference between the new and old conformation, which includes the short- and long-range interactions. R is the universal gas constant and T is the absolute temperature. If $\Delta E \leq 0$, the move is permitted. Otherwise, a random number will be generated to determine whether the move is successful or not. Determination for the permission of the movement by random number is applied to avoid the chain trapping at the local minima.
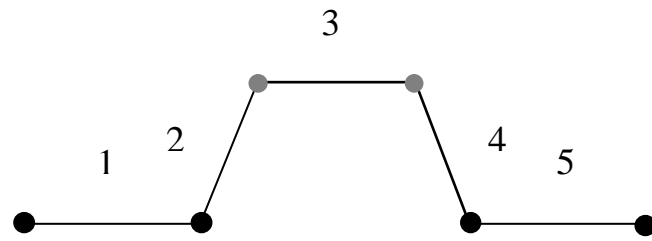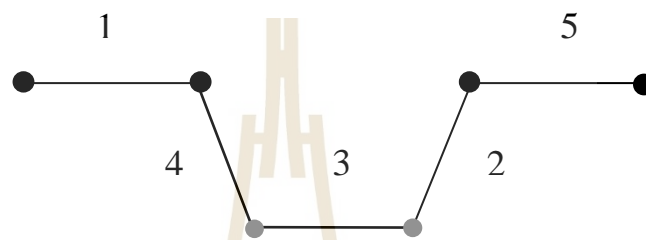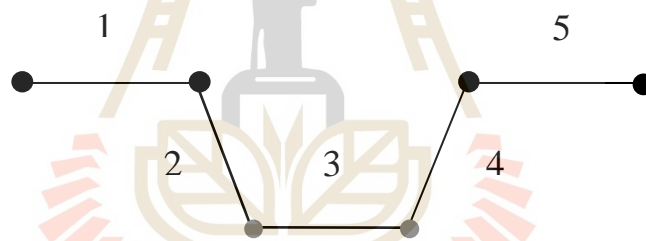
Figure 3.5 Schematic representation of two-bead pivot move. Two middle gray beads change their positions after the movement.

3.2.1.4 Short-range interaction

Simulation on the 2nnd lattice contains a Hamiltonian consisted of short-range and long-range interaction. The short-range interaction is defined by the intramolecular contribution of the chain conformation, based on the Rotational Isomeric State (RIS) models to depict the nature of the polymer chains. The statistical weight matrix used in the RIS model for PE is defined by: (Abe, et al., 1966)

$$\mathbf{U} = \begin{bmatrix} 1 & \sigma & \sigma \\ 1 & \sigma & \sigma\omega \\ 1 & \sigma\omega & \sigma \end{bmatrix}. \tag{3.2}$$

where $\sigma = \exp(-E_\sigma / RT)$,

$$\omega = \exp(-E_\omega / RT).$$

$E_\sigma,$ = 2.1 and E_ω = 8.4 kJ/mol for PE

The rows and columns of **U** are the statistical weights for the conformation of $(i\text{-}1)^{th}$ and i^{th} bond, respectively. The orders of indexing are t, g^+ and g^- for both row and column. The description of the statistical weight matrix in detailed for coarse-grained PE bonds was addressed earlier. (Doruker et al., 1996)

For the RIS model of PP, the one described by Suter, et al. (in 1975) is used *i.e.* E_η, E_τ and E_ω equal to 0.29, 3.9 and 8.0 kJ/mol, respectively. RIS model for PP is more complicated than that for PE since PP chains can have different stereochemical sequences, such as isotactic, syndiotactic and atactic. PP chains can be represented by the different statistical weight matrices for each type of configuration, such as *meso* and *racemic* diads. More detailed description is reported in previous publication. (Haliloglu, 1998) Different tacticity has the following statistical weight matrices.

$$U_d = \begin{bmatrix} \eta & 1 & \tau \\ \eta & 1 & \tau\omega \\ \eta & \omega & \tau \end{bmatrix} \tag{3.3a}$$

$$U_l = \begin{bmatrix} \eta & \tau & 1 \\ \eta & \tau & \omega \\ \eta & \tau\omega & 1 \end{bmatrix} \tag{3.3b}$$

$$U_{dd} = \begin{bmatrix} \eta\omega & \tau\omega & 1 \\ \eta & \tau\omega & \omega \\ \eta\omega & \tau\omega^2 & \omega \end{bmatrix} \qquad (3.3c)$$

$$U_{dl} = \begin{bmatrix} \eta & \omega & \tau\omega \\ \eta\omega & 1 & \tau\omega \\ \eta\omega & \omega & \tau\omega^2 \end{bmatrix} \qquad (3.3d)$$

$$U_{ld} = \begin{bmatrix} \eta & \tau\omega & \omega \\ \eta\omega & \tau\omega^2 & \omega \\ \eta\omega & \tau\omega & 1 \end{bmatrix} \qquad (3.3e)$$

$$U_{ll} = \begin{bmatrix} \eta\omega & 1 & \tau\omega \\ \eta\omega & \omega & \tau\omega^2 \\ \eta & \omega & \tau\omega \end{bmatrix} \qquad (3.3f)$$

In the simulations, the above statistical weight matrixes are applied to calculate the partition function in the discrete form. (Mattice and Suter, 1994)

$$Z = \prod_i U_i \qquad (3.4)$$

Then the bond probability of a specific state η at bond i could be expressed by

$$p_{\eta;i} = \frac{Z_{\eta;i}}{Z} = \frac{U_1 U_2 \cdots U_{i-1} U'_{\eta;i} U_{i+1} \cdots U_n}{Z} . \qquad (3.5)$$

Likewise, the probability of two different states neighbor bonds, for example, bond i-1 in ξ state and bond i in η state, can be written as

$$p_{\xi\eta;i} = \frac{Z_{\xi\eta;i}}{Z} = \frac{U_1 U_2 \cdots U_{i-1} U'_{\xi\eta;i} U_{i+1} \cdots U_n}{Z} \qquad (3.6)$$

The conditional probability $q_{\xi\eta;i}$, which is defined that bond i is in η state given the bond i-1 is in ξ state, has the following expression.

$$q_{\xi\eta;i} = \frac{p_{\xi\eta;i}}{p_{\xi;i-1}} \tag{3.7}$$

Throughout the simulation, the bond states will be changed before and after the movement. The probability can be calculated by the conditional probability of C–C bonds using Equation (3.8) if the bonds have the notation of Figure 3.6.

$$p_{\text{short}} = \frac{p_{\text{new}}}{p_{\text{old}}} = \frac{q^-_{\alpha\beta^*;i-1} q^+_{\beta^*\gamma^*;i-1} q^-_{\gamma^*\delta^*;i} q^+_{\delta^*\varepsilon^*;i} q^-_{\varepsilon^*\eta^*;i+1} q^+_{\eta^*\xi^*;i+1} q^-_{\xi^*\lambda;i+2}}{q^-_{\alpha\beta;i-1} q^+_{\beta\gamma;i-1} q^-_{\gamma\delta;i} q^+_{\delta\varepsilon;i} q^-_{\varepsilon\eta;i+1} q^+_{\eta\xi;i+1} q^-_{\xi\lambda;i+2}}. \tag{3.8}$$

Here, the sign (*) denotes the new state. The following logarithm expression is used to find the difference between short-range interactions before and after the move.

$$\Delta E_{\text{short}} = -RT \ln p_{\text{short}} \tag{3.9}$$
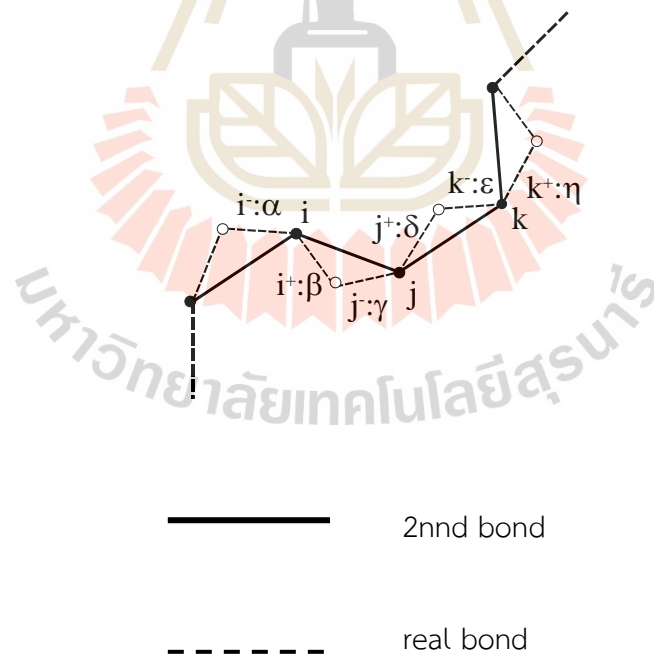
Figure 3.6 Schematic representation of a sub-chain on the 2nnd lattice and the corresponding detailed backbone chain on the underlying diamond lattice.

3.2.1.5 Long-range Interaction

The long-range interaction is a kind of non-bonded interaction which contains the intermolecular interaction and long-range intramolecular interaction, which can be achieved by modification using the portrayal of the second virial coefficient of a non-ideal ethane (for PE) or propane (for PP) gas using the Mayer function and the Lennard-Jones (LJ) potential energy function. (Cho and Mattice, 1997)

On 2nnd lattice, this interaction represents the interaction between two monomers, one at the origin and the other in the specified 2nnd lattice site. A symmetric spherical potential is acting between two monomers. From the flawed gas theory, (McQuarrie, 1976) the second virial coefficient can be written as

$$B_2 = \frac{1}{2}\int\{\exp[-\beta u(r)]-1\}d\boldsymbol{r} = \frac{1}{2}\int f d\boldsymbol{r}\,, \tag{3.10}$$

where, $\beta = 1/kT$; k is the Boltzmann constant. The Mayer function substitutes the integral in Equation 3.11. The integral in B_2 is separated into sub-integrals for each lattice cell and regrouped in each neighboring shell:

$$\begin{aligned} B_2 &= -\frac{1}{2}[-\int d\boldsymbol{r} + \sum_{1st}\int_{cell} f d\boldsymbol{r} + \sum_{2nd}\int_{cell} f d\boldsymbol{r} + \sum_{3rd}\int_{cell} f d\boldsymbol{r} + \cdots] \\ &= \frac{V_c}{2}[1 - \sum_{1st}<f>_{1st} - \sum_{2nd}<f>_{2nd} - \sum_{3rd}<f>_{3rd} - \cdots] \end{aligned}\,, \tag{3.11}$$

where V_c is the volume element $\int_{cell} d\boldsymbol{r}$ for one lattice cell of 2nnd lattice. $<f>$ is the cell averaged Mayer function,

$$<f> = \int_{cell} f d\mathbf{r} \Big/ \int_{cell} d\mathbf{r}\,, \tag{3.12}$$

In the calculation of $<f>$, the center of one monomer is fixed at the origin, while the other one is allowed to be anywhere in the given lattice cell. Therefore Equation 3.12 can be rewritten as

$$B_2 = \frac{V_c}{2}[1 - z_1\bar{f}_{1st} - z_2\bar{f}_{2nd} - z_3\bar{f}_{3rd} - \cdots]. \qquad (3.13)$$

z_i is the coordination number of the ith shell with the form of $10\,i^2 + 2$. The arithmetic means of $<f>$ gives the overall average Mayer function. The effective interaction parameter, u_i, representing the ith neighbor can be finally defined as

$$\exp(-\beta u_i) - 1 = \bar{f}_{ith} \qquad (3.14)$$

In this simulation, the LJ potential energy function with hard core is used to assure the volume exclusion.

$$u = \begin{cases} \infty & r < 2.5\text{Å} \\ u_{LJ} = 4\varepsilon\left[(\frac{\sigma}{r})^{12} - (\frac{\sigma}{r})^{6} \right] & r \geq 2.5\text{Å} \end{cases} \qquad (3.15)$$

Parameters used in the simulations are derived from experimental σ and ε values.

3.3 Simulation procedure on 2nnd lattice

The procedure of the simulation is listed as the following steps:

1. Set the desired chain number and chain length in the lattice to match the experimental density;
2. Select beads for the attempt of moves;
3. Retrieve the new configuration according to the rule of moves;
4. Check the excluded volume effect to remove double occupancy of lattice site;
5. Check bond reverse and unphysical collapse;
6. Calculate short- and long-range interactions;
7. Use the Metropolis rule to determine whether the move is permitted or not;
8. Record the chain configurations every set interval of MCS;
9. Analyze the configuration to obtain static and dynamic properties.

3.4 Film formation

Polymeric film can be initially constructed by adapting the method of Misra *et al.*[85] to lattice simulations. First bulk *NVT* simulations are carried out at 473 K with 85 parent chains of 48 beads each in a periodic box with a length of 30 lattice units (step length 2.5 Å) on each side and 22.4% of the site occupancy. After equilibration of this melt system, the periodic length of the simulation box will be extended in *z* direction to 90 lattice units for film formation. Then, equilibration run at same temperature is performed for at least 5×10^6 MCS. Another 5×10^6 MCS is needed to obtain data for analysis (snapshots are taken in every 10,000 MCS)

3.5 Crystallization

Polyethylene chains (both cyclic and linear) are generated randomly in the 2nnd simulation box with various chain length and chain number for bulk melts and thin films as shown in Table 3.4. For cyclic chains, it is first generated with large extension in one direction of periodic box. Then employed the fast-equilibration run to shrink the box and fold the cyclic-PE back to the appropriated density. While the linear-PE chains were generated using the normal method. Both systems are generated in bulk melts at 473K for 5 million MCS to reach the initial equilibration. Then the system temperature is dropped to 298K instantaneously and run for data collection up to 80 million MCSs. For annealing, the temperature will be changed to the target underneath its melting point in the range 360 K - 380 K.

Table 3.3 Long-range interaction (kJ/mol) of coarse-grained C_2H_4 units at various temperatures.

T (K)	1st shell	2nd shell	3rd shell
473	15.048	0.620	- 0.625
460	14.659	0.580	- 0.626
440	14.056	0.517	- 0.627
420	13.448	0.453	- 0.629
400	12.835	0.388	- 0.630
395	12.681	0.371	- 0.631
390	12.527	0.355	- 0.631
380	12.198	0.322	- 0.632
350	11.281	0.220	- 0.635
298	9.625	0.038	- 0.642

Table 3.4 Condition of each system for cyclic and linear PE crystallization simulation.

System	Box dimension (x,y,z) in lattice unit	Number of chain	Chain length (PE bead per chain)
Bulk 1	(16,16,16)	46	20
Bulk 2	(16,16,16)	23	40
Film 1	(24,24,72)	154	20
Film 2	(24,24,72)	77	40

CHAPTER IV

RESULTS AND DISCUSSION

There are four main parts in this chapters. Monte Carlo simulation of coarse-grained polymer models were employed in the first three chapters to investigate copolymer structures and dynamics at the melt state for different copolymer composition and sequence, molecular and surface properties of copolymer thin film as a function of comonomer content, and crystallization characteristics of linear and cyclic polymers. Subsequently, the effect of few ethylene defects on crystallization behavior of poly(ethylene-*ran*-propylene) as a function of comonomer content was studied by experimental techniques *i.e.* thermal analysis and X-ray scattering.

4.1 Structural and surface properties of poly(ethylene-ran-propylene) thin films

In this section, molecular simulation of coarse-grained copolymer model is developed and applied to study the variation of structural and surface properties for random copolymer thin films as a function of comonomer composition.

4.1.1 Copolymer model

The systems of 85 coarse-grained poly(ethylene-*ran*-propylene) chains containing 48 beads of ethylene and propylene units with regular stereochemical placement, in a random sequence were mapped onto the *2nnd* lattice. The length two connecting beads is 0.250 *nm* determined from the contour length of the backbone bond and the bond angle. The periodic boundary condition box with sides of length equal to 30 units given 15.15% bead occupancy which is equivalent to the simulated bulk density of polyethylene and polypropylene of 0.825 and 0.832 g/cm^3, respectively (closed to experimental values of 0.778 and 0.784 gcm^{-3}) (Orwoll, 1996).

All copolymer chains were generated randomly on the lattice points of the simulation box with periodic boundary condition with no double occupancy at the

same lattice position and the three states RIS models of ethylene-propylene copolymer as described by Mark (in 1972). The interactions dependent on only one bond torsional angle is called the first-order interaction. The statistical weight σ is for the conformation such that a CH or CH_2 group interact with another CH_2 group, where τ is for CH to interact with CH_3 group. For the conformation in which CH interact to both CH_2 and CH_3, the statistical weight is the product of $\sigma\tau$. This (τ, σ, $\sigma\tau$) parameter set is normalized to (η, 1, τ) where $\eta = \tau/\sigma$. The second-order interaction (ω << 1) is depended on two consecutive rotational angles which bring the CH_2/CH_3 groups into close proximity with strongly repulsive.

For CH_2-CH_2-CH_2 segment, the statistical weight matrix U_e is

$$U_e = \begin{bmatrix} 1 & \tau/\eta & \tau/\eta \\ 1 & \tau/\eta & \tau\omega/\eta \\ 1 & \tau\omega/\eta & \tau/\eta \end{bmatrix} \qquad (4.1.1)$$

where

$$\eta = \eta_0 \exp\left(-\frac{E_\eta}{kT}\right), \tau = \tau_0 \exp\left(-\frac{E_\tau}{kT}\right) \text{ and } \omega = \omega_0 \exp\left(-\frac{E_\omega}{kT}\right)$$

For the bond pairs at $CHCH_3$ group, the statistical weight matrix with d configuration is,

$$U_d = \begin{bmatrix} \eta & 1 & \tau \\ \eta & 1 & \tau\omega \\ \eta & \omega & \tau \end{bmatrix} \qquad (4.1.2)$$

The matrix U_l with 1 configuration can be obtained from U_d by interchange of the 2nd and 3rd rows and columns.

In the case of bond pairs separating two $CHCH_3$ groups, the statistical weight matrices are

$$U_{dd} = \begin{bmatrix} \eta\omega & \tau\omega & 1 \\ \eta & \tau\omega & \omega \\ \eta\omega & \tau\omega\omega & \omega \end{bmatrix} \qquad (4.1.3)$$

$$U_{dl} = \begin{bmatrix} \eta & \omega & \tau\omega \\ \eta\omega & 1 & \tau\omega \\ \eta\omega & \omega & \tau\omega\omega \end{bmatrix} \qquad (4.1.4)$$

The matrices U_{ll} and U_{ld} can be obtained from U_{dd} and U_{dl}, respectively, by the interchanges of the 2nd and 3rd rows and columns.

For CHCH$_3$-CH$_2$- CH$_2$, the matrices U_{de} and U_{le} are

$$U_{de} = \begin{bmatrix} \eta/\tau & \omega & 1 \\ \eta/\tau & 1 & \omega \\ \eta/\tau & \omega & \omega \end{bmatrix} \qquad (4.1.5)$$

where U_{1d} is obtained from U_{de} by the interchanges of the 2nd and 3rd rows and columns.

Similarly, for the bond pairs of CH$_2$-CH$_2$-CHCH$_3$, the matrices U_{ed} and U_{el} are

$$U_{ed} = \begin{bmatrix} \eta & \tau & 1 \\ \eta & \tau\omega & \omega \\ \eta\omega & \tau\omega & 1 \end{bmatrix} \qquad (4.1.6)$$

where U_{el} is related to U_{ed} as the usual relationship

For the coarse-grained RIS description of copolymer chains on *2nnd* lattice, the transformation from *2nnd* to diamond lattice can be related to two C-C bonds to each bead uniquely. The vector connecting bead *i* to *j* and bead *j* to *k*, are denoted by the 12 x 12 matrix which can be reduced to 16 3x3 blocks as (Haliloglu and Mattice, 1998)

$$\begin{bmatrix} A & B & A & B \\ B & A & B & A \\ A & B & A & B \\ B & A & B & A \end{bmatrix} \text{ and } A = \begin{bmatrix} a & b & c \\ c & a & b \\ b & c & a \end{bmatrix} B = \begin{bmatrix} b & c & a \\ c & d & b \\ d & b & c \end{bmatrix} \qquad (4.1.7)$$

where a = *tt* or *g+g+* state, b and c = *tg+, tg- , g+t, g⁻t, g+g+, g⁻g+,* and *collapse* state, d = *g⁻g-* or *reverse* state.

The intermolecular non-bonded interactions can be estimated using the temperature-dependent discretized Lennard-Jones (LJ) potential (Cho & Mattice, 1997) with the input parameters between propylene (P-P) and ethylene (E-E) beads as

ϵ/k_B=237.1 K and σ=5.118 Å, and ϵ/k_B=185.0 K and σ=4.400 Å, respectively (Poling, et al., 2002). For ethylene-propylene (E-P) interaction, the Lorentz-Berthelot averaging method gives ϵ/k_B=209.4 K and σ=4.759 Å (Takhulee & Vao-soongnern).. The first three shell energies at the simulation temperature at 473 K are: E–E (12.980, 0.101, –0.593 kJ/mol); P–P (26.693, 3.066, –1.087 kJ/mol) and E–P (18.400, 1.177, –0.880 kJ/mol). The first shell energy (u_1) is large due to highly repulsion interaction as the distance between beads (2.5 Å) is less than σ. The second shell (u_2) is on average between repulsive and attractive interaction. The third shell (u_3) is the attractive interaction in all cases whereas the other shell energies beyond u_3, being very small negative number close to zero as corresponding to the LJ attractive tail. In the simulations, we took the cut-off distance for the first three shells (equivalent to 0.750 nm) for the long-range energies to speed up the simulation as most of the time-consuming step in this simulation was from the calculation of intermolecular non-bonded interaction. It is important to include the attractive third shell energy to bring about the cohesion of polymer thin films as if only the first two repulsive shell energies were used, it would be impossible to form stable films.

4.1.2 Film formation

Independent coarse-grained poly(ethylene-*ran*-propylene) chains were place in the box with periodic boundary condition for bulk system of 30 × 30 × 30 units (equivalent to 75 × 75 × 75 Å³). After equilibration of the bulk, the length of one lattice size (Z direction) was increased to 90 units. This new dimension was long enough such that there was no effective interaction between the original chains with their self-replica and the effective periodic boundary condition was complimented only in two directions. From this technique, free-standing thin films were formed and then equilibrated.

4.1.3 Movement of the coarse-grained polymers

Single and pivot bead moves to the vacant sites were applied in this Monte Carlo simulation. The energies associated with the RIS models and the intermolecular interactions were used for the move acceptance using Metropolis criteria. A Monte

Carlo step (MCS) is equal to the mean number of moves required to change the position for every bead once. The equilibration of each system was evaluated by the end-to-end vector relaxation to lost memory from its initial orientation, and the chain center of mass to move to the distance larger than its radius of gyration (Clancy & Mattice, 2000). The method to generate the copolymer thin films need around 1- 2 million MCS in order to obtain equilibrated structures. Analysis of the properties was obtained by an average of the subsequent 10 million MCS after equilibration. Snapshots were taken every 10,000 MCS during this period.

Structural equilibration of poly(ethylene-*ran*-propylene) films at the molecular scale can be determined using the criterion of complete chain relaxation based on the normalized orientation autocorrelation functions (OACF) of the end-to-end vector $<R(t)R(0)>/<R^2>$. As shown in Figure 4.1.1a, OACFs for the extreme cases of both P_E = 0.0 and 1.0 rapidly decay to zero within 2 million MCS. In addition, as shown in Figure 4.1.1b, the mean square displacements (MSD) for the copolymer center of mass diffuse at the distance larger than $<Rg^2>^{1/2}$ of copolymer chains within 5 million MCS. As judged by MSD and OACF, structural equilibration of all copolymer chains in thin films could be archived within 5 million MCS at 473 K. To illustrate the structural and surface characteristics of poly(ethylene-*ran*- propylene) free standing thin film, Figure 4.1.2 present the sample snapshots of copolymer thin films at different ethylene fraction. In general, when copolymer chains contain more amount of ethylene units, copolymer films become thinner and have sharper surface.
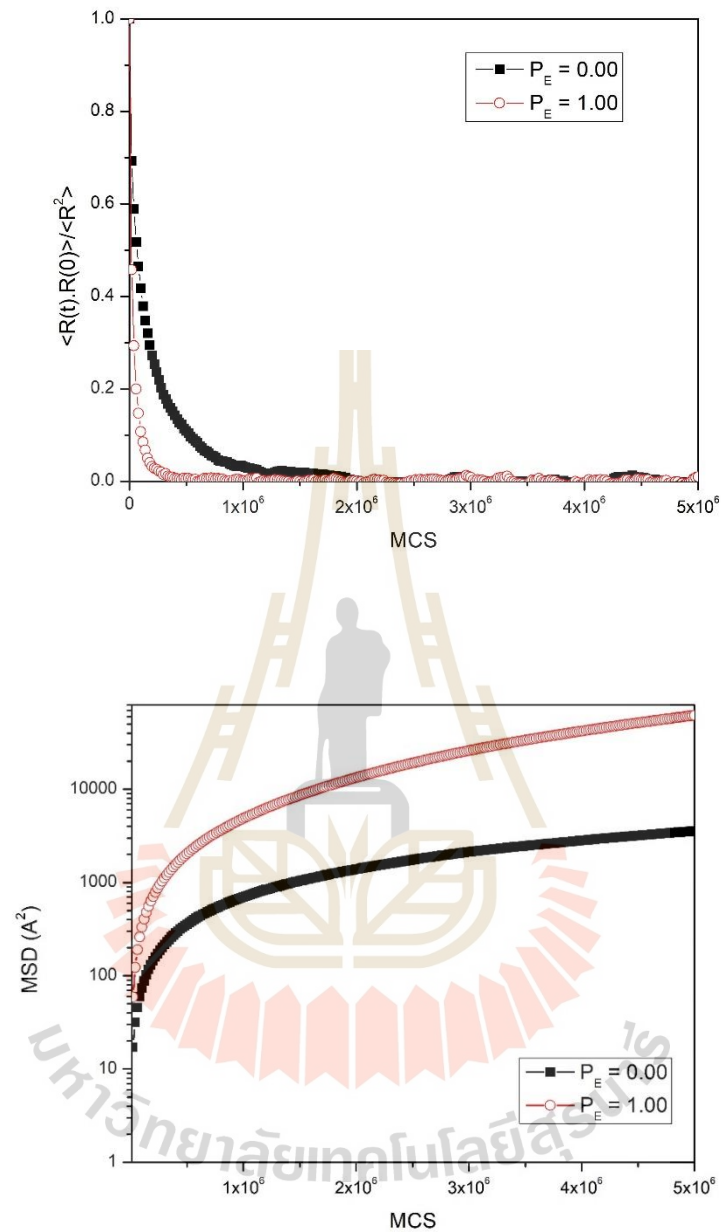
Figure 4.1.1 Structural relaxation of thin films through (a) the mean square displacement (MSD) for the center of mass and (b) the normalized orientation autocorrelation functions (OACF) of the end-to-end vector of poly(ethylene-*ran*-propylene) chains at ethylene fraction = 0.0 and 1.0.

P$_E$ = 0.00

P$_E$ = 0.60

P$_E$ = 0.20

P$_E$ = 0.80

P$_E$ = 0.40

P$_E$ = 1.00
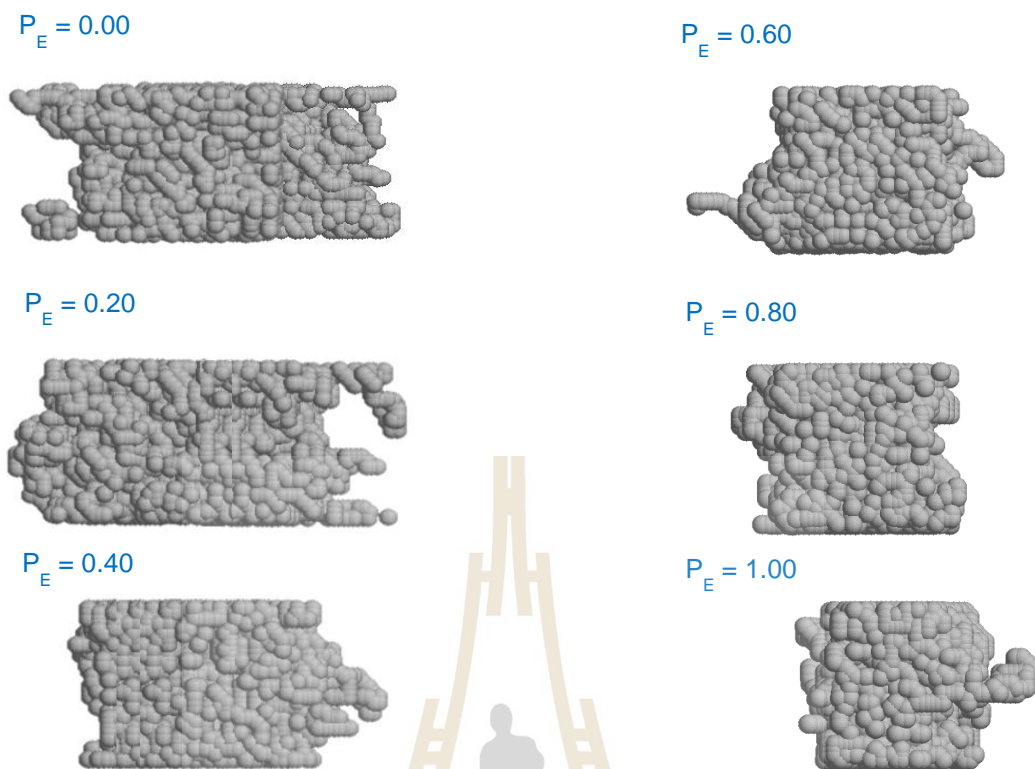
Figure 4.1.2 Sample snapshots for poly(ethylene-*ran*- propylene) free-standing thin film at different ethylene fraction.

4.1.4 Density profiles

The density profiles of poly(ethylene-*ran*-propylene) thin film can be evaluated by summing the number of coarse-grained beads in each bin volume and averaging for all chains from simulation trajectory as a function of displacement from the film mid plane (Z). The bead densities were then normalized by the bulk density relative to the system of 100% PE. In Figure 4.1.3, the relative density profiles are compared for all random copolymer films with different ethylene fraction (P_E). The increased density in the middle or bulk region is observed for larger P_E. To quantitatively analyze the characteristics of film density profiles as a function of P_E, the theoretical function developed by Helfand and Tagami (in 1972) was fitted to the relative density profiles of these random copolymer surfaces.

$$\rho(Z) = \frac{\rho_{bulk}}{2}\left[1 - tanh\left[\frac{Z}{w}\right]\right]$$ (4.1.8)

where $\boldsymbol{\rho}_{bulk}$ is the relative film density in the bulk region compared to 100% PE, Z is the distance from the film mid plane along the normal direction, R is the film thickness defined as the position where the density drops to 50 % of the relative bulk density, and w is the surface thickness (the correlation length). The Helfand-Tagami equation fits the density profiles quite well and the fitting parameters are listed in Table 4.1.1. Apparently, the relative densities in the bulk region become larger and the interfacial widths are sharper with increasing P_E. From Figure 4.1.4, the relative bulk density is nearly linear dependent with P_E. The ethylene content also causes films to become thinner (R) and narrower interfacial thickness (w). In general, when the film density increases as a function of ethylene content, copolymer thin films are more condensed, interfacial profiles are sharper and the interfacial width is sharper
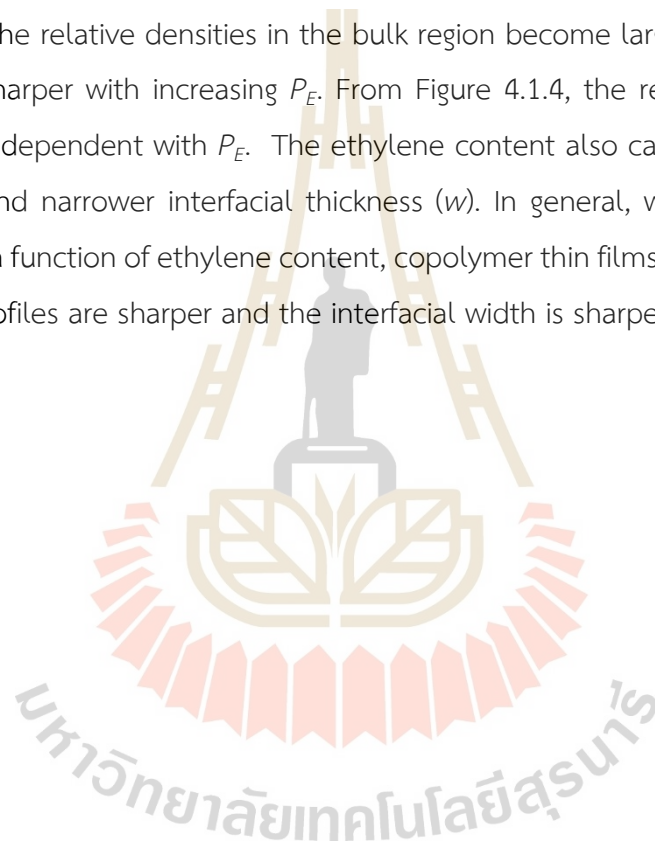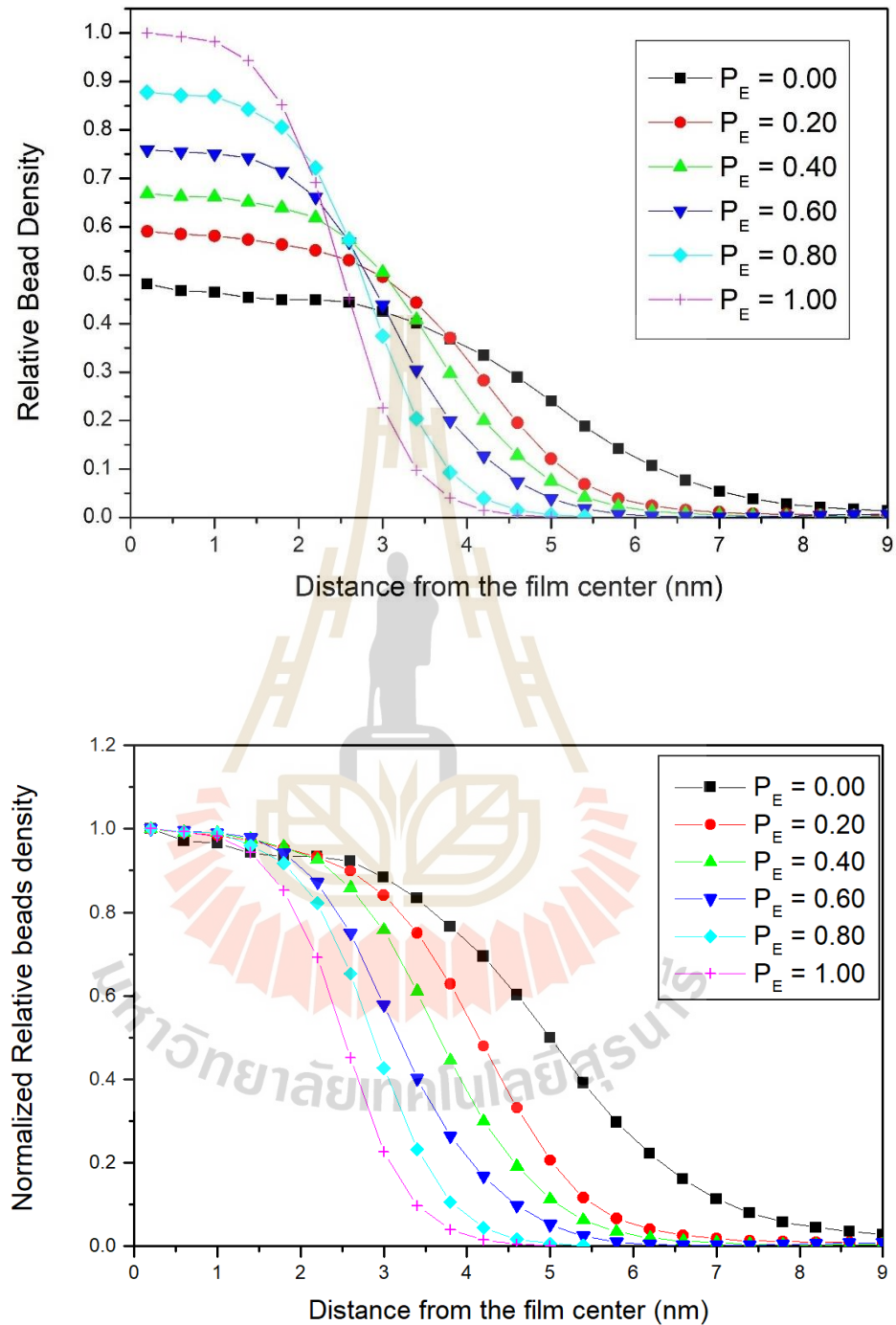
Figure 4.1.3 (a) The relative and (b) the normalized density profiles of poly(ethylene-*ran*-propylene) films as a function of *Z*.

Table 4.1.1 Parameters from density profile of poly(ethylene-*ran*-propylene) films at different ethylene fraction.

Ethylene Fraction	Relative beads density $\rho_{relative}$	Film thickness R (nm)	Interfacial thickness w (nm)
0.00	0.47	5.02	3.84
0.20	0.58	4.15	2.61
0.40	0.67	3.68	2.48
0.60	0.77	3.19	2.34
0.80	0.88	2.87	1.75
1.00	1.00	2.52	1.60
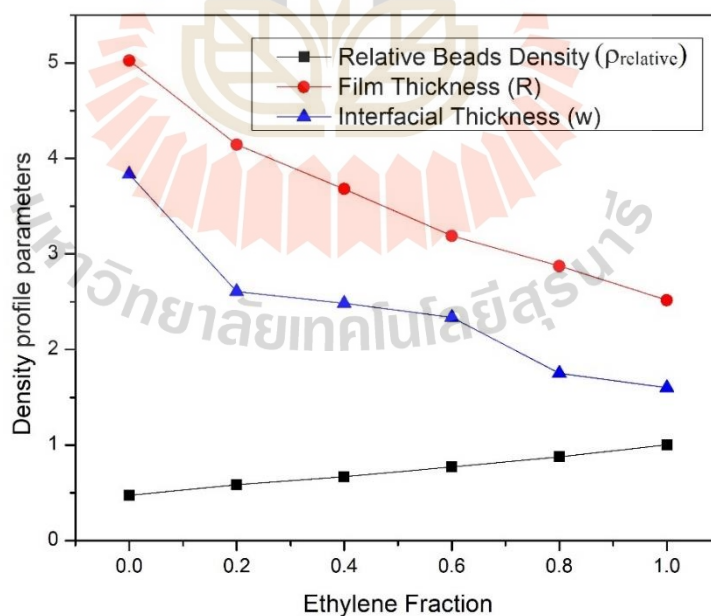
Figure 4.1.4 Surface characteristics of poly(ethylene-*ran*-propylene) films from the fitting with Eq. (4.1.8), at each ethylene fraction.

Next, the normalized profiles of the middle and end bead divided by total bead density of copolymer chains are depicted in Figure 4.1.5. In the bulk region of films, both end and middle bead densities are almost the same. In the region near film surface, the profiles of middle bead density tend to drop, while the end bead density increases significantly. The end beads are more located near the film surface and this effect is more apparent for films with larger amount of ethylene content. The end beads are located near the film surface as they have more mobility and thus need larger free volume. In the middle region of films, the structures pack more effectively. When the copolymer chains contain more repulsive propylene units, these monomer units and end beads are in competition to be located near the surface resulted in broader interfacial profiles.
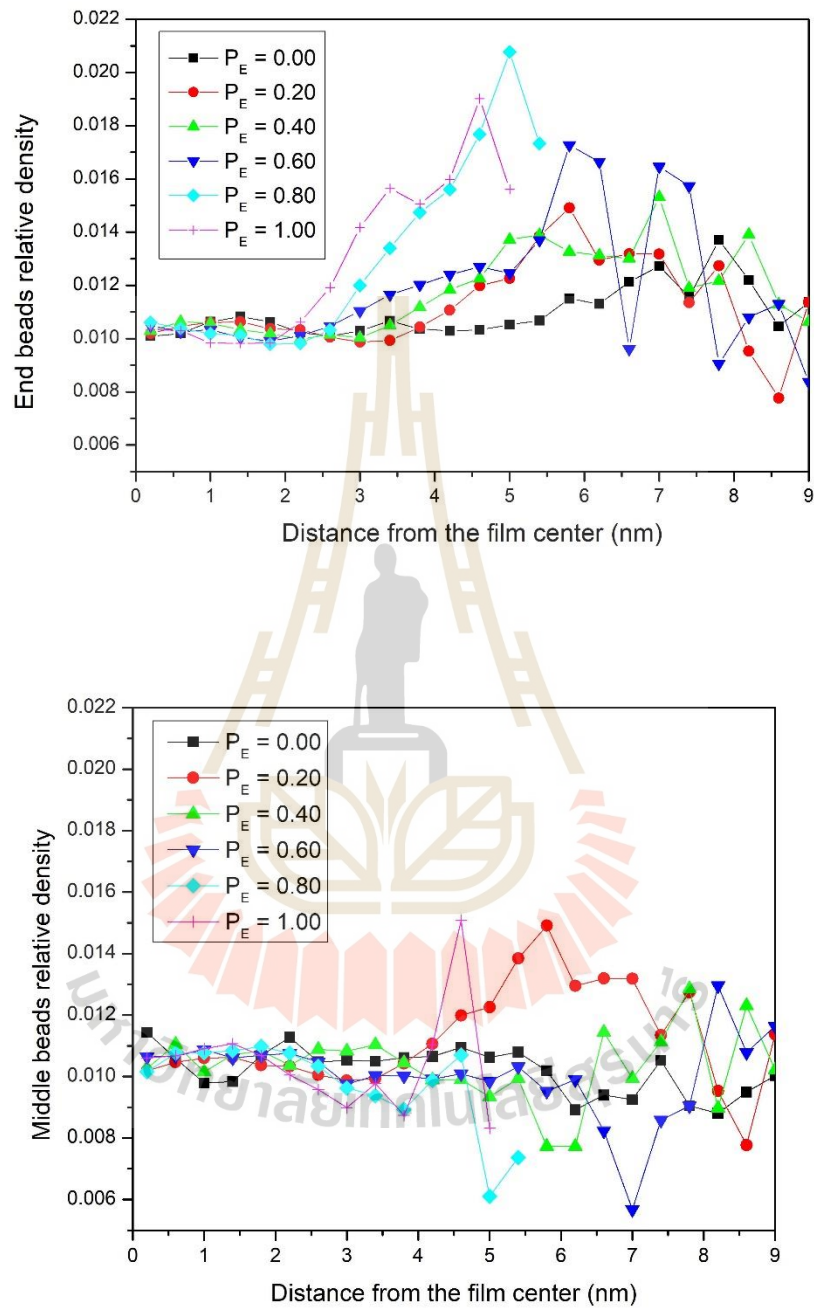
Figure 4.1.5 (a) Relative end bead densities and (b) relative middle bead densities as a function of *Z*.

        To further characterize the structures of poly(ethylene-*ran*-propylene) films,
Figure 4.1.6(a) presents the profiles for the chain center of mass and their cumulative
distribution as a function of Z. For the larger P_E, copolymer chains are more or less
uniformly distributed along the normal direction to the surface. For larger P_E, the
magnitudes are higher with sharper profiles. In opposite to the entropic effect for the
profiles of end beads, the behavior of chain centers of mass in the surface region is
from energetic contribution. For comparison, the cumulative distribution of chain
centers of mass for films with copolymer chains at different P_E are plotted in in Figure
4.1.6(b). Clearly, Films with larger amount of ethylene units have faster increase of
cumulative distribution of chain centers of mass and reach the plateau value at shorter
distance indicating copolymer chains are more densely packed as ethylene units are
less repulsive than that of propylene beads.
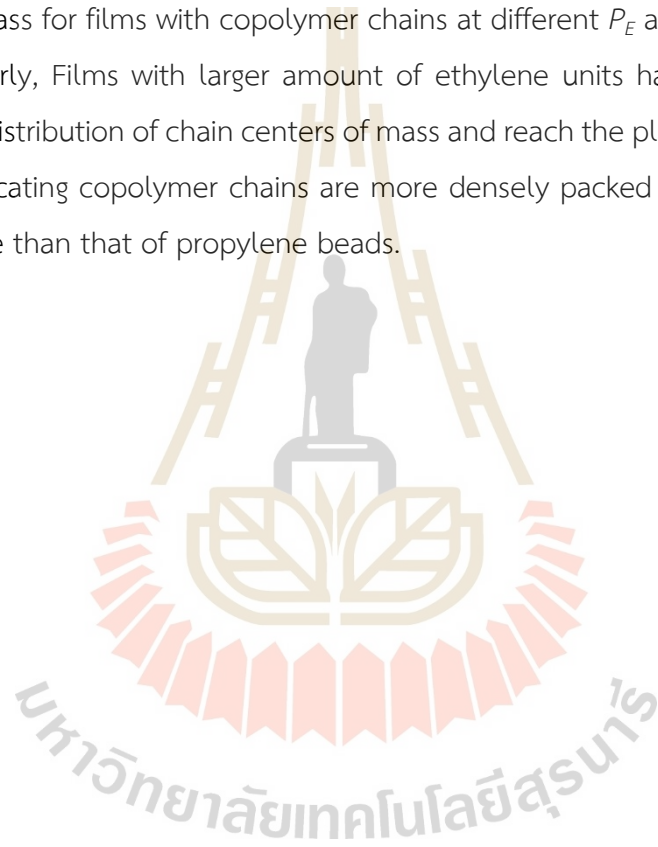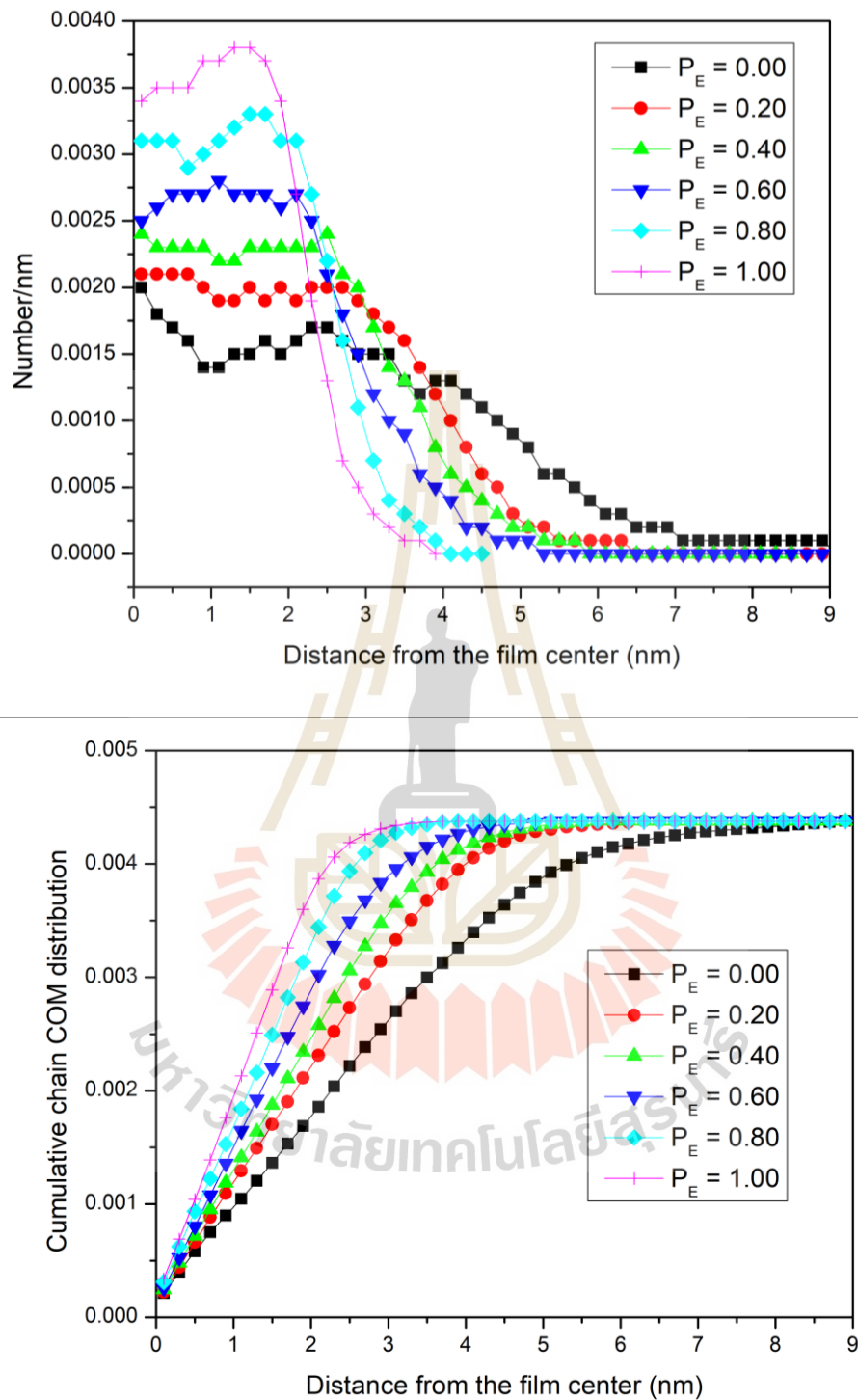
Figure 4.1.6 (a) The distribution for the copolymer chain center of mass and (b) the corresponding cumulative distribution

4.1.5 Bond orientation

Bond arrangement defined from the chord vectors which connect the backbone atom i to $i + 2$, can be determined in term of the order parameter as follows:

$$S = \frac{1}{2}\langle 3(cos^2\theta) - 1\rangle \qquad (4.1.9)$$

where θ is the angle between the chord vectors and the perpendicular axis to the film surface. Bond is considered to orient in parallel or normal direction to the surface when S = -0.5 or 1.0, respectively. Random orientation is defined when the order parameter S = 0.0. Figure 4.1.7 depicts the orientation parameter for all chord vectors. All profiles exhibit similar trend for the chord arrangement as a function of Z. Apparently, chord vectors are quite randomly oriented in most region of thin film except near the surface. Copolymer chains containing more repulsive propylene beads have order parameter closer to 0. Interestingly, the bond orientation become slightly more anisotropic in the surface region for the copolymer chains with larger amount of ethylene content. Similar results in the past simulation were also reported (Doruker and Mattice, 1998), the middle bonds tend to orient parallelly near the free surface, while the end beads tend to orient perpendicular to the surface. As the end beads are segregated near the surface, the overall order parameters are increased near the free surface.
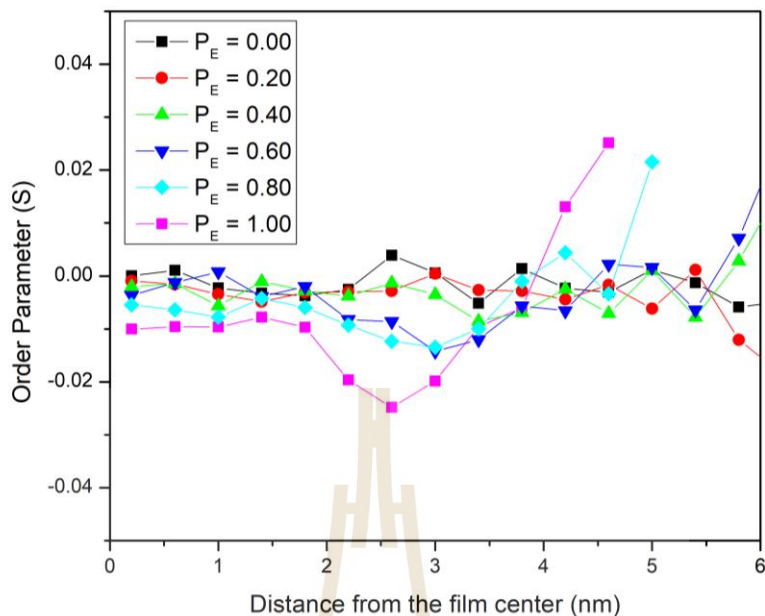
Figure 4.1.7 The order parameter for all chord vectors as a function of Z

4.1.6 Molecular properties

The mean square end-to-end vector, $<R_e^2>^{1/2}$, and the mean square radius of gyration, $<R_g^2>^{1/2}$ of copolymer chains were calculated for quantitative analysis of the average molecular size of copolymers in free-standing films as presented in Table 4.1.3 as a function of ethylene content. Both $<R_e^2>^{1/2}$ and $<R_g^2>^{1/2}$ tend to decrease for larger ethylene content implying that copolymer chains are more compacted as ethylene beads are less repulsive interaction compared to propylene units. In addition, the $<R_e^2>/<R_g^2>$ ratios are close to 6 for all systems implying that the chain length used in this simulation is long enough to be consistent with theoretical prediction (Fixman, 1962).

To view the overall chain shape, an equivalent ellipsoid of polymer chain is defined by three major axes ($L_1 > L_2 > L_3$) which can be obtained from the diagonalization of the radius of gyration tensor (Solc and Stockmayer, 1971). The theoretical random flight chain model predicts the ratio of $L_1^2 : L_2^2 : L_3^2$ = 11.7:2.7:1. The $L_1^2 : L_2^2 : L_3^2$ ratios from our simulation determined at different ethylene contents are presented in Table 4.1.3. The normalized ratio of the largest and smallest axes are presented in Figure 4.1.8(a) and 4.1.8(b). These eigenvalues are relatively unchanged

in the region near the center of films and then L_1 drops while L_3 increase near the surface which are related to the chain flattening near the surface. The major axes are slightly changed as a function of ethylene fraction. To analyze the change of molecular shapes quantitatively, the normalized asphericity ($b/R_g{}^2$) was determined by $b = L_1^2 - 1/2(L_2^2 - L_3^2)$ as presented in Table 4.1.3 and Figure 4.1.8c. Simulation results imply that copolymer chain with larger ethylene content become more compact shape and the chain shape factor (asphericity) decreases in the direction toward the film surface as a result of chain flattening. The shape distortion of copolymer chains in thin film should be related not only to the co-monomer content but also the confinement from impenetrable free surfaces.

Table 4.1.2 The root mean square radius of gyration $<R_g{}^2>^{1/2}$ and the root mean square end-to-end vector $<R_e{}^2>^{1/2}$ for copolymer chains in thin films.

P_E	0.00	0.20	0.40	0.60	0.80	1.00
$<R_e{}^2>^{1/2}$ (nm)	31.26 ± 27.01	30.78 ± 26.71	30.90 ± 26.75	30.95 ± 26.91	30.54 ± 26.64	30.60 ± 26.86
$<R_g{}^2>^{1/2}$ (nm)	12.72 ± 8.32	12.58 ± 8.26	12.61 ± 8.29	12.61 ± 8.34	12.52 ± 8.28	12.54 ± 8.34
$<R_e{}^2>/<R_g{}^2>$	6.04	5.99	6.00	6.03	5.95	5.96

Table 4.1.3 Three molecular major axes and the relative asphericity for copolymer chains.

P_E	$\langle L_1^2 \rangle : \langle L_2^2 \rangle : \langle L_3^2 \rangle$	$\langle b \rangle / \langle R_g^2 \rangle$
0.00	9.90:2.65:1	0.602
0.20	9.53:2.62:1	0.594
0.40	9.66:2.63:1	0.599
0.60	9.25:2.60:1	0.591
0.80	8.43:2.51:1	0.589
1.00	8.75:2.52:1	0.593
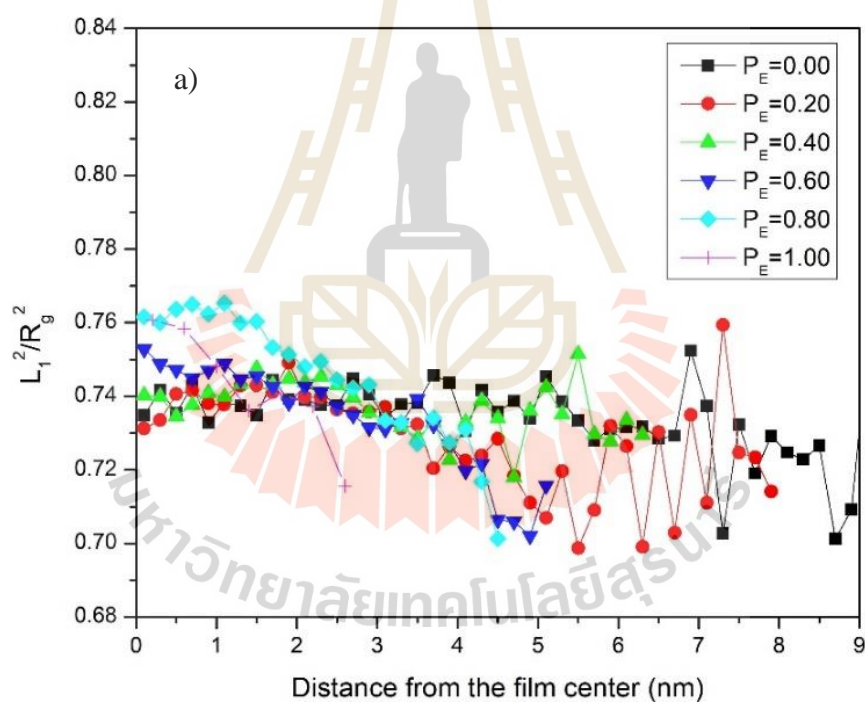
Figure 4.1.8 The normalized major axes of copolymer chains, (a) L_1/Rg^2, (b) L_3/Rg^2 and (c) the chain shape factor (asphericity) as a function of Z for different ethylene fraction.
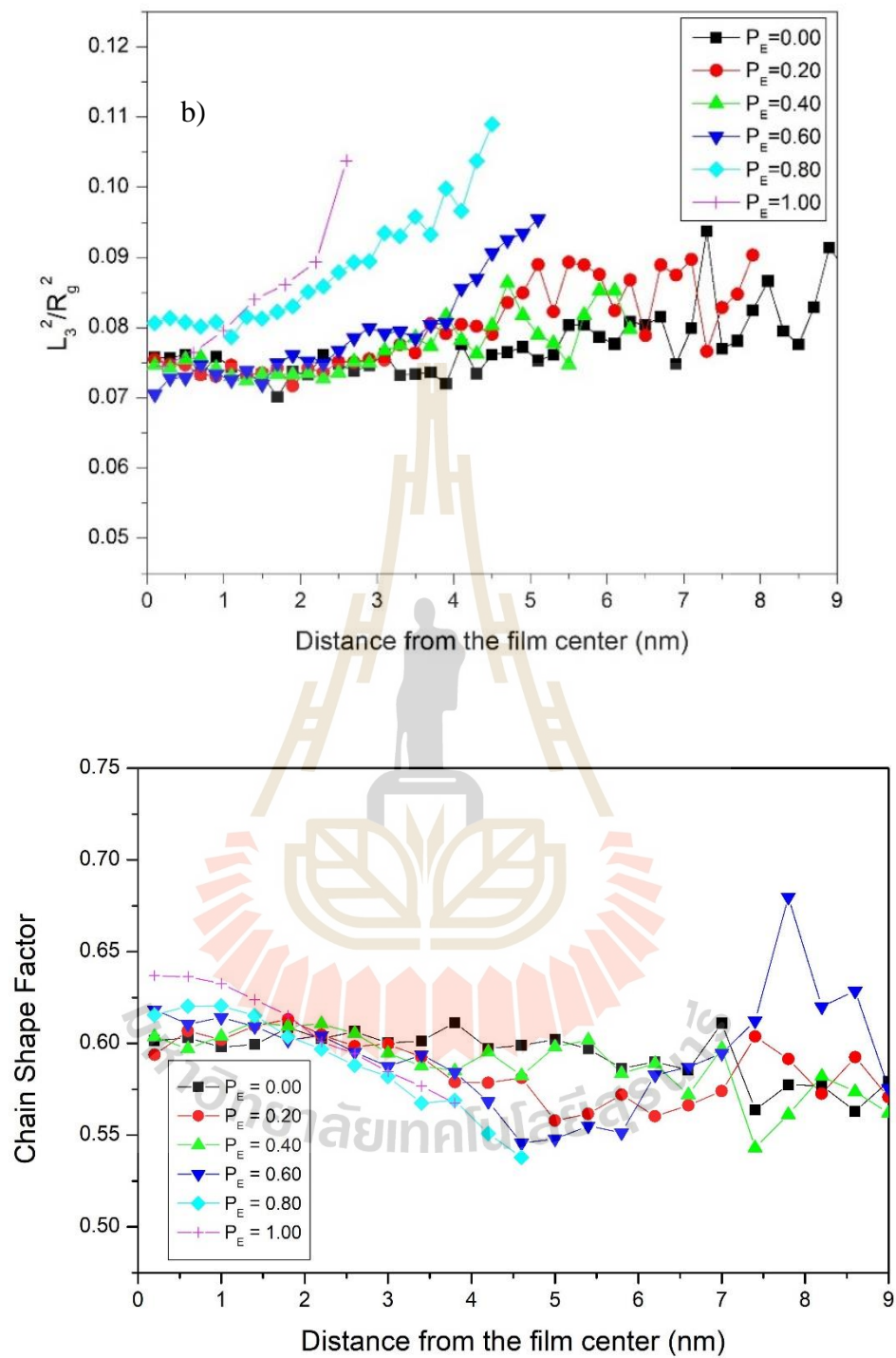
Figure 4.1.8 (Continued) (b) and (c).

To study more about the change of chain dimension in parallel and perpendicular direction to the film surface, the radius of gyration component of copolymer chains versus the distance from the film center is depicted in Figure 4.1.9 where xy and z refer to the average of X-Y and Z component, for parallel and perpendicular to the film surface, respectively. The parallel (X-Y) and perpendicular (Z) components are getting smaller along the distance from the film center with increasing ethylene content and is decreased for chains close to the surface. These findings are also from the chain flattening as chain centers of mass are located close to the surface. Chains become flatter as a function of higher ethylene content.

4.1.7 Chain orientation

Using similar definition to the chord orientation in Eq. (4.1.9), the order parameter of the longest (L_1) axes of copolymer chains in reference to the normal vector to the film surface is presented in Figure 4.1.10. The orientation of L_1 is quite randomly isotropic in the bulk region of films and the magnitude of L_1 order parameter is slightly proportional to ethylene content. The chains become more anisotropic orientation with larger amount of ethylene content (in other words, chain become more random orientation for larger amount of more repulsive propylene units). Toward the free surface, L_1 tends to orient in parallel direction to the film surface. This anisotropy at the surface region become more apparent for copolymer films contain larger amount of ethylene fraction as ethylene beads have less repulsive interaction. Denser film structures are formed and copolymer chains are slightly more oriented as a function of ethylene fraction.
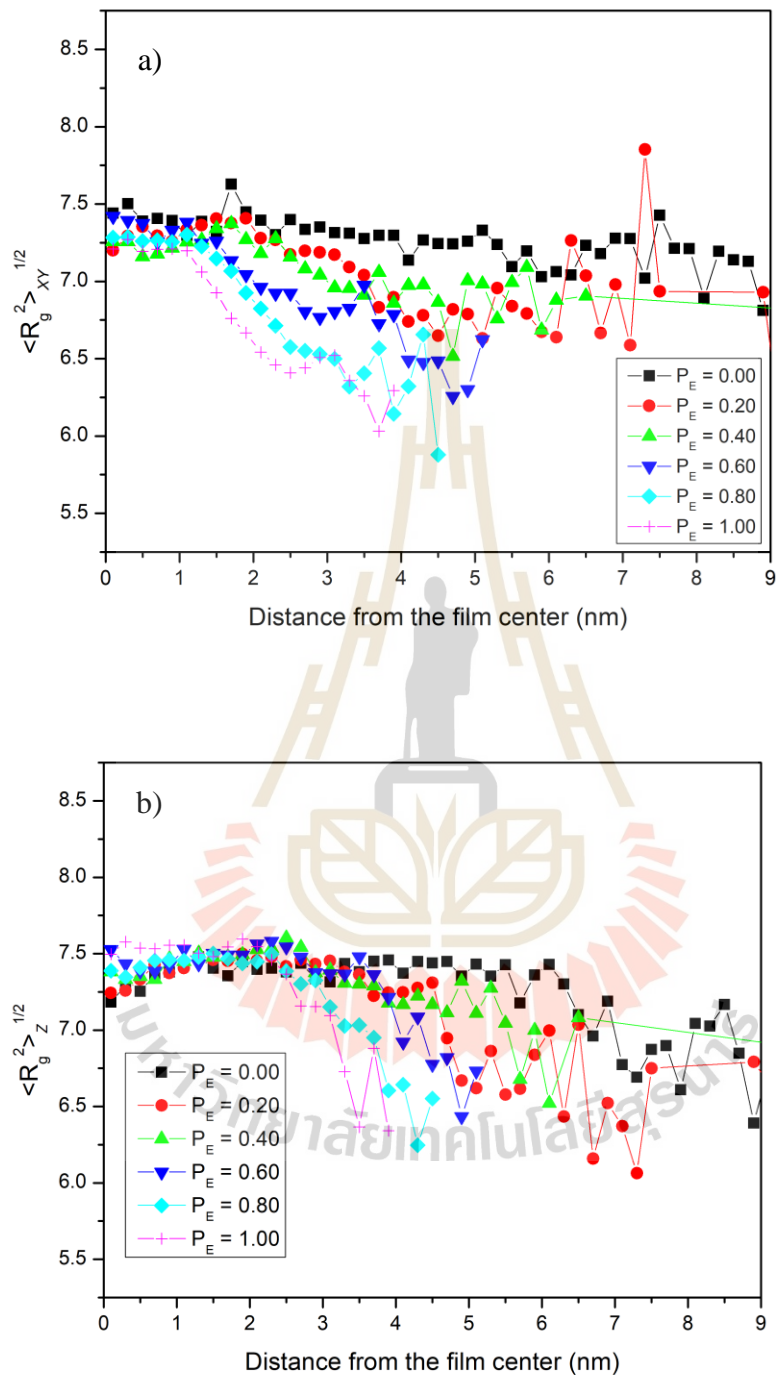
Figure 4.1.9 The components of the mean-squared radius of gyration of copolymer films in (a) the parallel (X-Y) and (b) perpendicular (Z) direction.
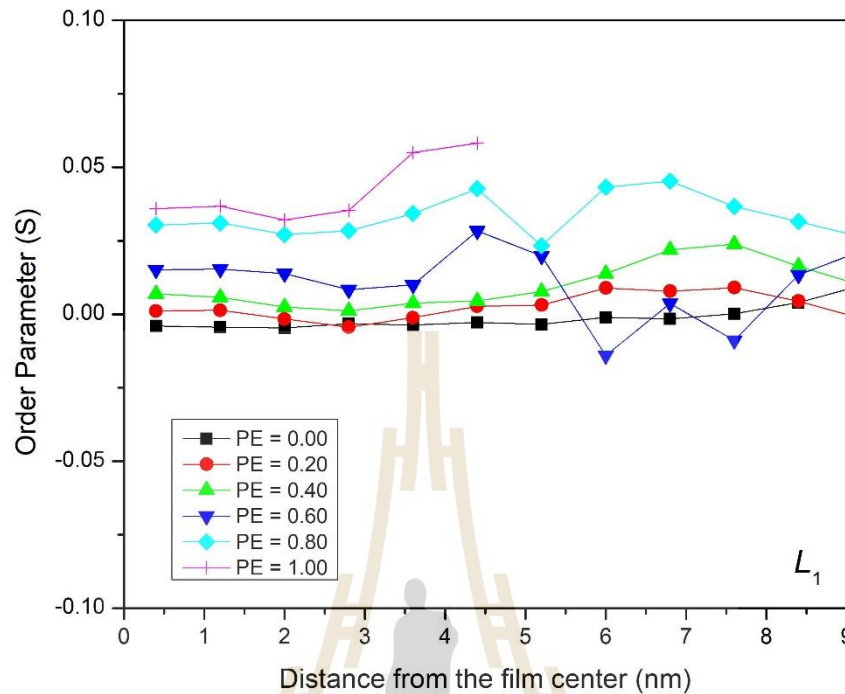
Figure 4.1.10 The arrangement of the longest (L_1) axes of copolymer chains as a function of Z with different ethylene content.

4.1.8 Summary

Structural and surface properties of poly(ethylene-*ran*-propylene) free stand thin film with different ethylene fraction were investigated using Monte Carlo simulation of coarse-grained copolymer model on the *2nnd* lattice. The relative bead densities near the mid-plane center of films are relatively constant and significantly dropped in the surface region. The profiles become denser with sharper surface for copolymer films with larger ethylene content. The chain ends are more segregated while the middle beads are decreased in the free surface region and this observation become more signify for copolymer with more ethylene fraction. The bonds prefer to orient perpendicularly to the surface due to end bead segregation and are slightly sensitive to ethylene fraction in copolymer. For chain properties, the largest axis tends to orient in parallel to the film surface and the orientation become more isotropic for

copolymer chain with less ethylene fraction. Chain size in normal direction become contraction along the direction from the film center and is decreased in the region close to the surface, while the molecular size in parallel direction component has no noticeable changed. Molecular shape in term of asphericity becomes more distorted as a function of ethylene content. The overall size of copolymer chains near the surface was also slightly changed. For chain orientation, the largest molecular axis tends to oriented in a parallel direction to the film surface, and relatively changed toward random orientation for less ethylene content. It should be noted that the data are wide fluctuation for the bond and chain properties in the low-density region near the surface probably due to the small number of observations.

4.2 Effect of monomer composition and sequence on molecular and dynamic properties of ethylene-propylene random copolymer melts

In this section, the effect of comonomer composition and sequence placed as the regular pattern at fixed ethylene fraction (P_E) on the structures and dynamics of ethylene-co-propylene copolymer melts are reported.

4.2.1 Model and method

Ethylene-propylene random copolymer (EPRC) were modeled as coarse-grained chains mapped on the *2nnd* lattice, which E bead is represented for ethane unit, -CH$_2$-CH$_2$-, and P bead is represented as propane unit, -$CH_2CH(CH_3)$- with *d* configuration. Coarse-grained ethylene beads are consolidated on C$_2$H$_2$ backbone carbon atoms and propylene beads on the same C$_2$ backbone bonded to the methyl side group.

The second nearest diamond lattice (*2nnd*) lattice is a high coordination lattice constructed by elimination of every second position from the diamond lattice with the step length of 2.5 Å determined from the contour length of the backbone bond and the bond angle. The lattice has 10i^2+2 coordination numbers in the ith shell, identical to the closest packing of FCC lattice. The periodic boundary condition box with sides of length equal to 30 units. The lattice is occupied by the fraction of the site = 0.1185

which provides more computational efficiency of the bead movement and is equivalent to a density of 0.75 g/cm^3. Temperature is kept at 473 K so that polymer chains are in the melt stage.

Copolymer chains were represented by the Rotational Isomeric State (RIS) model of ethylene-propylene copolymer [23]. For CH_2-CH_2-CH_2 segment, the statistical weight matrix U_e is

$$U_e = \begin{bmatrix} 1 & \tau/\eta & \tau/\eta \\ 1 & \tau/\eta & \tau\omega/\eta \\ 1 & \tau\omega/\eta & \tau/\eta \end{bmatrix} \tag{4.2.1}$$

where

$$\eta = \eta_0 \exp\left(-\frac{E_\eta}{kT}\right), \tau = \tau_0 \exp\left(-\frac{E_\tau}{kT}\right) and\ \omega = \omega_0 \exp\left(-\frac{E_\omega}{kT}\right)$$

For the bond pairs at $CHCH_3$ group, the statistical weight matrix with d configuration is,

$$U_d = \begin{bmatrix} \eta & 1 & \tau \\ \eta & 1 & \tau\omega \\ \eta & \omega & \tau \end{bmatrix} \tag{4.2.2}$$

The matrix U_l with 1 configuration can be obtained from U_d by interchange of the 2nd and 3rd rows and columns.

In the case of bond pairs separating two $CHCH_3$ groups, the statistical weight matrices are

$$U_{dd} = \begin{bmatrix} \eta\omega & \tau\omega & 1 \\ \eta & \tau\omega & \omega \\ \eta\omega & \tau\omega\omega & \omega \end{bmatrix} \tag{4.2.3}$$

For $CHCH_3$-CH_2- CH_2, the matrices U_{de} is

$$U_{de} = \begin{bmatrix} \eta/\tau & \omega & 1 \\ \eta/\tau & 1 & \omega \\ \eta/\tau & \omega & \omega \end{bmatrix} \tag{4.2.4}$$

Similarly, for the bond pairs of CH_2-CH_2-$CHCH_3$, the matrices U_{ed} is

$$U_{ed} = \begin{bmatrix} \eta & \tau & 1 \\ \eta & \tau\omega & \omega \\ \eta\omega & \tau\omega & 1 \end{bmatrix} \tag{4.2.5}$$

The intermolecular non-bonded interactions can be estimated using the temperature-dependent discretized Lennard-Jones (LJ) potential with the input parameters between propylene (P-P) and ethylene (E-E) beads as $\varepsilon/k_B=237.1$ K and $\sigma=5.118$ Å, and $\varepsilon/k_B=185.0$ K and $\sigma=4.400$ Å, respectively. For ethylene-propylene (E-P) interaction, the Lorentz-Berthelot averaging method gives $\varepsilon/k_B=209.4$ K and $\sigma=4.759$ Å. The first three shell energies at the simulation temperature at 473 K are: E–E (12.980, 0.101, −0.593 kJ/mol); P–P (26.693, 3.066, −1.087 kJ/mol) and E–P (18.400, 1.177, −0.880 kJ/mol).

Boltzmann-weighted chain generating algorithm was used for the initial melt stage equilibration. Phase space was rapidly sampled on the following equilibrium Monte-Carlo simulation. Single and pivot bead moves to the unoccupied sites were carried out in this Monte Carlo simulation. The energies correlated with the RIS models and the intermolecular interactions were applied for the move allowance using Metropolis criterion. The equilibration of each system was assessed by the end-to-end vector relaxation to eliminate its initial orientation memory, and the chain center of mass to move to the distance surpass its radius of gyration. The data collecting stage of equilibration for the long-range energy performed by the combined single bead and pivot moves of Monte-Carlo simulation of 80 million Monte-Carlo steps (MCS). One Monte-Carlo step is defined as the mean number of moves required to undertake the movement of every bead once. The Metropolis criterion for accepting the movement is considered using the probabilities of before and final states. The algorithm for dynamical Monte-Carlo is appropriate to represent molecular mobility and the Monte-Carlo Steps (MCS) can be proportional to real time.

The simulations of EPCR were composed of 85 chains, each chain contained 48 beads. E and P were represented for ethylene and propylene units, respectively, with regular stereochemical placement, in a random sequence. The ethylene fraction (P_E) was varied at 0.00, 0.25, 0.50, 0.75 and 1.00. Different patterns of comonomer sequence repeating units at each set at P_E = 0.25, 0.50 and 0.75 are listed in Table 4.2.1, 4.2.2 and 4.2.3, respectively.

4.2.2 Results and discussion

The rotational and translational mobility of ethylene-co-propylene random copolymer (EPRC) at the ethylene fraction (P_E) = 0.00, 0.25, 0.50, 0.75 and 1.00 with random monomer sequences are presented as the orientational autocorrelation function (OACF) for the end-to-end vector ($<\boldsymbol{R}(t)\cdot\boldsymbol{R}(0)>$) and the average mean-square displacement for the center-of-mass (MSD) in Figure 4.2.1(a) and 4.2.1(b), respectively. Chain mobility of EPRCs is strongly increased as a function of ethylene content for both OACF and MSD. The increased diffusion rates are not linearly dependent on P_E values but in the order of 0.75 >> 0.50 > 0.25. In this study, EPRC chains with identical P_E values used in Figures 4.2.1 and 4.2.2 but with different chain pattern were investigated to gain more understanding of the correlation of monomer sequence with conformation and dynamics of EPRCs.
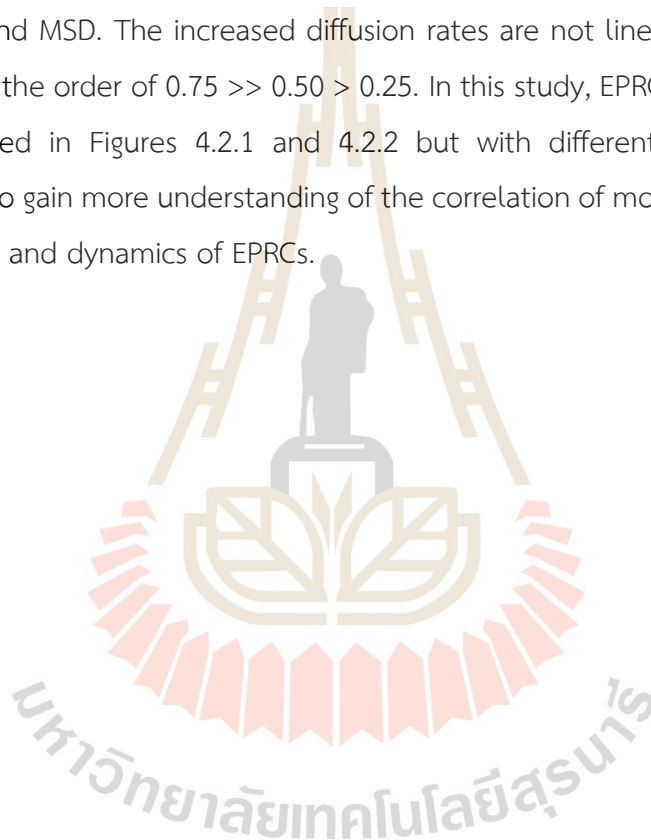
Figure 4.2.1 (a) Decay of the orientational autocorrelation function (OACF) for the end-to-end vector and (b) the mean-square displacement (MSD) for ethylene-co-propylene random copolymer melts at P_E = 0.00, 0.25, 0.50, 0.75 and 1.00.

4.2.2.1 Copolymer at P_E = 0.25

At P_E = 0.25, there exist 4 possible sequences, namely EEPPPPPP, EPEPPPPP, EPPEPPPP and EPPPEPPP. The OACF of the aforementioned sequences are presented in Figure 4.2.2(a). It is obvious that the EEPPPPPP and EPEPPPPP sequences, which has more "block-like" character, decay at a much faster rate than the alternating sequences as: EEPPPPPP $\geq$ EPEPPPPP > EPPEPPPP $\geq$ EPPPEPPP. Similarly, the average mean-square displacements of the center-of-mass (MSD) also exhibit a similar trend in which EEPPPPPP > EPEPPPPP > EPPEPPPP > EPPPEPPP in Figure 4.2.2(b). Relative diffusion coefficients for all monomer sequences were calculated based on the MSD as a function of the number of MCS and the results are listed in Table 4.2.1. These data suggests that the mobility of copolymers increases as a function of the length of propylene sequence.

The relative diffusion coefficients can be divided the into two groups for the (A) fast and (B) slow diffusion of copolymer sequence. For group A, the longer P block (EEPPPPPP and EPEPPPPP) sequences diffuses obviously faster than the group B with shorter P block (EPPEPPPP and EPPPEPPP) sequences. The correlation of chain mobility with molecular dimension and chain rigidity as represented by radius of gyration and the characteristic ratio, respectively, is not clear. It was observed that the EPPPEPPP sequence exhibits the smallest magnitude suggesting the more compact chains and higher flexibility should have higher mobility. Nevertheless, for the case of two sequences (EPPPEPPP and EPEPPPPP) with almost the same chain rigidity, the EPPPEPPP sequence has much higher mobility. Thus, the intrachain factors (molecular dimension and chain flexibility) is not only the factor to govern the dynamics of EPRC melts at low ethylene fraction (P_E = 0.5).

The local intermolecular packing can be characterized using the intermolecular pair correlation function (PCF) defined as the probability of finding one monomer at a distance r from another monomers. On the discrete lattice space, PCF is defined based on the shell ith, instead of the normal definition based on a continuous distance, r. This discretized form of the pair correlation function can be defined as:

$$g_{MM}(i) = \frac{1}{(10i^2+2)V_M n_s} \sum n_{MM}(i), \qquad\qquad (4.2.6)$$

Where V_M is the volume fraction of monomers in the system, n_s is the number of snapshots from the simulation, and $n_{MM}(i)$ is the number occupancy of monomer in the ith shell from other monomers from different chains. As shown in Figure 4.2.3, all four sequences have significant difference in the second to the fourth shell where the EEPPPPP and EPEPPPP sequences exhibit lower PCFs values. This result implies that these two sequences have less effective interchain packing. Examining the radii of gyration and characteristic ratios of these two sequences, the results suggest that intermolecular packing plays a more important role than intrachain effect in determining the copolymer mobility at low ethylene fraction (P_E = 0.5).
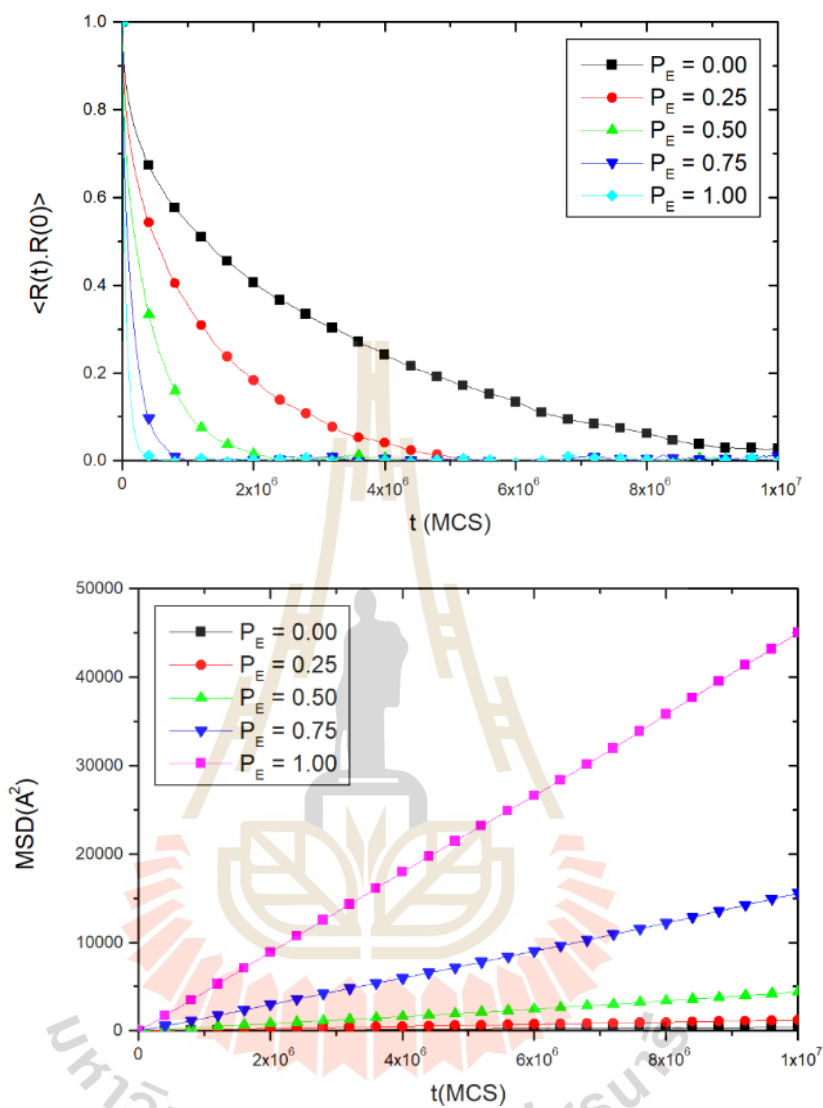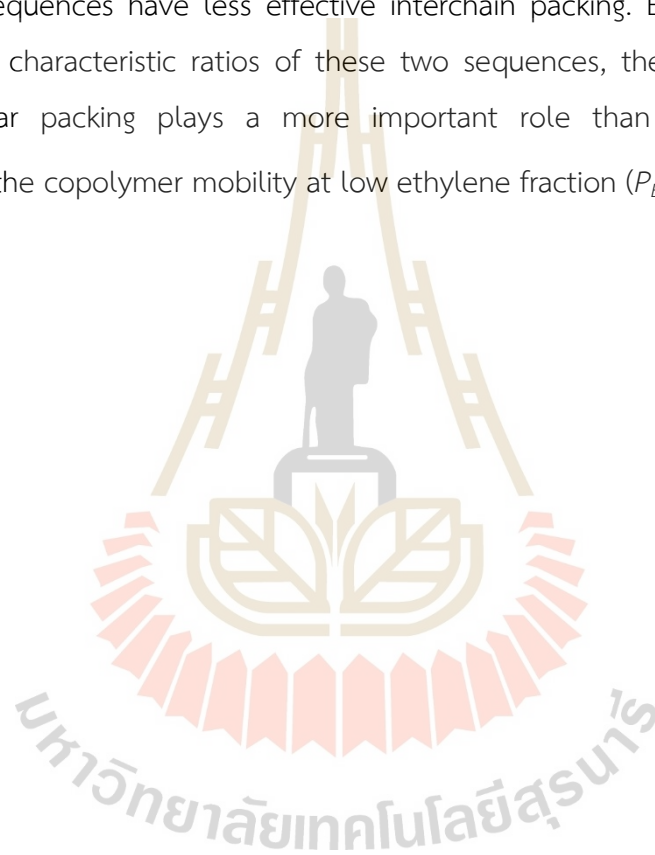
Figure 4.2.2 (a) Decay of the orientational autocorrelation function (OACF) for the end-to-end vector and **(b)** the mean-square displacement (MSD) for EPRC melts at P_E = 0.25, with different co-monomer sequences.

Figure 4.2.3 Intermolecular pair correlation function (PCFs) of EPRC melts with different co-monomer sequences at P_E = 0.25.

Table 4.2.1 Comonomer sequences, the mean square radius of gyration, $<R_g^2>^{1/2}$ $(\mathring{A})$, the characteristic ratio, $<r^2>_0/nl^2$, the relative intermolecular PCFs in the third shell, $g_{tatol}(3)$ and the relative diffusion coefficient, D of EPRC melts at P_E = 0.25.

Group	Sequences	$<R_g^2>^{1/2}$	C_n (RIS)	*relative $g_{tatol}(3)$*	relative D
A	EEPPPPPP	12.18	4.05	0.86	1.78
	EPEPPPPP	12.04	3.93	0.89	1.51
B	EPPEPPPP	12.18	4.09	1.02	1.10
	EPPPEPPP	12.00	3.90	1.00	1.00

4.2.2.2 Copolymer at P_E = 0.50

Figure 4.2.4(a) depicts the decay of the end-to-end vector autocorrelation functions of 10 monomer sequences of EPRC at P_E = 0.50. Obviously, all copolymer chains achieved equilibration quite fast and the decay rates are relatively difference. More apparently, all sequences can have distinguishable MSDs over a given period of time as shown in Figure 4.2.4(b) and demonstrate quite distinguishable lines. The MSDs from the raw data are used to determine the relative diffusion coefficient (*D*) as presented in Table 4.2.2. Again, these data also suggests that the block-like sequences exhibit faster diffusion. The relative motion can be ordered as: PPPPEEEE > PPPEPEEE > PEPPEEPE > PEPEPEPE > PPEEPPEE = PPPEEEPE > PPEPPEEE > PPEPEPEE. Note that the order for the translational motion is different from those for rotational motion.

All intermolecular PCFs of EPRC melts for each co-monomer sequence at P$_E$ = 0.50 have quite similar pattern with the most distinguishable at the 3rd shell. In general, the block-like and alternating sequence can be distinguishable from other patterns. In addition, the block-like (PPPPEEEE) sequence has the largest chain dimension but exhibit faster mobility than the PPPEPEEE sequence. Hence, there might be the effect from comonomer arrangement on molecular mobility stronger than other structural properties in this case. An insertion of different monomer to break up the continuous sequence seem to slow down the chain rotational motion. Three copolymer sequences with the slowest mobility are PPEPPEEE > PPEPEPEE > PPPEPEEPE. From Table 4.2.2, the relative diffusion coefficients can be divided into four groups (A > B > C > D). The average chain dimension can be arranged for each group as: A = D < B < C. The average relative magnitudes for the 3rd shell of PCFs are not significant difference but can be ordered as: A < B < C < D. As expected, the general trend of chain diffusion seems to inversely depended on molecular dimension and intermolecular packing (except group D exhibit the slowest diffusion possible due to the highest intermolecular packing dominating its small dimension). Interestingly, the copolymer with perfectly alternated (PEPEPEPE) sequence is not the slowest diffusion but can diffuse faster than other 5 sequences.

In group A, when the first three maximum diffusions rates are considered, all these three sequences containing PPP blocks have smaller chain dimension but higher local intermolecular packing (Figure 4.2.5 and Table 4.2.2). The diffusion seems to be affected by the chain dimension. For lower diffusion coefficient in group B, most of copolymer chains have rather alternating sequence (except PPPEEEPE). Unlike the situation in group A, the alternating sequences tend to give larger chain dimension and higher intermolecular packing. In overall, the relative diffusion rates of are relatively about the same. For the diffusion behavior in group C, PPEPPEEE and PPEPEPEE sequences have almost the same diffusion rate. Except the packing density, the molecular size and chain rigidity of PPEPPEEE sequence are higher than the PPEPEPEE pattern. It can be conferred that lower chain packing maybe the reason to have slightly faster diffusion for PPEPPEEE sequence even though both chains contain PPEP block. For the remaining pattern, the PPEPEEPE sequence has smallest molecular size but the highest intermolecular packing. The slowest different rate should be governed by the preferred local packing than other groups.

Furthermore, the acceptance rate of MC moves can be employed to quantify the diffusion of these sequences by comparing the mobility of E and P units. In general, moving of consecutive E pattern is relatively faster than continuous P sequence. The EPE segment has faster mobility than PEP units. Comparing between 4 units, the acceptance rate can be ordered as EEPP, PPEE > PEEP > EPPE > EPEP, PEPE. These results suggested that the diffusion of PEPEPEPE sequence was faster than others because it contains more EPE or PEP segments as well as it has more flexible chain. The diffusion of EPRC melts depends not only on both intramolecular contribution and intermolecular interaction. The intermolecular packing seems to be more influence than the intramolecular contribution at an intermediate ethylene composition (P_E = 0.25 and 0.50).
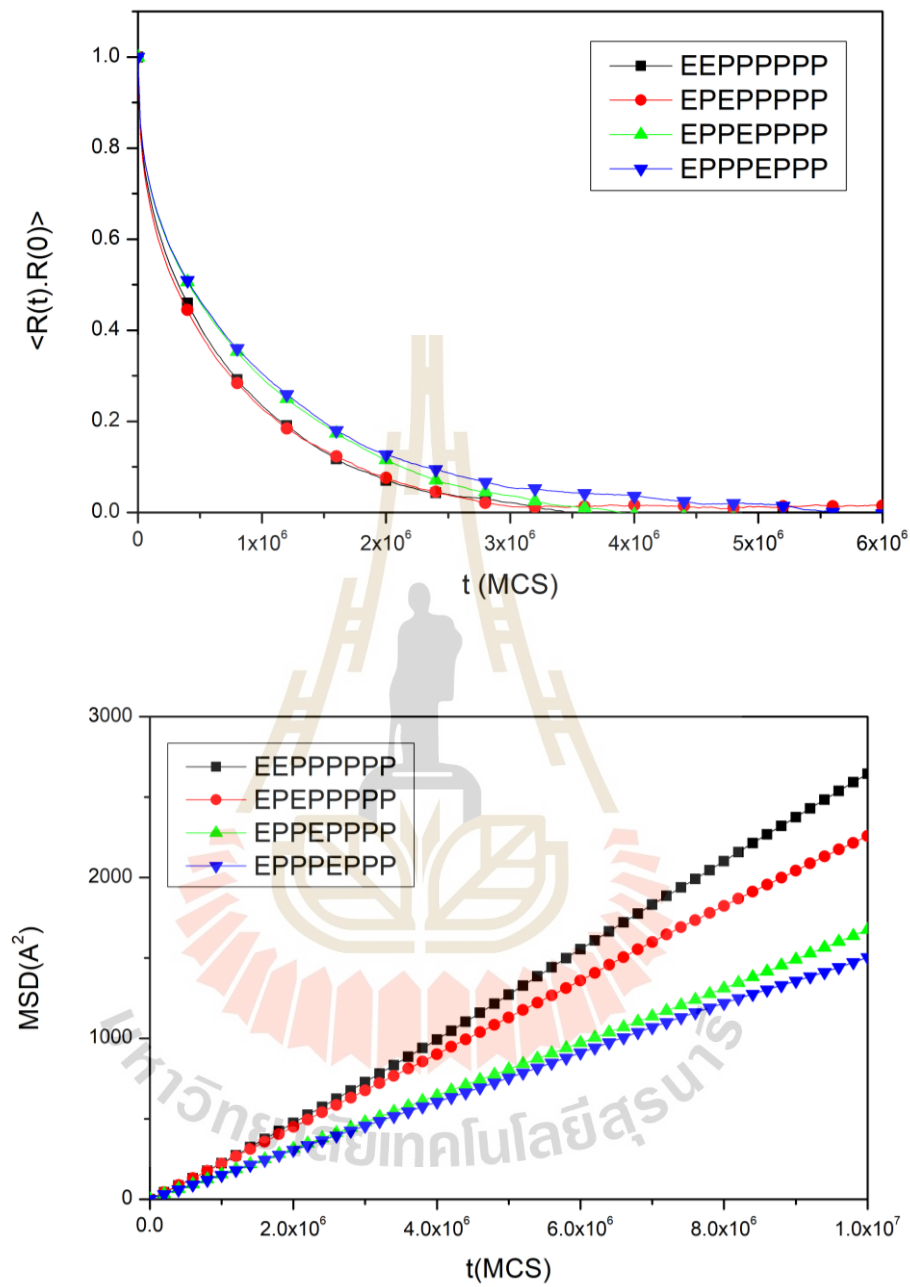
Figure 4.2.4 (a) Decay of the orientational autocorrelation function (OACF) for the end-to-end vector and **(b)** the mean-square displacement (MSD) for EPRC melts at P_E = 0.50, with different co-monomer sequences.
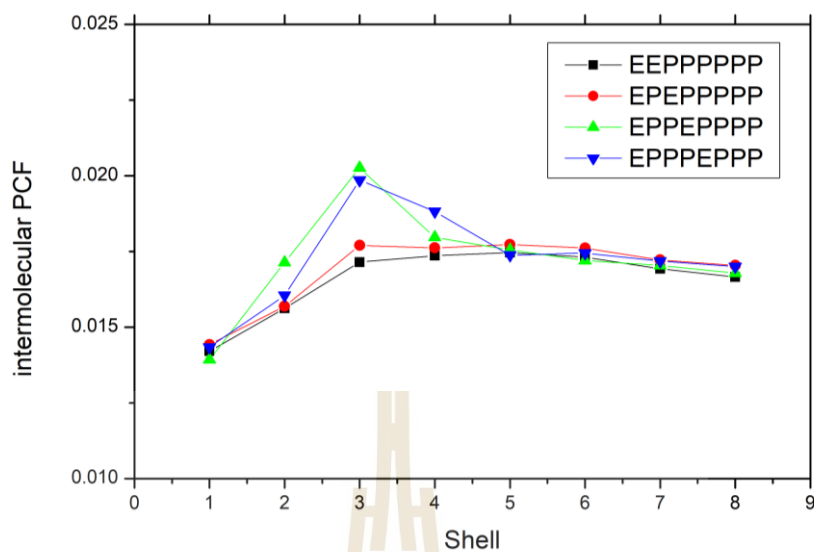
Figure 4.2.5 Intermolecular PCFs of PE-*i*PP melts at P_E = 0.50, with different co-monomer sequences.

Table 4.2.2 Comonomer sequences, the mean square radius of gyration, $<R_g^2>^{1/2}$ $(\mathring{A})$, the characteristic ratio, $<r^2>_0/nl^2$, the relative intermolecular PCFs in the third shell, $g_{tatol}(3)$ and the relative diffusion coefficient, D of EPRC melts at $P_E = 0.5$

Group	Sequences	$<R_g^2>^{1/2}$	C_n (RIS)	relative $g_{tatol}(3)$	relative D
A	PPPEEPEE	12.27	4.09	1.06	1.24
	PPPPEEEE	12.39	4.20	0.97	1.20
	PPPEPEEE	12.24	4.07	1.03	1.16
	Average	12.30		1.02	1.20
B	PEPPEEPE	12.48	4.30	1.06	1.01
	PEPEPEPE	12.35	4.19	1.00	1.00
	PPEEPPEE	12.46	4.24	1.06	0.98
	PPPEEEPE	12.34	4.17	1.01	0.98
	Average	12.41		1.03	0.99
C	PPEPPEEE	12.64	4.43	1.03	0.89
	PPEPEPEE	12.57	4.36	1.05	0.88
	Average	12.61		1.04	0.89
D	PPEPEEPE	12.31	4.11	1.05	0.77

4.2.2.3 Copolymer at $P_E = 0.75$

Figure 4.2.6(a) depicts the decay of the end-to-end vector autocorrelation functions of copolymers with four different comonomer sequences with a fixed $P_E = 0.75$. The OACFs of all chain sequences decay to zero within 2 million MCS and are quite similar and difficult to distinguish. On the other hand, the MSDs for the longer consecutive ethylene sequence (PPEEEEEE and PEPEEEEEE) exhibit higher mobility in the translational motion than the shorter ones (PEEPEEEE and PEEEPEEE) as depicted in Figure 4.2.6(b). Accordingly, the relative diffusion coefficients listed in Table 3 can be ordered as: PEPEEEEEEE > PPEEEEEEE > PEEPEEEE > PEEEPEEE.

The intermolecular PCFs for all monomer sequences at P_E = 0.75 are compared in Figure 4.2.7. All four sequences exhibit almost identical PCFs. As a result, the intermolecular packing of all copolymers is not correlated well with chain mobility. Upon investigation of the radii of gyration, characteristic ratios and the values of the third cell of the PCFs, it is clearly that the fast-moving sequence, specifically PEPEEEEEE and PEPEEEEE are not correlated well with the characteristic ratio and have similar chain packing. Difference in chain translational motion is related to the monomer sequence. Copolymers with long consecutive ethylene sequence tend to form more random coil conformation. This is rather comparable to the case in which P_E = 0.25 in which long consecutive propylene units with *meso* diads cause the helix-like sequence that leads to less chain packing, thereby increasing their mobility. Although, the intermolecular interaction appeared to be not the factor to control the mobility of the chains in the case of P_E=0.75. Despite PPEEEEEE sequence has its size approaching to that of PEEEPEEE sequence, it moves faster due to a raising of the acceptance rate for longer ethylene sequence. The slowest mobility is seen for PEEEPEEE sequence which is the shortest EEE sequence interrupted by M unit. The consecutive ethylene block sequence seems to exhibit noticeable faster diffusion, so the effect of intramolecular contribution seems to be dominant in governing the diffusion at high ethylene composition (P_E = 0.75).
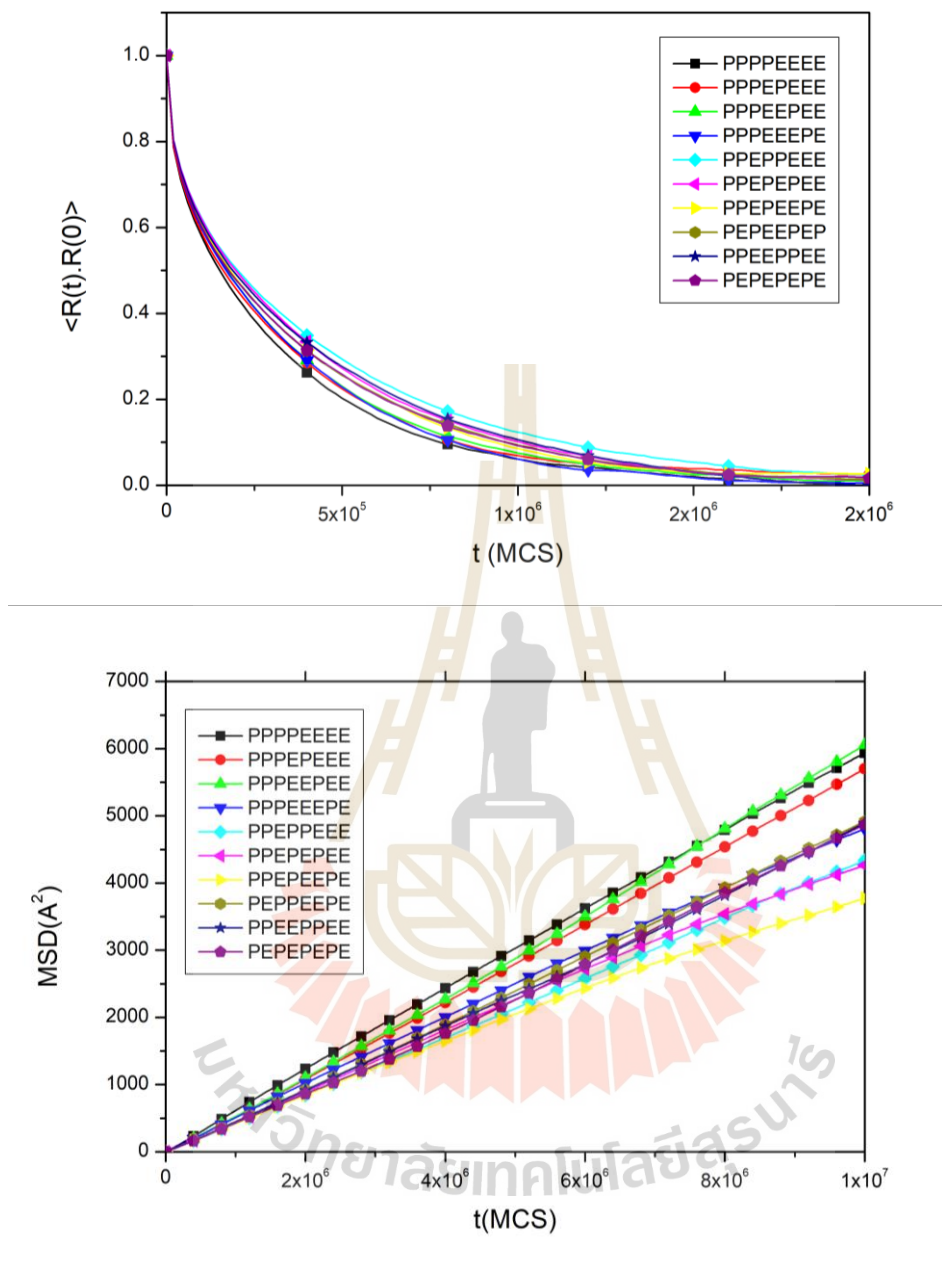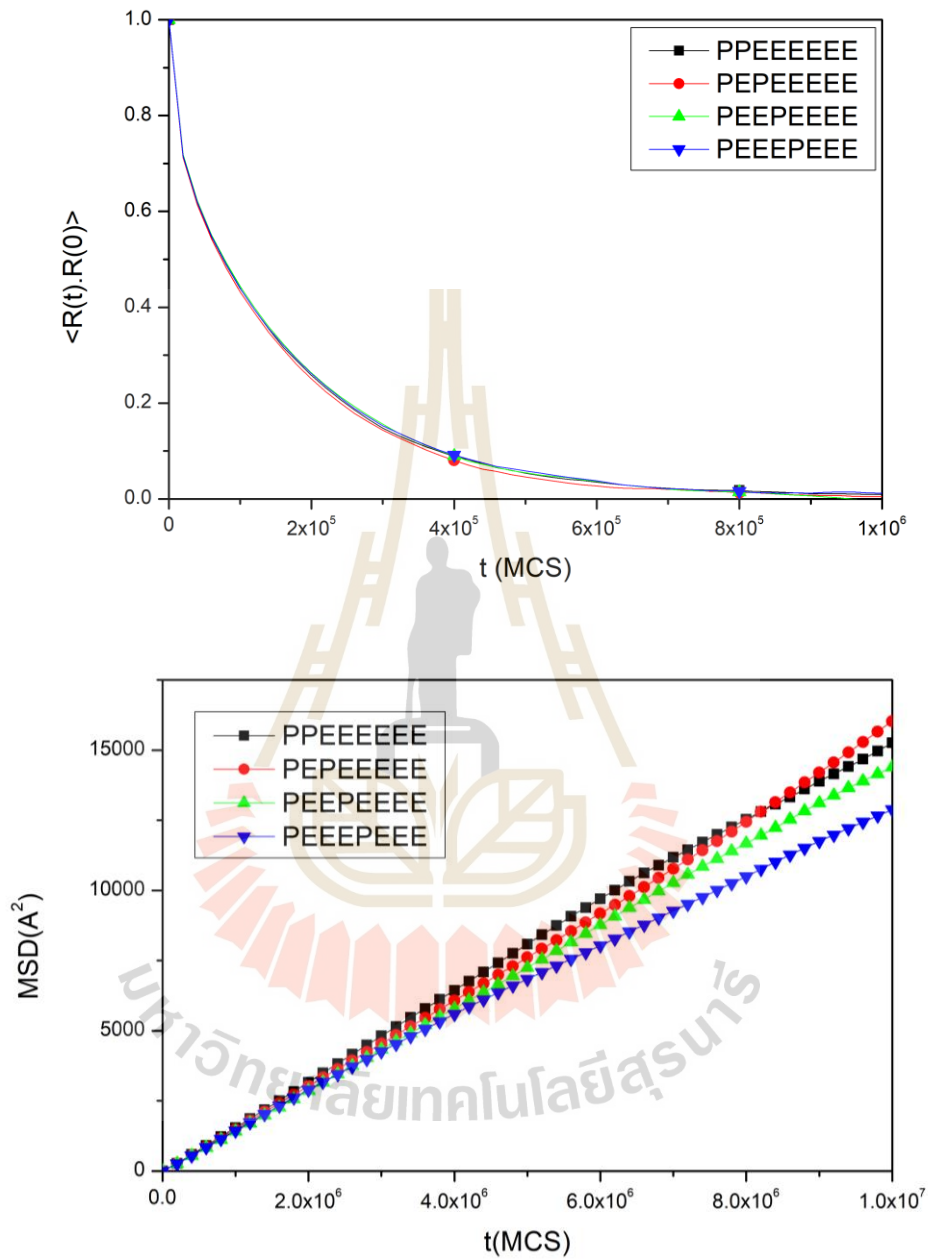
Figure 4.2.6 (a) Decay of the orientational autocorrelation function (OACF) for the end-to-end vector and **(b)** the mean-square displacement (MSD) for EPRC melts at P_E = 0.75, with different co-monomer sequences.
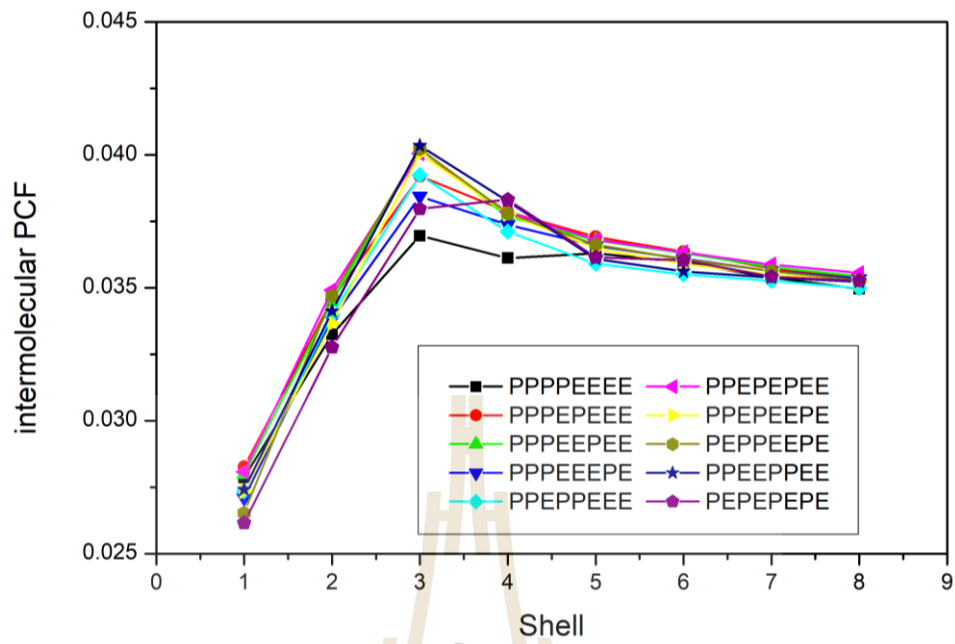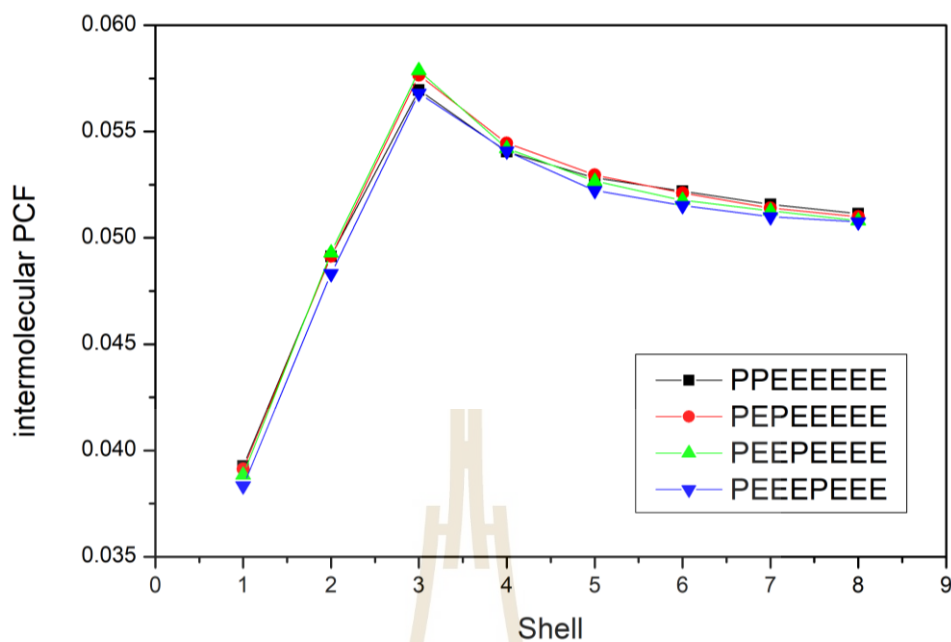
Figure 4.2.7 Intermolecular PCFs for EPRC melts at P_E = 0.75, with different co-monomer sequences.

Table 4.2.3 Repeating sequences, the mean square radius of gyration, $<R_g^2>^{1/2}$ $(\mathring{A})$, the characteristic ratio, $<r^2>_0/nl^2$, the relative intermolecular PCFs in the third shell, $g_{tatol}(3)$ and the relative diffusion coefficient, D of EPRC at P_E = 0.75 .

Sequence	$<R_g^2>^{1/2}$	C_n (RIS)	relative $g_{tatol}(3)$	relative D
PEPEEEEE	12.69	4.44	1.02	1.24
PPEEEEEE	12.80	4.52	1.00	1.21
PEEPEEEE	12.73	4.48	1.02	1.14
PEEEPEEE	12.71	4.45	1.00	1.00

4.2.3 Summary

Monte Carlo simulations of coarse-grained copolymer model were employed to investigate molecular and dynamic characteristics of EPRC melts. EPRC chains were consisted of the fixed fractions of ethylene monomers (P_E = 0.25, 0.50, and 0.75). The variation of comonomer sequences on EPRC can influence the conformational properties in term of molecular size and chain rigidity especially for low ethylene content but with some exception in few patterns. Simulation results imply that the intrachain interaction exhibited itself in the radius of gyration (chain dimension) and in the characteristic ratio (chain stiffness) and interchain interaction in term of the pair correlation function contributed to the dynamic properties of the copolymers differently depending on the P_E value and the specific monomer sequence. At low to intermediate (P_E = 0.25 and 0.5), EPRC chains exhibit higher mobility so long as the chains contain block-like structure. Copolymers with long consecutive monomers of the same type tend to have faster mobility than those with more randomly mixed comonomers. EPRC chains with low P_E have higher molecular packing efficiency for the patterns close to alternating sequence, resulting in slower mobility. At high P_E = 0.75, the chain dynamics are quite similar for all comonomer sequence due to large amount of ethylene beads. Nevertheless, the intramolecular interaction seems to play more crucial role than the intermolecular packing in determining the chain mobility especially for copolymer with long ethylene block sequence.

4.3 Crystallization characteristics of isotactic polypropylene with ethylene defects

In this section, the effect of few ethylene defects on crystallization characteristics of isotactic polypropylene is investigated by experimental techniques including differential scanning calorimeter (DSC) and synchrotron small angle x-ray scattering (SAXS).

4.3.1 Differential Scanning Calorimeter

For non-isothermal crystallization, the kinetics of this process can be evaluated from the thermogram of heat flow versus temperature. Figure 4.3.1 depicts the non-isothermal DSC thermograms of MH001, MH002, RPP02, RPP03, and RPP05 at six cooling rates from 5 to 30 °C/min. The crystallization onset temperature (T_i), and peak temperature (T_p) are listed in Table 4.3.1 With increasing the cooling rate, both T_i and T_p have a tendency shift to lower temperature. The lower cooling rate cause the crystallization to start earlier. The relative crystallinity, X(T) as a function of temperature can be obtained from the following equation:

$$X(\text{T}) = \frac{\int_{T_i}^{T} (dH/dT)\mathrm{dT}}{\int_{T_i}^{T\infty} (dH/dT)\mathrm{dT}} \qquad (4.3.1)$$

where dH is the enthalpy of crystallization within a miniature time interval dT, T_i and $T\infty$ are the onset and the end crystallization temperatures, respectively.
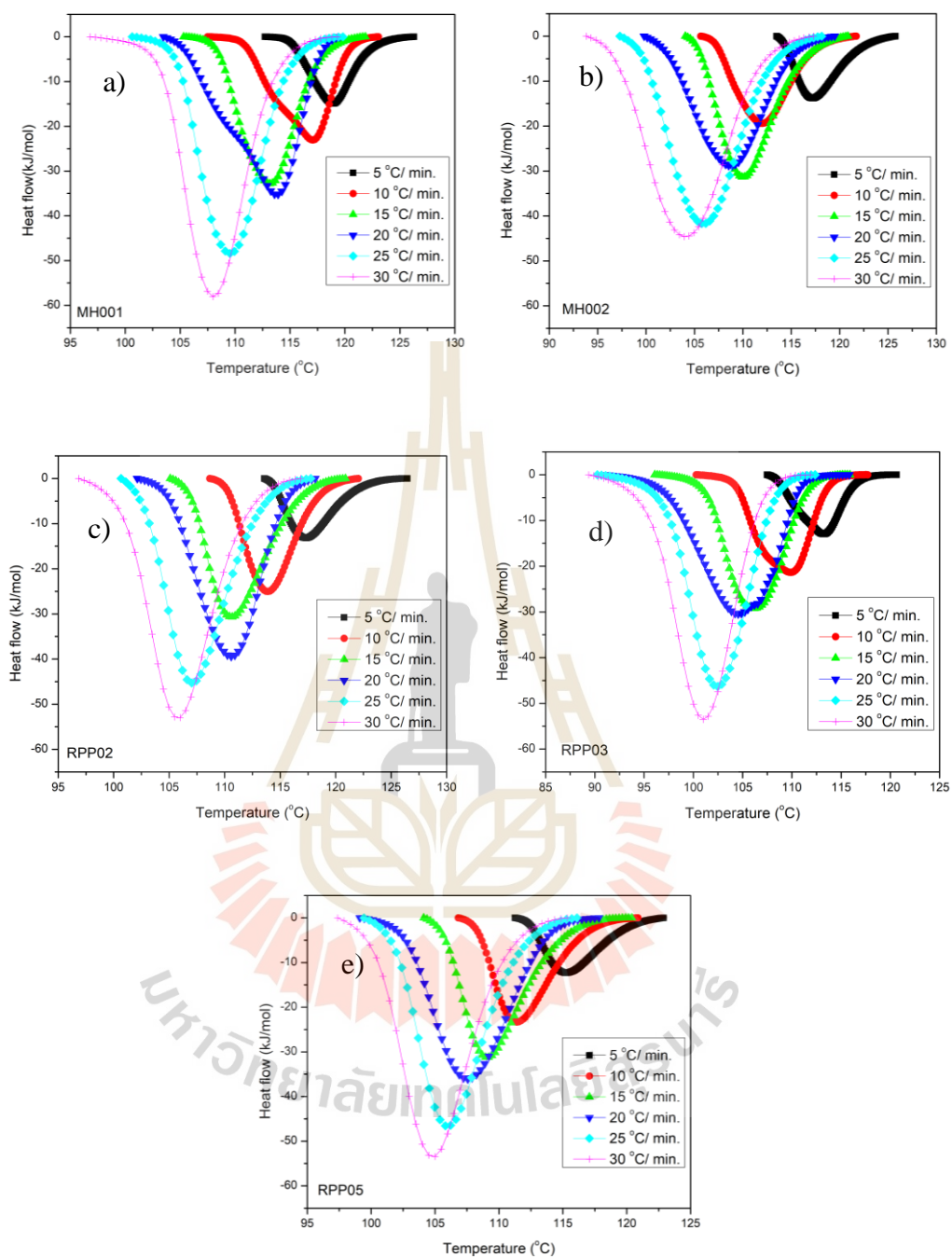
Figure 4.3.1 DSC thermograms of polypropylene sample with ethylene defect a) MH001, b) MH002, c) RPP02, d) RPP03 and e) RPP05 at various cooling rates.

The relative degree crystallinities at each cooling rates as a function of temperature can be determined by Eq. (4.3.1). Figure 4.3.2 shows the relationship between X(T) and temperature which all curves are sigmoidal. Obviously, the changes in percent of crystallinity for all polymers is depended on the cooling rate. As the temperature of sample gradually decreases, the crystallization rates are found to increase and indicate the presence of slow nucleation, fast primary crystallization and then slow secondary crystallization stages in different temperature ranges. The sigmoidal curves in Figure 4.3.2 presents the change in sample crystallinity with temperature. The changes of inflection points are significantly affected by different cooling rates. Higher cooling rate cause the shifting of crystallization region.
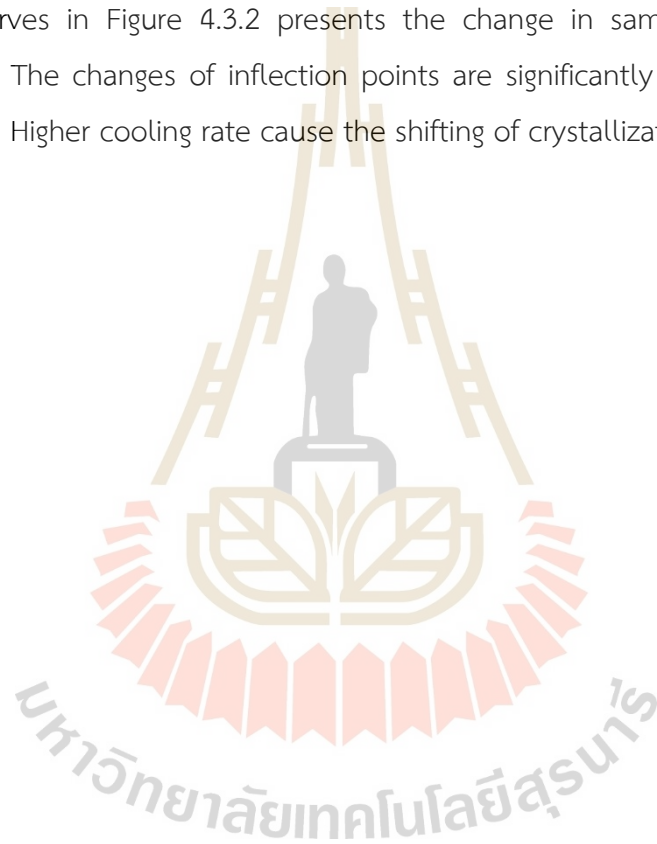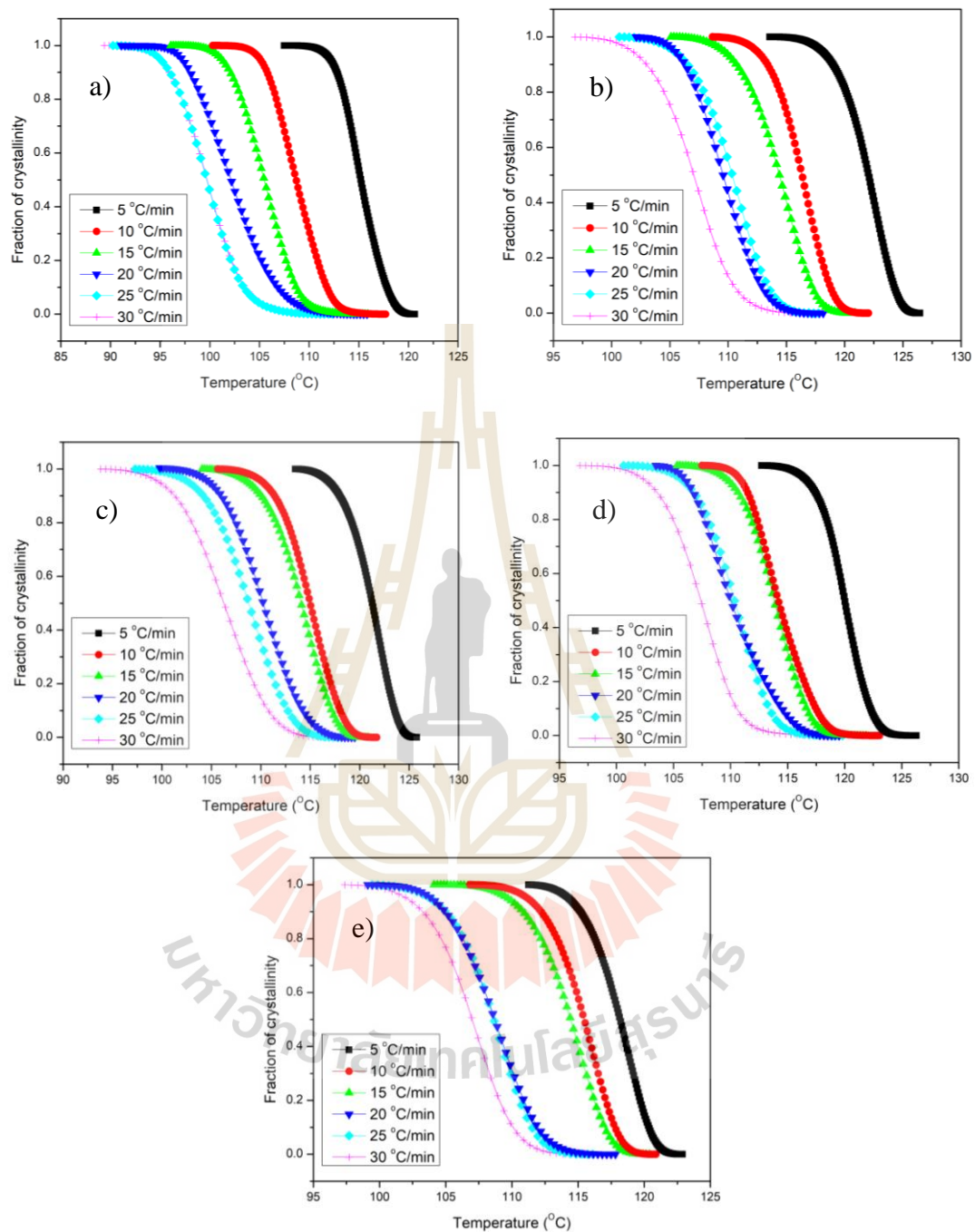
Figure 4.3.2 Relative crystallinity as a function of temperature of a) MH001, b) MH002, c) RPP02, d) RPP03 and e) RPP05 at various cooling rates.

For nonisothermal crystallization, the time and temperature have the relationship as:

$$t = \frac{|T_0 - T|}{\phi} \qquad (4.3.2)$$

where t is the crystallization time, T_0 is the temperature at which crystallization starts ($t = 0$), T is the crystallization temperature and ϕ is the cooling rate. Figure 4.3.3 presents the relative crystallinity $X(t)$ as a function of time (t). All these curves are sigmoidal shape. As the cooling rate increases, it takes less time to crystallize. The half-time ($t_{1/2}$) is defined to measure the overall rate of non-isothermal crystallization. As listed in Table 4.3.2, $t_{1/2}$ decreases with the increasing cooling rates.

Next, the Avrami, Ozawa and Mo models were employed to analyze quantitatively the kinetics of non-isothermal crystallization. The Avrami model was developed for the case of isothermal crystallization and need modification (Avrami, 1939; Avrami, 1940). The original Avrami model is in the form as:

$$1 - X(t) = \exp\left(-Zt^n\right) \qquad (4.3.3)$$

or

$$\log\left[-\ln\left(1 - X(t)\right)\right] = n\log t + \log Z \qquad (4.3.4)$$

where $X(t)$ is the relative degree of crystallinity at time t, n is the constant to specify the type of nucleation and the growth dimension and Z is non-isothermal crystallization rate constant. Although, the physical meanings of Z and n are not for the non-isothermal case in principle, it still can give good perception into the kinetics of non-isothermal crystallization.
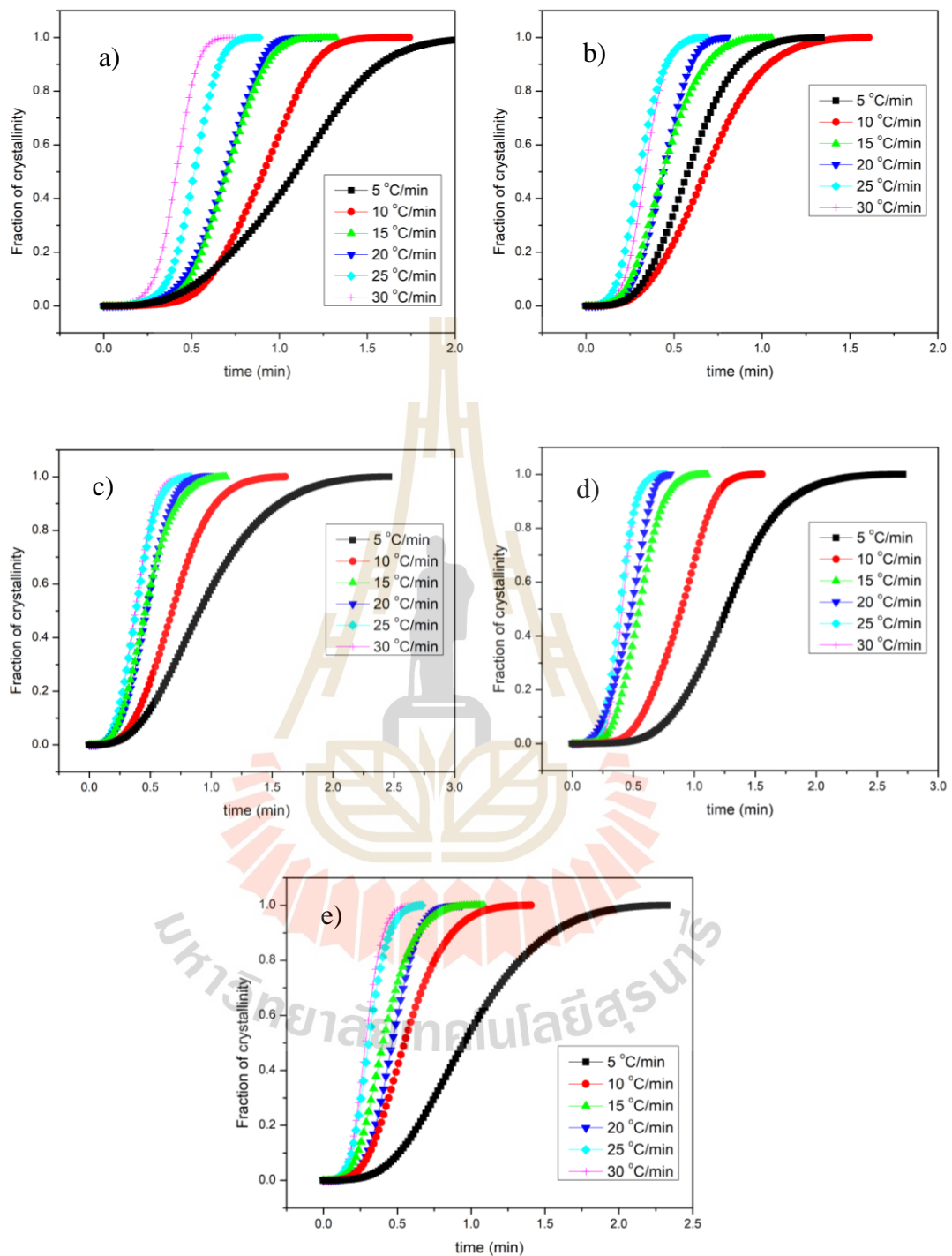
Figure 4.3.3 Fraction of crystallinity versus crystallization time of a) MH001, b) MH002, c) RPP02, d) RPP03 and e) RPP05 at various cooling rates.

Later, Avrami equation was modified by Jeziorny (in 1978) for the case of non-isothermal crystallization by

$$\log(Z_c) = \frac{\log Z}{\Phi} \qquad (4.3.5)$$

Where Z_c is the overall rate constant and Φ is the cooling rate. Based on this modification, the plot between log[-ln(1-X(t))] and log t is analyzed in Figure 4.3.4. The Avrami exponent (n), non-isothermal crystallization rate constant (Z) and the overall rate constant (Z_c) can be evaluated from the slope and intercept from Figure 4.3.4 and Eq. (4.3.5) as presented in Table 4.3.1. An increase of Z as a function of the cooling rate means that the crystallization become faster in the cooling experiment. Although the exponents (n) exhibit scattered data, n for RPP05 is still larger than other samples at the same cooling rate. Z_c for MH001 (iPP with no ethylene content) is the highest and decrease slightly for the sample with small ethylene content (RPP02: 0.16%) and then increase for RPP05 (ethylene content = 0.59%).
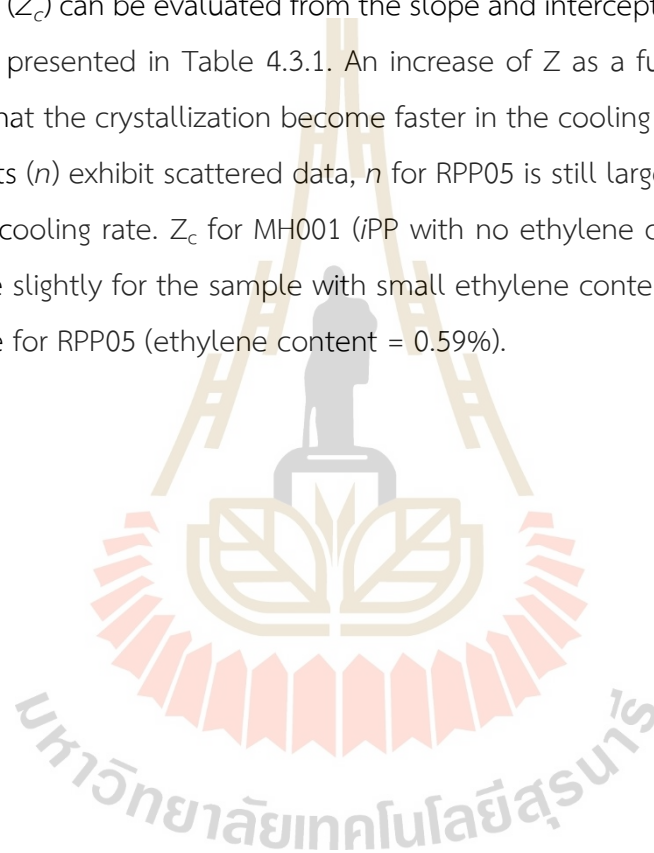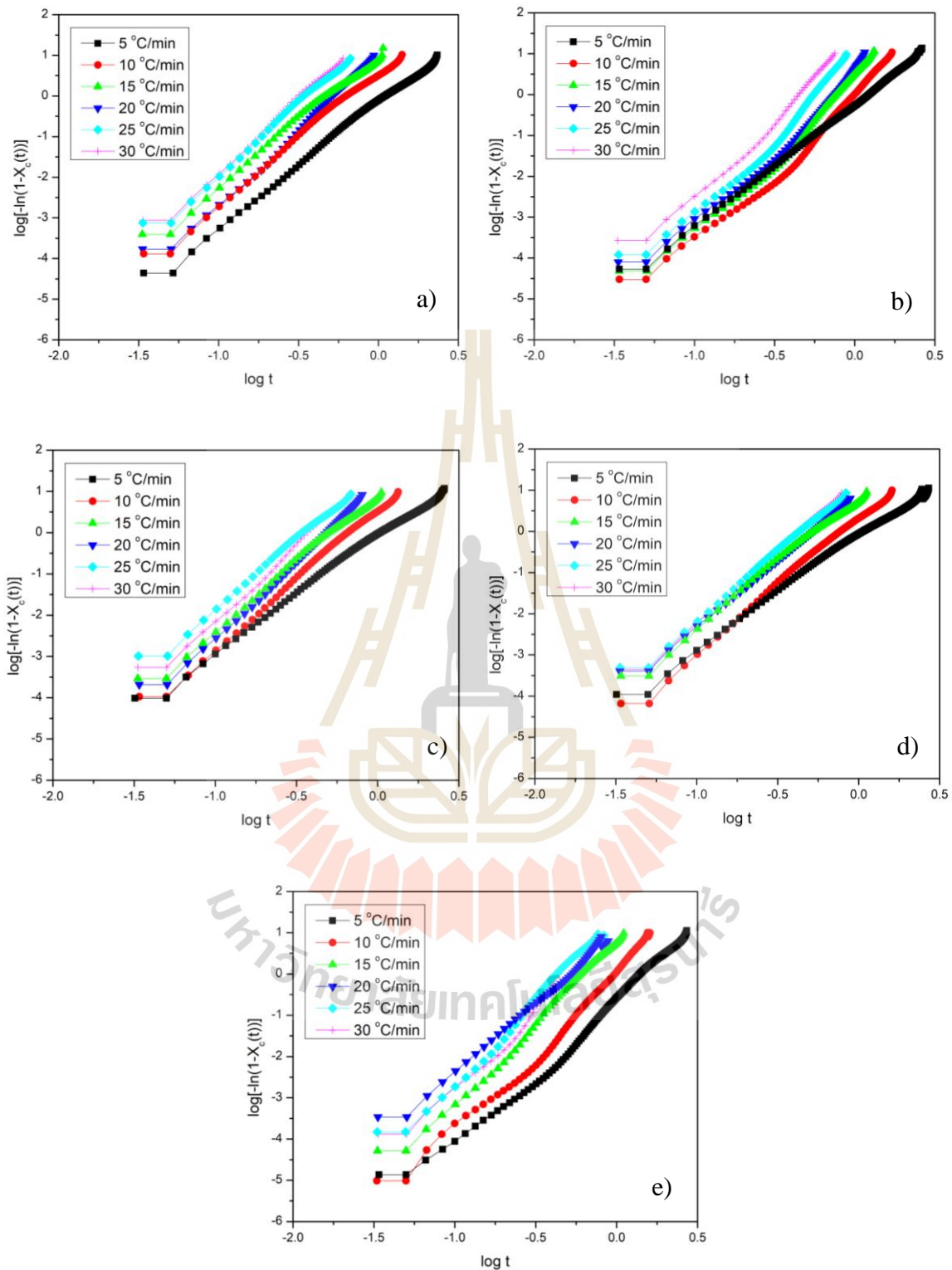
Figure 4.3.4 Avrami plots for the crystallization of a) MH001, b) MH002, c) RPP02, d) RPP03 and e) RPP05 samples at various cooling rates.

Table 4.3.1 Avrami parameters for non-isothermal crystallization of polymer samples.

Sample	Φ °C/min	T_p °C	T_i °C	$t_{1/2}$ min	Z_c	n
MH001 (PPE000)	5	118.58	122.32	1.28	1.79	2.77
	10	117.09	120.82	0.91	1.20	2.88
	15	112.92	117.84	0.56	0.95	3.50
	20	113.92	117.52	0.49	0.88	3.42
	25	109.44	114.32	0.39	0.92	3.53
	30	107.97	113.32	0.41	0.96	3.26
MH002 (PPE009)	5	117.44	122.32	0.91	0.98	2.92
	10	111.86	118.32	0.69	0.87	3.62
	15	110.17	116.31	0.46	0.83	3.54
	20	107.89	115.81	0.47	0.90	3.25
	25	105.43	113.48	0.39	0.88	3.56
	30	103.94	112.81	0.38	0.89	3.63
RPP02 (PPE016)	5	116.39	121.84	0.89	0.96	3.06
	10	114.08	118.34	0.58	0.86	3.49
	15	110.93	116.84	0.44	0.84	3.52
	20	110.58	115.34	0.44	0.89	3.55
	25	107.46	112.78	0.30	0.85	3.60
	30	105.48	111.87	0.34	0.90	3.51
RPP03 (PPE185)	5	113.46	116.36	1.09	1.10	3.04
	10	109.89	113.36	0.91	1.19	2.77
	15	106.53	110.86	0.71	1.05	3.00
	20	103.94	109.86	0.69	1.01	2.97
	25	102.48	108.36	0.52	0.98	3.12
	30	101.00	106.90	0.42	0.94	3.25
RPP05 (PPE059)	5	114.38	120.36	0.96	1.04	3.22
	10	110.20	116.86	0.56	0.83	3.52
	15	108.26	114.86	0.41	0.81	3.59
	20	107.44	113.86	0.47	0.92	3.39
	25	106.47	111.84	0.30	0.85	3.72
	30	105.00	111.67	0.29	0.86	3.77

Taking into account for the cooling rate on the non-isothermal crystallization, Ozawa (in 1971) modified the original Avrami model by assuming that the crystallization proceeds similar to at constant cooling rate and the new model is;

$$1 - X(T) = \exp\left(-\frac{P(T)}{\Phi^m}\right) \qquad (4.3.6)$$

$$\log\left[-ln\left(1 - X(T)\right)\right] = \log P(T) - m \log\Phi \qquad (4.3.7)$$

where $X(T)$ is the fraction of polymer crystallinity at temperature T, m is the Ozawa exponent, and $P(T)$ is the cooling function related to nucleation and crystal growth rates. Based on Ozawa model, the plots between log[-ln(1-X(T))] and log Φ at each temperature are presented in Figure 4.3.5 and the linear line should be obtained. The kinetic parameters m and $P(T)$ can be determined. Obviously, all the plots are not quite linear and the Ozawa model may be inadequate to explain the non-isothermal crystallization. Next, another suitable model should be used.
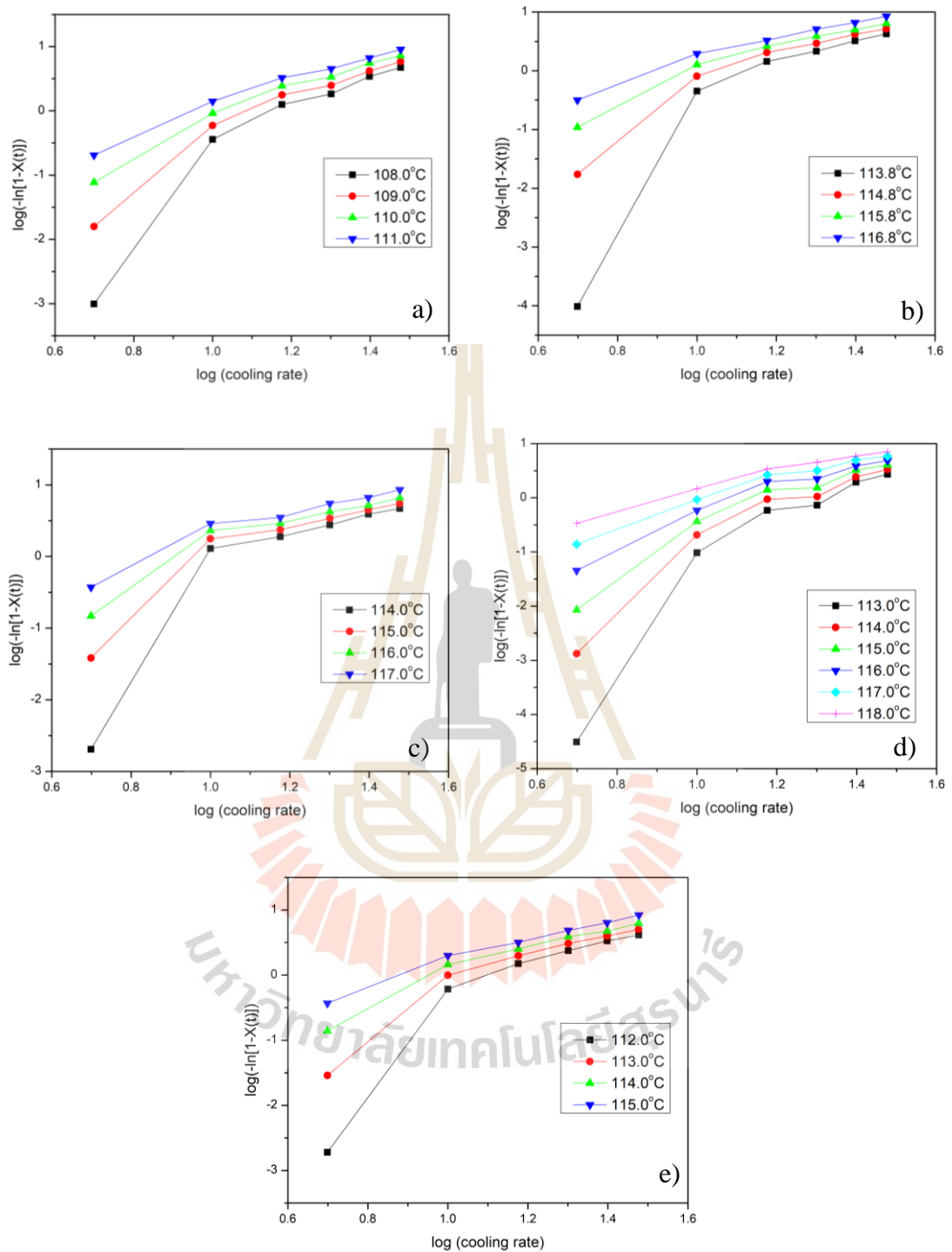
Figure 4.3.5 Ozawa plots for the crystallization of a) MH001, b) MH002, c) RPP02, d) RPP03 and e) RPP05 at various temperature.

Mo *et al.* (Liu, Mo, Wang, et al., 1997) tried to analyze the non-isothermal crystallization by the combination of Avrami with Ozawa model to:

$$\log \Phi = \log F(T) - a \log t \qquad (4.3.8)$$

Where $(T) = [P(T)/Z]^{1/m}$, $a = n/m$, (n and m are the Avrami and Ozawa exponents, respectively). $F(T)$ is the cooling rate at the selected crystallinity in the unit of crystallization time. A set of linear plots based on Eq. (3.8) at different crystallinities are presented in Figure 4.3.6, and the parameters a and log $F(T)$ can be retrieved from the slope and intercept.

As demonstrated in Figure 4.3.6, the plot between log Φ and log t gives a linear line at each degree of crystallinity, and the parameters a and $F(T)$ are listed in Table 4.3.2. $F(T)$ increase as a function of the relative crystallinity. The larger relative crystallinity, the faster the cooling rate is needed. From the magnitude of $F(T)$, the overall crystallization rate of MH001 (or PPE000) is the fastest, while the slowest one is MH002 (or PPE009). Nevertheless, there is no specific correlation between $F(T)$ and ethylene content. However, these data set is correlated well with the expanded Avrami equation.
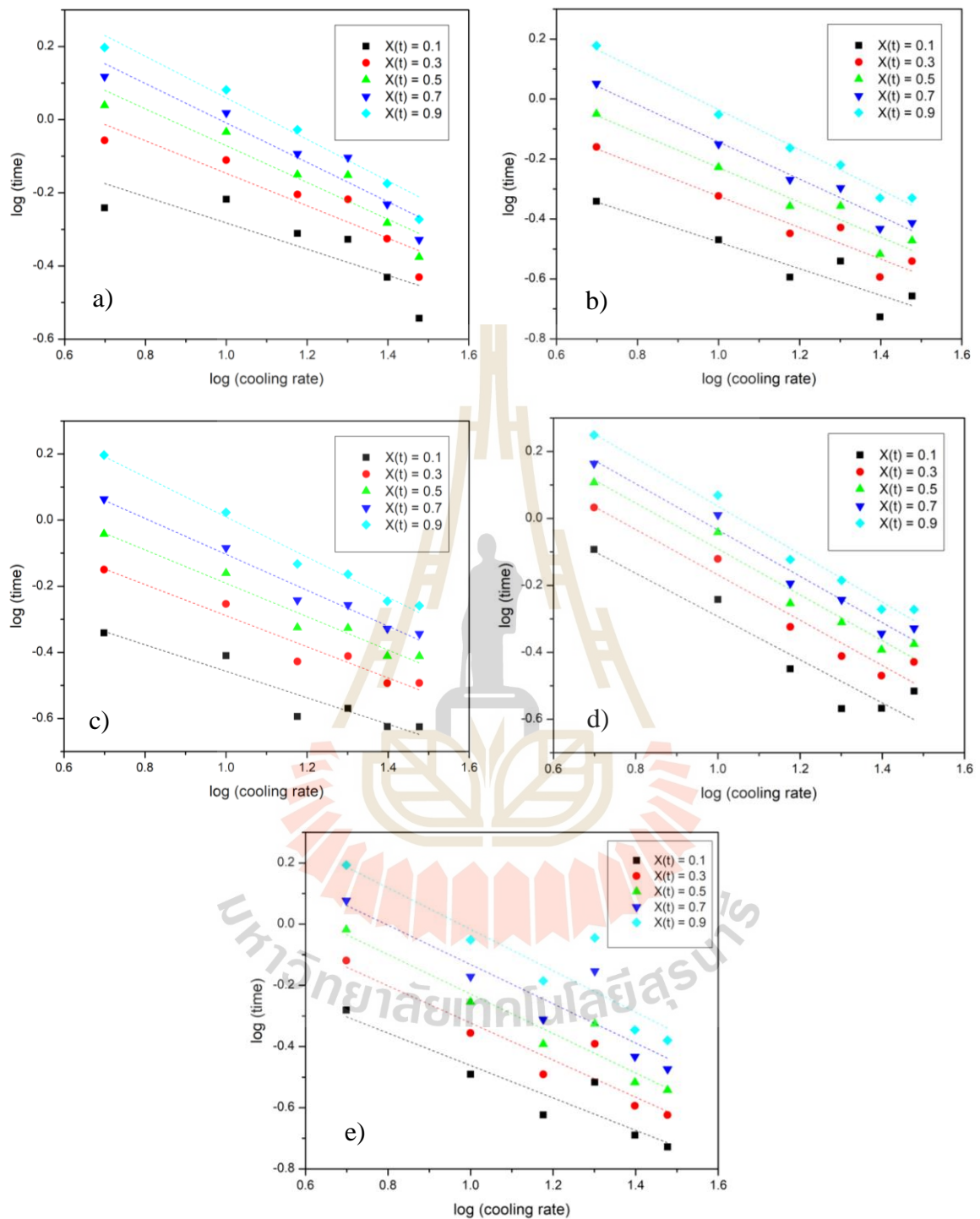
Figure 4.3.6 The combined Avrami and Ozawa plots for a) MH001, b) MH002, c) RPP02, d) RPP03 and e) RPP05 at selected crystallinity, $X_c(t)$.

Table 4.3.2 Non-isothermal crystallization kinetic parameters from the combined Ozawa and Avrami model for all samples.

Sample	X(t)	a	F(T)
MH001	0.1	0.65	2.26
(PPE000)	0.3	0.68	3.23
	0.5	0.69	3.93
	0.7	0.69	4.55
	0.9	0.72	5.68
MH002	0.1	0.40	0.88
(PPE009)	0.3	0.47	1.52
	0.5	0.51	2.06
	0.7	0.54	2.76
	0.9	0.61	4.14
RPP02	0.1	0.44	0.93
(PPE016)	0.3	0.52	1.59
	0.5	0.58	2.23
	0.7	0.62	3.00
	0.9	0.67	4.29
RPP03	0.1	0.36	1.19
(PPE185)	0.3	0.44	1.98
	0.5	0.50	2.70
	0.7	0.54	3.39
	0.9	0.57	4.24
RPP05	0.1	0.53	1.17
(PPE059)	0.3	0.61	1.92
	0.5	0.65	2.61
	0.7	0.64	3.24
	0.9	0.68	4.57

In overall, DSC results for non-isothermal condition show that the sample with ethylene defects crystallize slower than the neat *i*PP probably due to lower chain diffusion rate. These samples also have lower enthalpy of crystallization which may be related to better nucleation ability as the crystallization should be nucleation-dominated. Avrami analysis indicates that the crystal dimension for *i*PP-E sample is closed to 3D at the higher ethylene content. There is an increment in crystallization rate as a function of cooling rate. At any cooling rate, normal iPP crystallizes faster than *i*PP-E implying that the non-isothermal crystallization should be diffusion-dominated.

4.3.2 Synchrotron Small Angle X-ray Scattering

SAXIT software (Soontaranon and Rugmai, 2012) was used to reduce 2D-SAXS patterns to 1D-SAXS profile by circularly averaging these 2D patterns. Subsequently, the Lorentz corrected SAXS profile could be obtained from the beam intensity after correction with sample transmission and background scattering subtraction, then multiplying by q^2 (Vonk and Kortleve, 1967) where q is the scattering vector (Pilz *et al.*, 1979):

$$q = (4\pi/\lambda) \sin \theta \qquad (4.3.9)$$

λ is the X-ray wavelength and 2θ is the scattering angle defined by:

$$2\theta = \tan^{-1} (D/L) \qquad (4.3.10)$$

where D is the path length from the origin to the data point on the detector plane and L is the distance from sample to detector.

The semi-crystalline polymers can be analyzed in term of some properties, for instance, the crystalline volume fraction, the crystalline/amorphous electron densities difference, which is proportional to the total scattering intensity. SAXS profiles can be the fingerprint of lamellar structure in polymer. In this work, the SAXS patterns of *i*PP with and without small amount ethylene defect were recorded to study the role of monomer defect on the crystallization characteristics.

In this part, the paracrystalline model was used to determine the morphological parameters, such as the average long period (L) and the average lamellar thickness (L_c). Bragg's correlation length ($L_B = 2\pi/q_{max}$, where q_{max} is the scattering vector at the maximum intensity) can also be used to find the average long period (Xia *et al.*, 2001). This model assumes the long-range disorder of lattice affects the amorphous layer and crystalline component. Thus, both amorphous layer and crystalline phases are treated equally in the interpretation of paracrystalline structure (Crist, 1973) and this model can also give the average lamellar thickness obtained by the fitting the SAXS data with the equation (Vaĭnshteĭn, 1966).

$$I(q) = C * \left\{ \begin{array}{l} I_0 exp(-\sigma_{in}^2 q^2)\overline{|F(q,L)|^2}S(q) \\ +aq^{-x} + \frac{b}{1+q^2+\xi^2} + \frac{I_{0b}}{1+(|q-q_0|\xi_0)^m} \end{array} \right\} + k \qquad (4.3.11)$$

where C, I_0, a, b, x, and k are adjustable parameters. The SAXS peak and crystalline structure can be described by the first term while the exponential $exp(-\sigma^2 in q^2)$ is from the interface between crystalline and amorphous phase. The diffusive scattering is defined by the second term as the power-law model. The third term represents the scattering of random polymer chains by the Ornstein-Zernike function. The broad peak defined by the fourth term to describe the scattering of amorphous phase. The form factor of the averaged crystalline lamella can be expressed as:

$$\overline{|F(q,L)|^2} = \frac{1}{\sqrt{2\pi}\sigma_L} \int_{-\infty}^{\infty} |F(q,x)|^2 exp\left(-\frac{(x-L)^2}{2\sigma_L^2}\right) dy \qquad (4.3.12)$$

The form factor of crystal with lamella thickness L is:

$$F(q,L) = \frac{\sin\left(\frac{qL}{2}\right)}{\frac{qL}{2}} \qquad (4.3.13)$$

The structure factor, $S(q)$, is derived from the interference between the scattered X-ray of lamellae oriented in one dimension, which can be expressed by:

$$S(q) = \frac{1-|G(q)|^2}{1-2|G(q)|\cos(q\alpha)+|G(q)|^2} \qquad (4.3.14)$$

where **α** is the average long period. *G(q)* is the Fourier transform of the Gaussian distribution function of long period given by:

$$G(q) = F[H(y)] \qquad (4.3.15)$$

The original form before the Fourier Transform is:

$$H(y) = \frac{1}{\sqrt{2\pi\sigma_a}} exp\left(-\frac{(y-\alpha)^2}{2\sigma_\alpha^2}\right) \qquad (4.3.16)$$

where **σ** is the standard deviation of the distribution of long period.

In this analysis, SAXS data for the crystallization were recorded at 130 °C every 5 minutes for 1 hour of crystallization times for all samples (PPE000, PPE009, PPE016, PPE059, and PPE185 with the percentage of ethylene content per mol = 0.00%, 0.09%, 0.16%, 0.59% and 1.85% respectively).
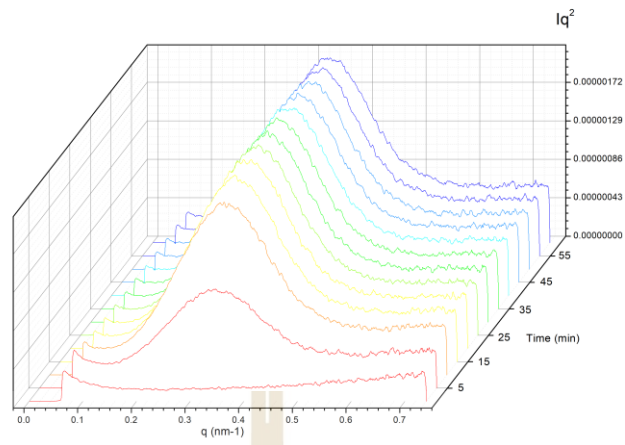
(a)
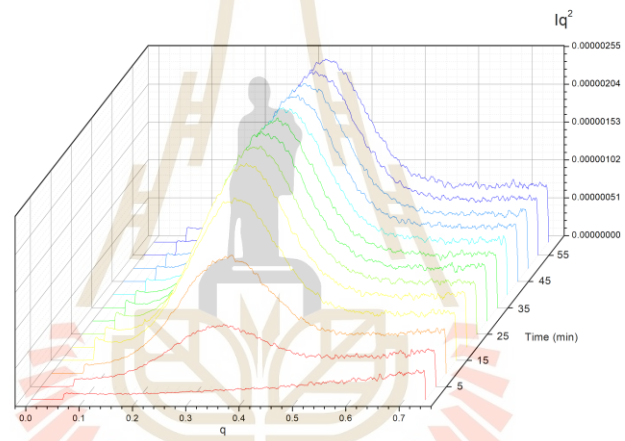
(b)
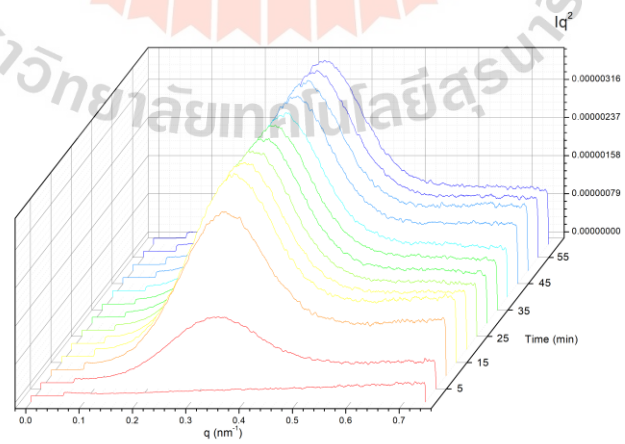
(c)

Figure 4.3.7 Evolution of SAXS profiles for isothermal crystallization at 130 ^{o}C of (a) PPE000, (b) PPE009, (c) PPE016, (d) PPE059, and (e) PPE185 samples
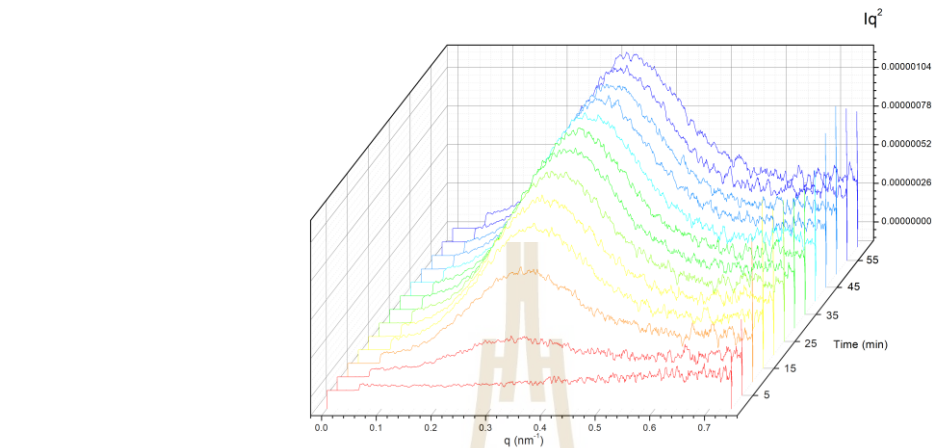
(d)
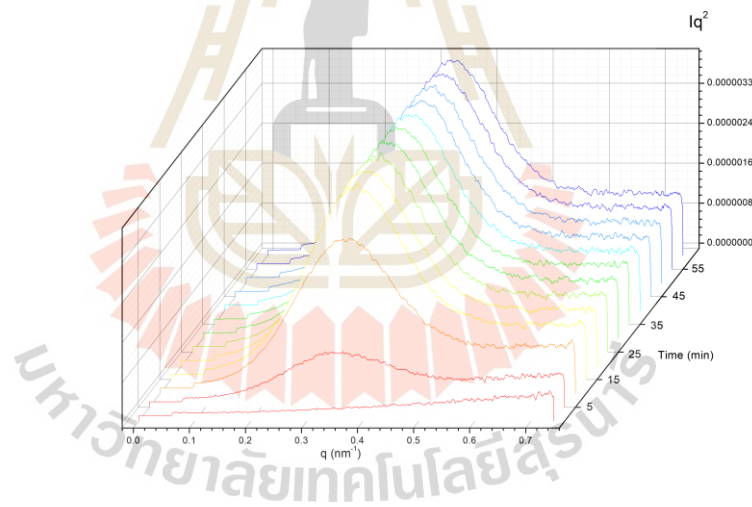
(e)

Figure 4.3.7 (Continued) (d) and (e)

It is noted that there was no observation peak for SAXS profiles in non-isothermal crystallization experiment for all polymer samples. The crystallization can be observed in the isothermal condition as seen from the difference of SAXS profile as a function of time. From Figure 4.3.7, fully crystallization can be confirmed after 20 minutes due to no significant change of the peak maxima.

The maximum intensities are plotted to monitor the progress of crystallization for all polymer samples for qualitatively comparison but not for quantitative comparison crystallinity due to the unequal amount of each sample in the specimen. The crystallizations had progressively growth from an initial stage and then reached the equilibration after 20 min. Data fluctuations can be seen due to the electron flux movement during the experiment. The maximum intensity for RPP03 sample (the highest amount of defect) tend to increase from 20 to 60 min. while the others are relatively constant. The amount of monomer defect was largely affected on the crystallization kinetics.
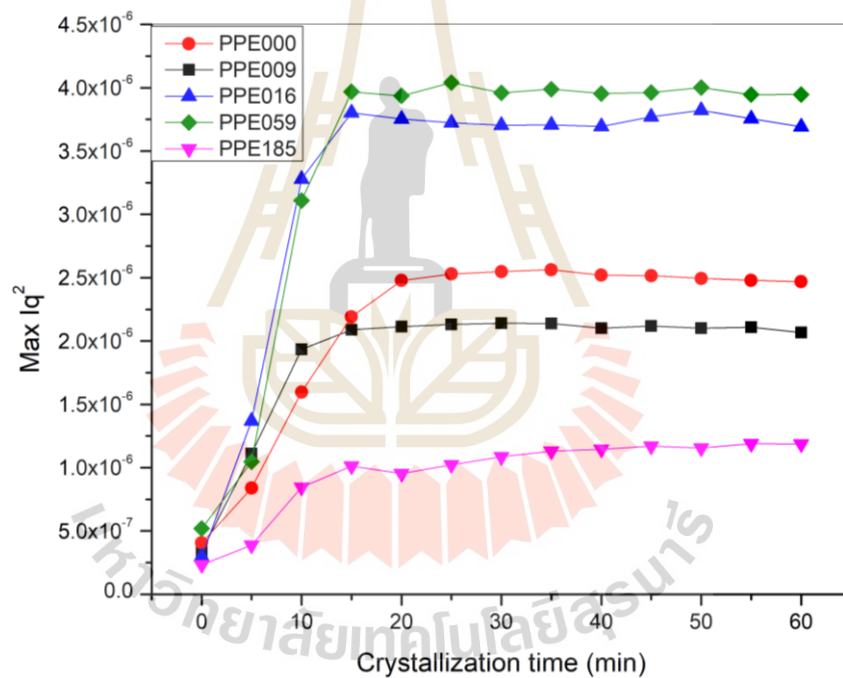
Figure 4.3.8 The evolution of maximum intensity (Iq^2) as a function of crystallization time.
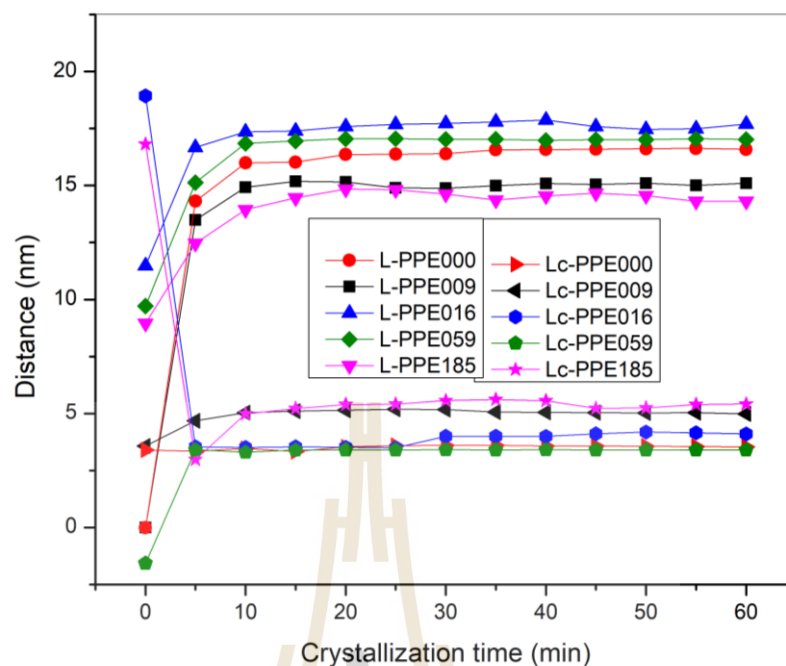
Figure 4.3.9 Evolution of the lamella thickness (L_C) and long-period parameter (L) as a function of crystallization time.

Results from the paracrystalline fitting give the lamella thickness (L_C), the size of crystal layer, and the long-period parameter (*L*), the length of amorphous plus and crystal region. Figure 4.3.10 shows that L_C of RPP03 (highest defect) is the highest (5.42 nm) accompanied with the lowest L (14.31 nm). For MH002 (*i*PP homopolymer) sample, L_c has the smallest (3.54 nm) with *L* = 16.59 nm. The lamella thickness (L_c) and long period parameter (L) for each sample become higher as a function of the crystallization time. The magnitude of L_c may be a very high due to the error from the undesired form of non-crystallized sample during the fitting step. In Figure 4.3.10 and 4.3.11 depict the relationship for the intensity maximum and the crystal structure parameters, respectively, with the percentage of ethylene defect.
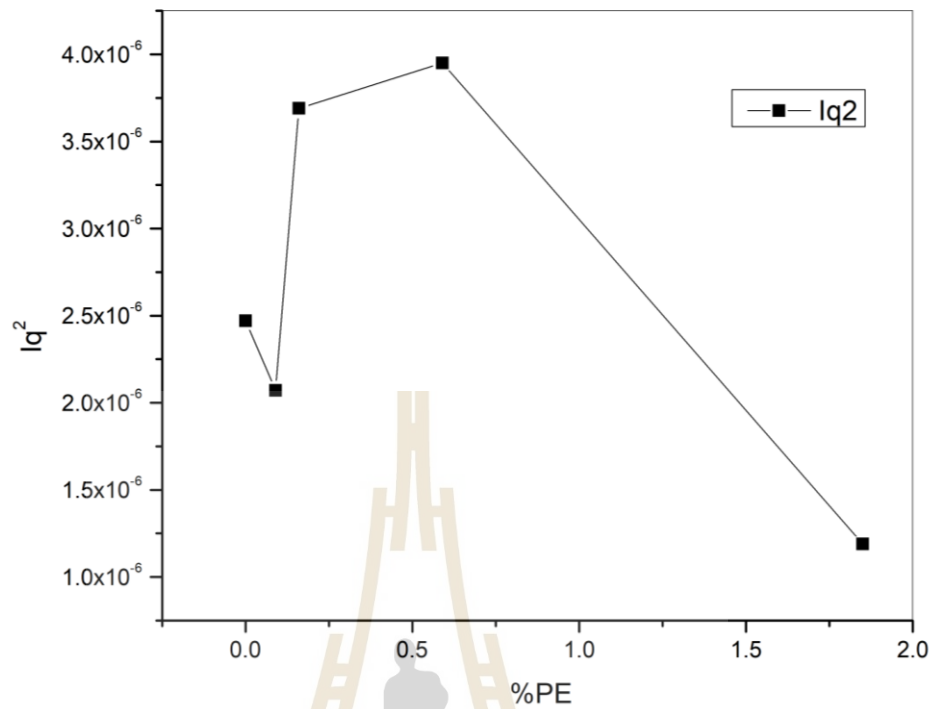
Figure 4.3.10 The change in Iq^2 with the percentage of ethylene defect.
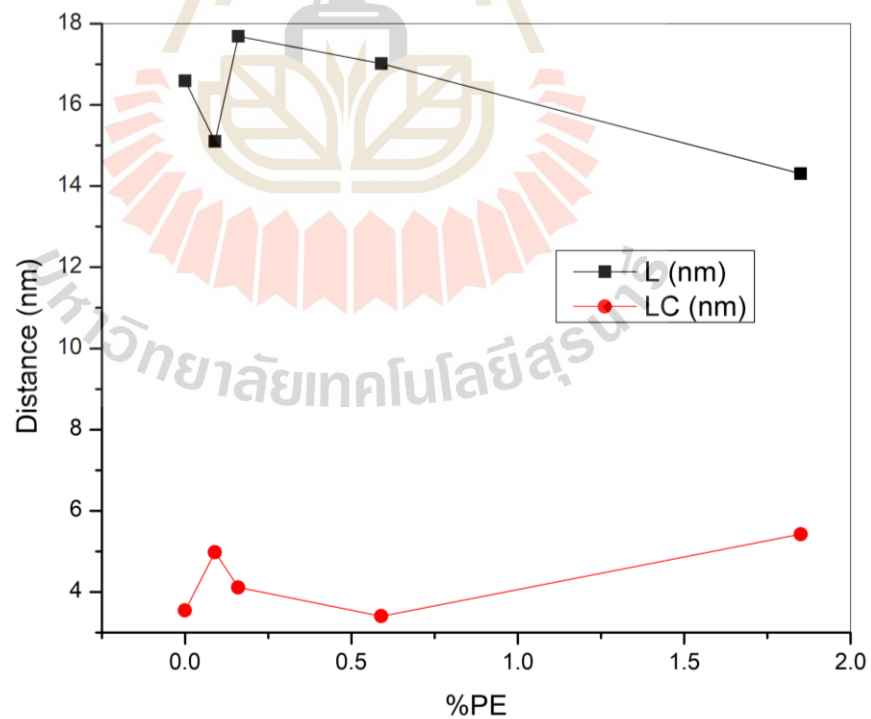
Figure 4.3.11 The lamella thickness (L_c) and long-period parameter (L) as a function of the percentage of ethylene defect from the fitting by paracrystalline model.

Table 4.3.3 Structural parameters of *i*PP at each ethylene defect as fitted by the paracrystalline model.

	%PE	L (nm)	L_C (nm)	Iq^2
MH001	0.09	15.10	4.98	2.07E-06
MH002	0.00	16.59	3.54	2.47E-06
RPP02	0.16	17.69	4.11	3.69E-06
RPP03	1.85	14.31	5.42	1.19E-06
RPP05	0.59	17.02	3.40	3.95E-06

From Figure 4.3.10 and 4.3.11, results show that Iq^2 and the crystal structure parameters from fit by paracrystalline model are not correlated well with the amount of ethylene defect. It is noted that the method to use 1-D electron density correlation function should be better to obtain structural information of these polymer samples as depicted in Figure 4.3.12.

The proposed diagram to describe structural evolution during isothermal crystallization is presented in Figure 4.3.10 to guide SAXS analysis. Polymer chains are needed to stay close to each other before crystallization and X-ray scattering signals are from electron density fluctuations which is related to the spinodal decomposition *i.e.* high density regions initiate nucleation (Crist, 1973; Terrill et al.,1998; Heeley et al.,2003).

Imai et al. (in 1992) proposed the mechanism that these dense regions are from parallel interactions of polymer segments with the lengths must surpassed the critical value (persistence length), about 2.38 nm for iPP as estimated by Zhuetal (Zhu, Yan and Fang 2001). As time progresses, chains can be folded and assemble the stacked lamellae growing in the radial direction to form the spherical structure at sub-micron scale (Imai and Kaji, 2006) which can be detected by SAXS.
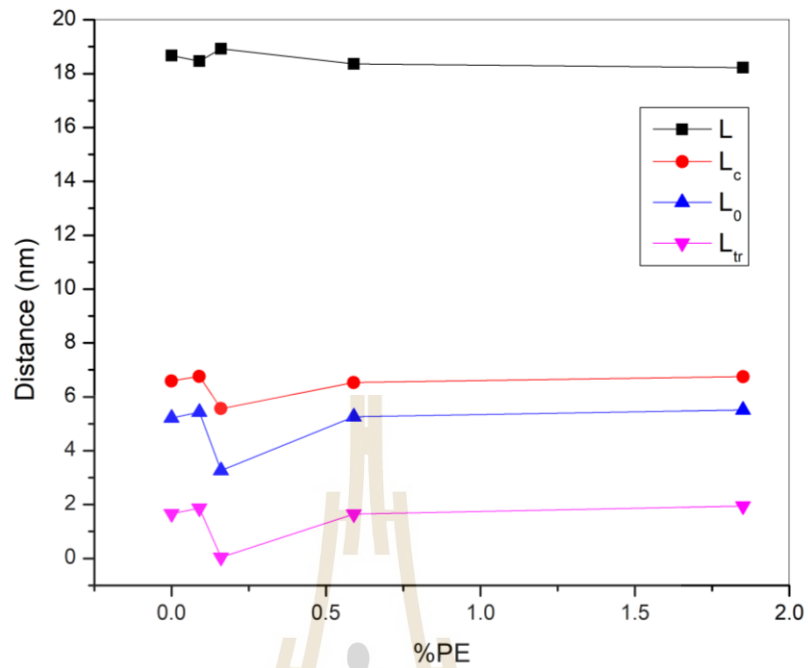
Figure 4.3.12 Lamella thickness (L_c), lamellar core thickness (L_0), interface thickness (L_{tr}), and long-period parameter (L) as a function of the percentage of ethylene defect from 1D-electron correlation function.
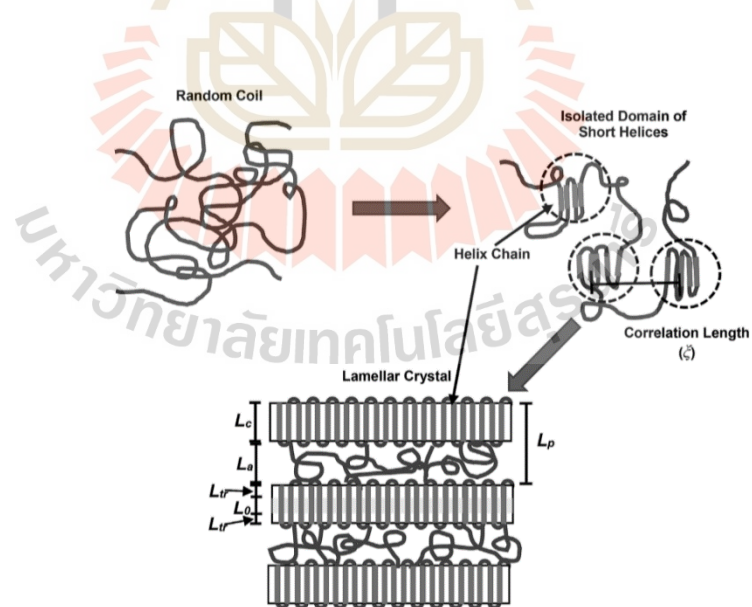
Figure 4.3.13 Schematic illustrating structure evolution of iPP under isothermal treatment (Imai et al., 1992).

The morphological parameters, such as the long period (L_p) and the average lamellar thickness (L_c) can be better determined using the 1D-electron density correlation function, $K_{(z)}$. Note that the long period can also be calculated from the first maximum at the lowest scattering angle by employing Bragg's law in the SAXS profiles as given by:

$$L_B = \frac{2\pi}{q_{max}} \tag{4.3.17}$$

where q_{max} is scattering vector at maximum intensity. This method assumed that the long-range disorder of the lattice affects the amorphous layer and crystalline component's size fluctuations. Therefore, each phase is treated equally to define the paracrystalline macrolattice [30]. The structural parameters of stacked lamellae can be determined using the 1D-electron density correlation function, $K_{(z)}$. The two-phase model composed of the alternatively stacked crystalline and amorphous layers is presumed. $K_{(z)}$ can be expressed by (Strobl and Schneider, 1980).

$$K_{(z)} = \left\langle \left[\eta_{(z')} - \langle \eta \rangle \right] \left[\eta_{(z+z')} - \langle \eta \rangle \right] \right\rangle = 2 \int_0^\infty \pi^{-1} q^2 I_{(q)} \cos(qz) \, dq \tag{4.3.18}$$

where $\langle \, \rangle$ is the ensemble average, $\eta(z)$ and $\langle \eta \rangle$ are the electron densities along the normal direction of lamella and the averaged electron density, respectively (Rungswang et al., 2015 and Rungswang et al., 2017).

The correlation function was calculated from Eq. (4.3.18) and the model is presented in Figure 4.3.13. Multiple points on the $K_{(z)}$ curve can give several structural parameters including the average lamellar thickness (L_c), the long period (L_p), the average interface thickness (D_{tr}) and the average core thickness (D_0). In addition, the amorphous-layer thickness (L_a) can also be determined as $L_a = L_p - L_c$. All these parameters derived from $K_{(z)}$ for all samples 5 at 130°C are displayed in Table 4.3.4.

The parameters derived from 1-D electron density correlation function presented in Figure 4.3.14 and Table 4.3.4 give similar trends of L and L_C compared with the paracrystalline model. L and L_C values from this technique are less difference. Nevertheless, L and L_C are not directly correlated to the amount of PE defect. For

example, RPP02 (0.16% of ethylene defect) has the shortest L_C but the longest L even if this sample has the least defect content.
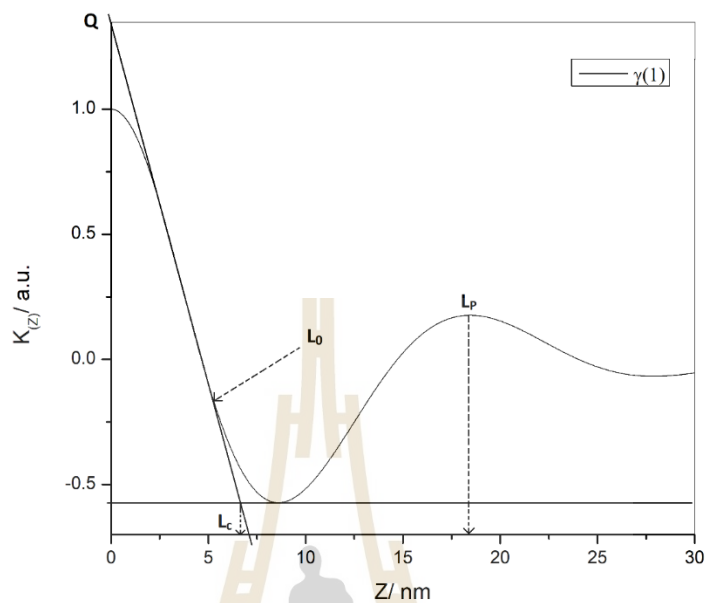
Figure 4.3.14 The method of 1-D electron density correlation function to determine lamellar parameters.

Table 4.3.4 Parameters of semi-crystalline structure *i*PP samples with ethylene defect from the method of 1-D electron density correlation.

	%PE	L	L_C	L_0	L_{tr}
PPE009	0.09	18.46	6.76	5.43	1.87
PPE000	0.00	18.67	6.59	5.22	1.66
PPE016	0.16	18.93	5.56	3.27	0.04
PPE185	1.85	18.23	6.75	5.51	1.95
PPE059	0.59	18.36	6.53	5.26	1.65

4.3.4 Summary

Crystallization of *isotactic* polypropylene with a small amount of ethylene defects was investigated by differential scanning calorimetry (DSC) and synchrotron small angle X-ray scattering (SAXS). The crystallization is slowed down for *i*PP with ethylene defects. Isothermal crystallization kinetics of these samples was fit by Avrami analysis and the results suggest that the dimension crystal growth (n) and the crystallization rate (k) tend to increase for *i*PP with ethylene defects. For SAXS analysis, both paracrystalline model and electron density correlation function were used to estimate the long period (D) and the lamellar thickness (L). The D is increased for *i*PP with ethylene defects such that there were higher amorphous (La) and L, but lower L/D ratio than L-*i*PP. the degree of crystallinity is lower for for *i*PP with defects, this result agrees with DSC and SAXS.

4.4 Molecular simulation of the crystallization of linear and cyclic polymers

In recent years, cyclic polymers can be prepared and are interesting materials with new properties. Understanding the physics of crystallization of cyclic in comparison to linear polymer should be significant for polymer science. In this part, molecular simulation is employed to investigate the effect of polymer chain topology on structural formation of cyclic and linear polyethylene models upon cooling from the melt to crystallization temperature.

4.4.1 Polymer model

Low molecular polyethylene (PE) model was coarse-grained to keep only every second carbon in the backbone and mapped onto the *2nnd* lattice . Polymer systems were composed of 46 linear $C_{40}H_{82}$ or cyclic $C_{40}H_{40}$ chains (equivalent to 20 beads) placed randomly in the 2nnd box of 18x18x18 dimension .The distance from beads *i*

to $i+1$ = 0.25 nm .The intrachain interactions was handled by the Rotational Isomeric State (RIS) model of PE. The 9x9 statistical weight matrix was condensed to 3x3 dimension which includes three new parameters, *a*, *b* and *c*, in addition to σ and ω as:

$$\mathbf{U_{PE}} = \begin{bmatrix} 1 & \sigma & \sigma \\ 1 & \sigma & \sigma\omega \\ 1 & \sigma\omega & \sigma \end{bmatrix} \rightarrow \mathbf{U_{2nnd}} = \begin{bmatrix} 1 & 4\sigma & 2\sigma\sigma(1+\omega) \\ 1 & 4a & 2b\sigma(1+\omega) \\ 1 & 4b & 2c(1+\omega) \end{bmatrix} \qquad (4.4.1)$$

where $\sigma = \sigma_0 \exp(-E_\sigma/kT)$, $\omega = \omega_0 \exp(-E_\omega/kT)$ and $a = \sigma\omega^{1/8}$, $b = \sigma\omega^{1/4}$ and $c = \sigma^2\omega^{1/2}$.

Interchain interactions were represented by Lennard-Jones (LJ) potential in the lattice form. The interaction parameter u_i at the ith shell can be obtained as:

$$\exp\left(-\frac{u_i}{k_B T}\right) - 1 \equiv \bar{f}_i \qquad (4.4.2)$$

The LJ parameters for PE are ε/k_B = 185 K and σ = 4.4 Å. Only the first three shell parameters were applied to increase the speed of simulation.

4.4.2 Simulation

A single bead moves were allowed for each PE bead on *2nnd* lattice as the self-avoiding random walk. Each bead was chosen randomly to move to the empty position and accepted according to the Metropolis criteria.

$$P_{move} = \min[1, P_{LR}P_{new}/P_{old}] \qquad (4.4.3)$$

where P_{LR} is the Boltzmann weights from long-range interaction for each move and P_{new}/P_{old} is the probability ratio for moving bead to a new site. Monte Carlo step (MCS) was defined when all the beads are moved once by average. Data analysis was obtained by an ensemble average of the 80 million MCS after equilibration at 298 K. Data was recorded every 10,000 MCS during this period for subsequent analysis.

4.4.3 Results and discussion

4.4.3.1 Equilibration

Simulation was performed by stepwise cooling from the molten state at 473 K and equilibrated at each step for 10 million MCS (473 → 400 → 350 → 298 K). Then, the crystallization was monitored at 298 K for 80 million MCS equilibration for crystallization. Figure 4.4.1 presents the results for intra-, inter-chain and total energies for linear and cyclic PE systems during the crystallization at 298 K. System energetics was a conventional way to validate thermodynamic equilibration. The energy change became stable after 20 million MCS, for both systems. The intramolecular energy for cyclic system is higher than that of the linear system because of more amount of high energy (*gauche*) conformation whereas the intermolecular energy for linear system is lower due to better chain packing that pull more beads to the shells with attractive interaction. In overall, cyclic systems have higher total energies implying that the intrachain energy is dominated. Nevertheless, the equilibration as determined by energetics alone may be not enough. For the purpose of validate the equilibrium, chain properties including the relaxation of the end-to-end vector (mid-to-end vector for cyclic chain) and the mean square displacement for the center of mass were evaluated.
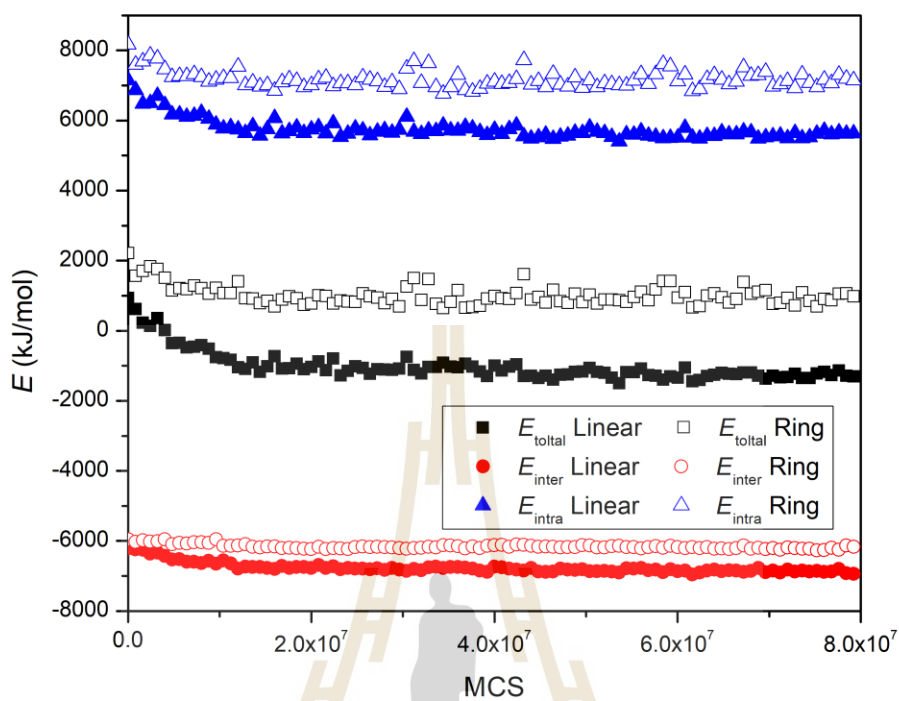
Figure 4.4.1 Total (E_{total}), intermolecular (E_{inter}), and intramolecular energy (E_{intra}) of the linear and ring polymers as a function of MCS at 298K.

The orientational auto-correlation function (OACF) and the mean-squared displacement (MSD) were determined to evaluate the equilibration in term of rotational and translational relaxation of polymers. The OACF can be formulated both from the head-to-mid vector *i.e.* the vector connecting the head bead to middle bead, $<\mathbf{M}(t).\mathbf{M}(0)>/(\mathbf{M}^2)$ and the bond vector, $<\mathbf{m}(t).\mathbf{m}(0)>/<\mathbf{m}^2>$. The MSD of the chain center of the mass, g_{cm} can be defined as

$$g_{cm}(t) =< [r_{cm}(t) - r_{cm}(0)]^2 >$$

(4.4.1)

Here, $r_{cm}(t)$ and $r_{cm}(0)$ are the coordinates of the chain center of the mass at time *t* and *0*, respectively. The angle bracket means ensemble average.

The OACF of the end-to-end and mid-to-end vectors were used for linear and cyclic chains, respectively, to justify the system relaxation. It is seen that cyclic chains are relaxed readily whereas it is hard to justify for the linear chains. Nevertheless, bond relaxation for both linear and cyclic systems can be decayed to the value less than 1/e which is justified for the equilibration at least at the bond level. The MSD of the center of mass also exhibit that both chains can diffuse to the distance larger than its molecular dimension i.e. radius of gyration (R_g) to confirm the equilibration. In general, the MSD of linear chains is significantly higher than that of ring polymer.
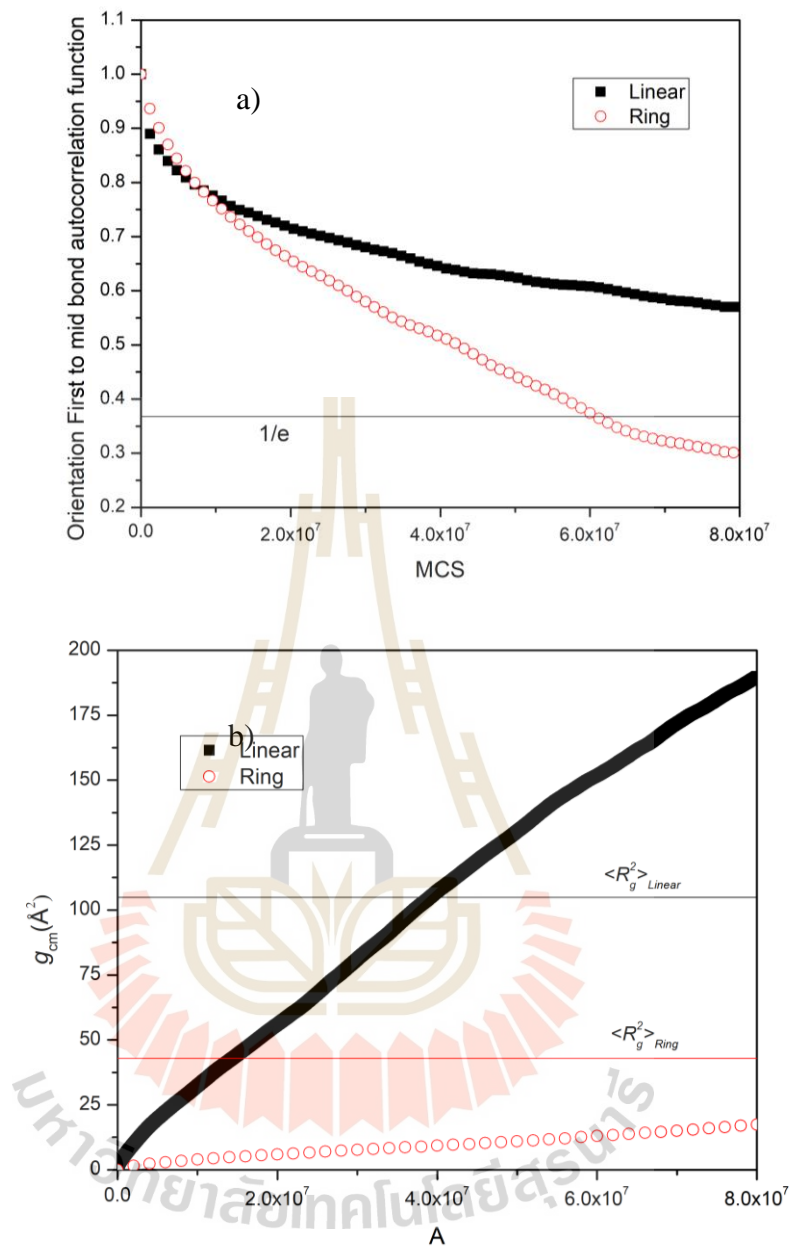
Figure 4.4.2 (a) OCAF and (b) MSD of linear and cyclic PE as function of MCS at 298 K. The horizontal dashed line in MSD is the mean square radius of gyration of polymer chains.

Figure 4.4.3 illustrates the final snapshots of the ordered structures of coarse-grained model of linear and ring PE at 298 K. Apparently, the linear PE is similar to crystal structure with one domain whereas the cyclic system is composed of multiple ordered domains.
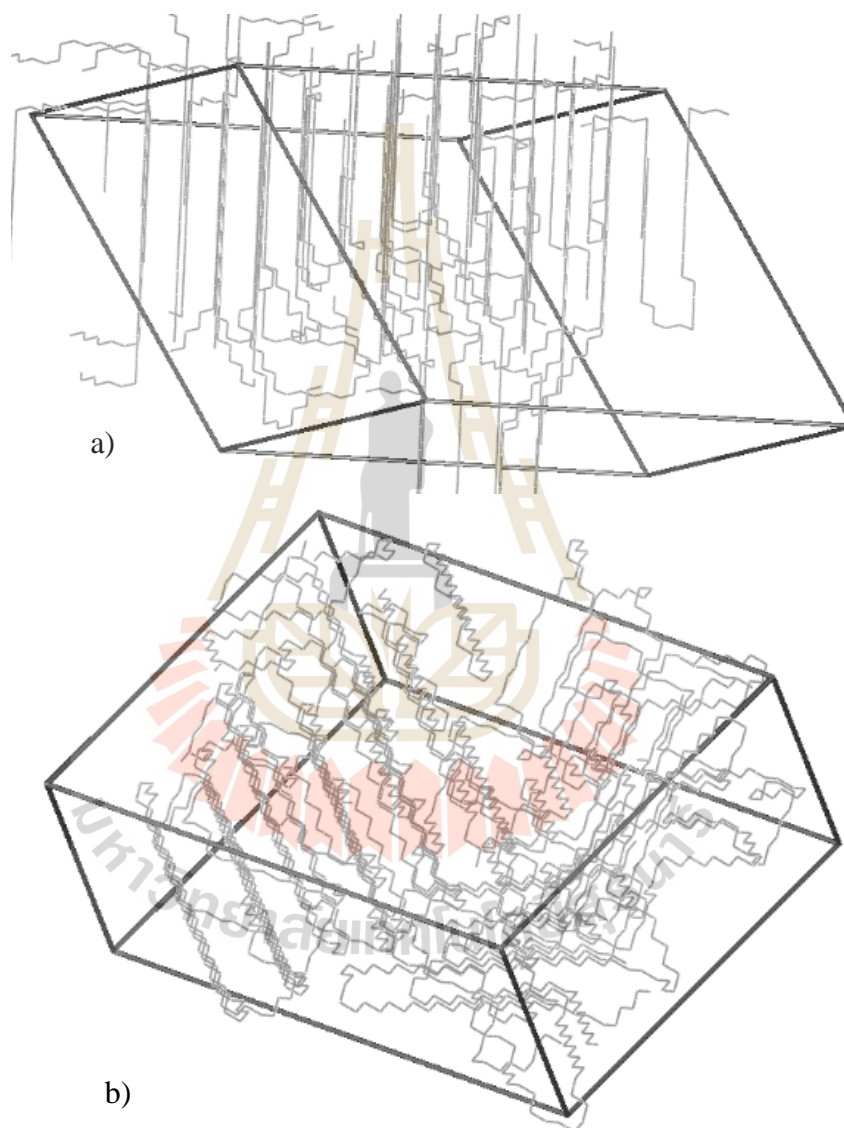
Figure 4.4.3 The final structure of (a) linear and (b) ring PE after 8×10^7 MCS at 298 K.

4.4.3.2 Chain conformation

The structure formation process at the local scale can be examined by the looking at the conformational change. In Figure 4.4.4, the time dependence of the fraction of *trans* state at each temperature at 473, 400, 350 and 298 K is presented. The *trans* fraction is relatively small at the beginning compared to the intermediate step where it increases dramatically. In general, the fraction of *trans* should reach 1.0 for the fully crystallization *i.e.* all polymer chains are completely elongated. For these simulation results, the fraction of *trans* reach the constant value about 0.8 indicating that polymer chains still have some *gauche* states. Interestingly, the fraction of *trans* is increased even in the period that the global orientational order does not occurred (see also at Figure 4.4.6(b)). These findings imply that polymer chains have to stretch first and the orientation can take place afterward during the crystallization process.

To compare the crystallization between linear and cyclic PE chains at the molecular level, Figure 4.4.4 depicts the evolution of *trans* fraction at 298 K. After 20 million MCS, the fraction of *trans* states reach 0.8354 ± 0.0079 and 0.7047 ± 0.0063 for linear and cyclic chains, respectively. As expected, the *trans* fraction of linear chains is higher. These results imply that linear chains should be able to form crystal structure better than the cyclic polymer. As seen in Figure 4.4.3b, the crystallization for cyclic chains is possible with the ordered structures containing multiple domains.
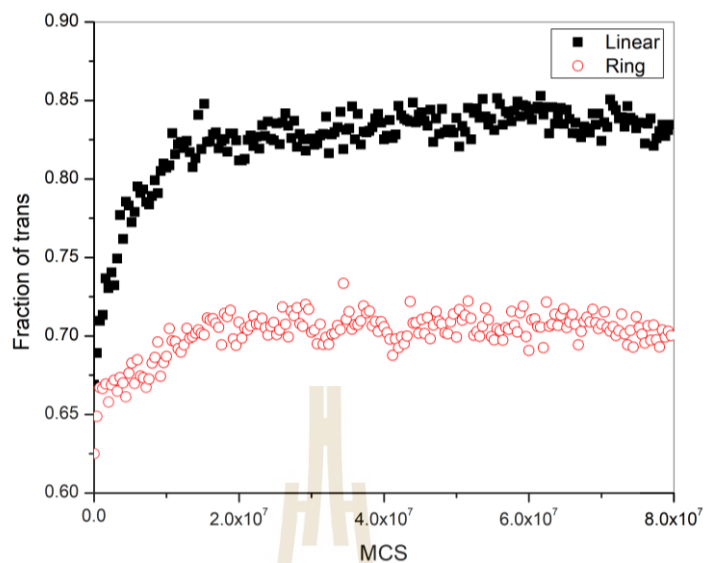
Figure 4.4.4 Evolution of *trans* fraction as a function of MCS for linear and cyclic PE chain at 298 K.

4.4.3.3 Overall chain conformation

The overall chain conformation can be described by the mean square radius of gyration for linear and ring chains denoted by $<R^2_{g,L}>$ and $<R^2_{g,R}>$, respectively to represent the overall expansion and distortion of chains. As shown in Figure 4.4.5, both $<R^2_{g,L}>$ and $<R^2_{g,R}>$ increase with simulation time and reach constant values at later time. In addition, the $<R^2_{g,L}>/<R^2_{g,R}>$ ratio at 473 K is around 2.1 $\pm$ 0.1 which is closed to 2.0 from theoretical prediction for polymer melt at long chain limit. The $<R^2_{g,L}>/<R^2_{g,R}>$ ratio change from 2.1 $\pm$ 0.1 to 2.3 $\pm$ 0.1 at 473 K and 298 K, respectively. The strongest increase of $<R^2_{g,L}>/<R^2_{g,R}>$ ratio is observed during the first 15 million MCS at 298 K.
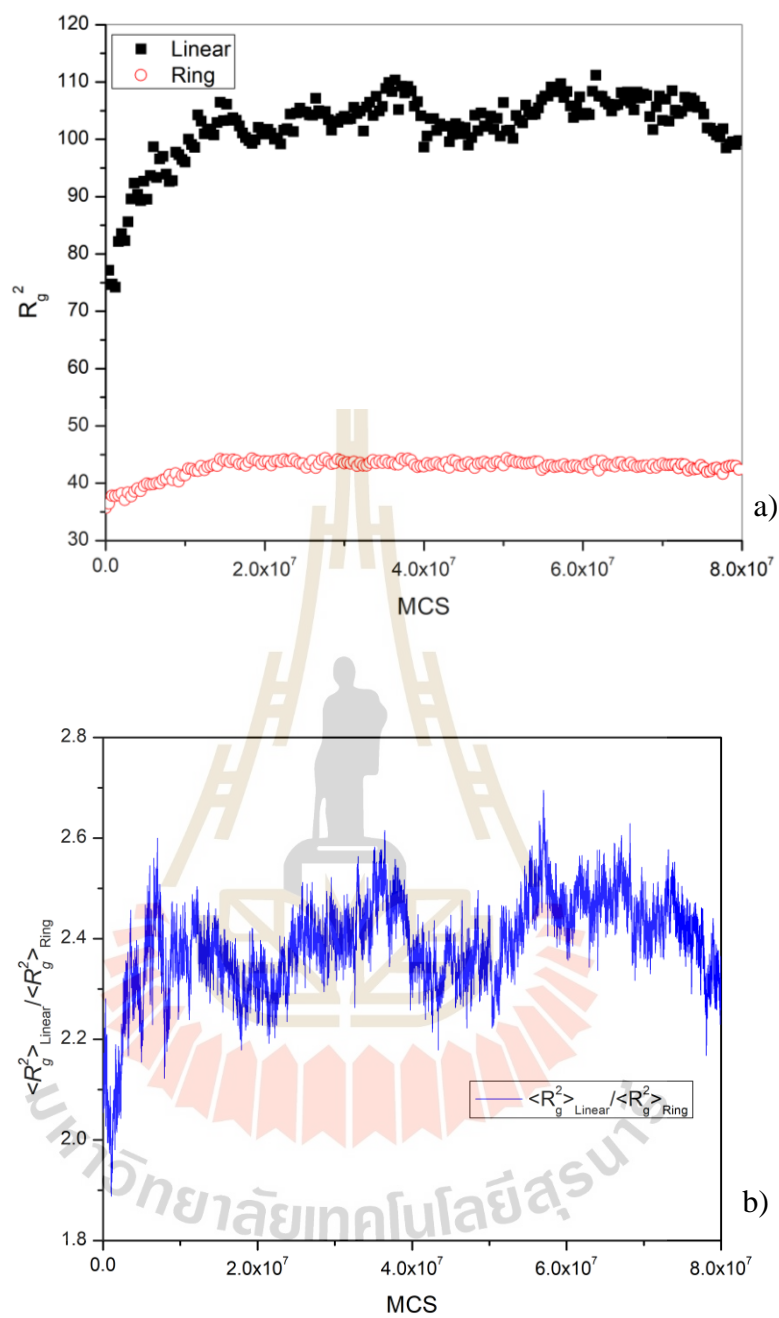
Figure 4.4.5 (a) Mean square radius of gyration $<R^2_g>$ for linear vs ring PE and (b) $<R^2_g>_{Linear}/<R^2_g>_{Ring}$ as a function of MCS of polyethylene.

Then, the components of $<R^2_g>$ in the directions of *x, y* and *z* axes, represented by $<R^2_{gx}>$, $<R^2_{gy}>$ and $<R^2_{gz}>$ in a laboratory-fixed coordinate system, are investigated and presented in Figure 4.4.6. For the purpose of revealing the anisotropy of the expansion of these independent parent chains in each direction, the polymer coordinates can be determined after reverse mapping using Eq. (4.4.5).

$$\begin{bmatrix} x \\ y \\ z \end{bmatrix} = \begin{bmatrix} 1 & cos60° & cos30°\sqrt{3} \\ 0 & sin60° & sin30°\sqrt{3} \\ 0 & 0 & \sqrt{2}/\sqrt{3} \end{bmatrix} \begin{bmatrix} \bar{x} \\ \bar{y} \\ \bar{z} \end{bmatrix} \qquad (4.4.5)$$

Upon crystallization, the linear polymer chain in Figure 4.4.6a has the largest $<R^2_{gz}>$ due to chain expansion in the crystallization process which is the preferred direction for chain elongation. On the other hand, there is no general trend for the expansion of cyclic polymer because there is no specific trend for $<R^2_{gx}>$, $<R^2_{gy}>$ and $<R^2_{gz}>$ which are about the same values as seen in Figure 4.4.6b. The linear chains can form one domain crystal which are oriented in one direction while the cyclic chains form multiple domain crystal oriented in many different ways.
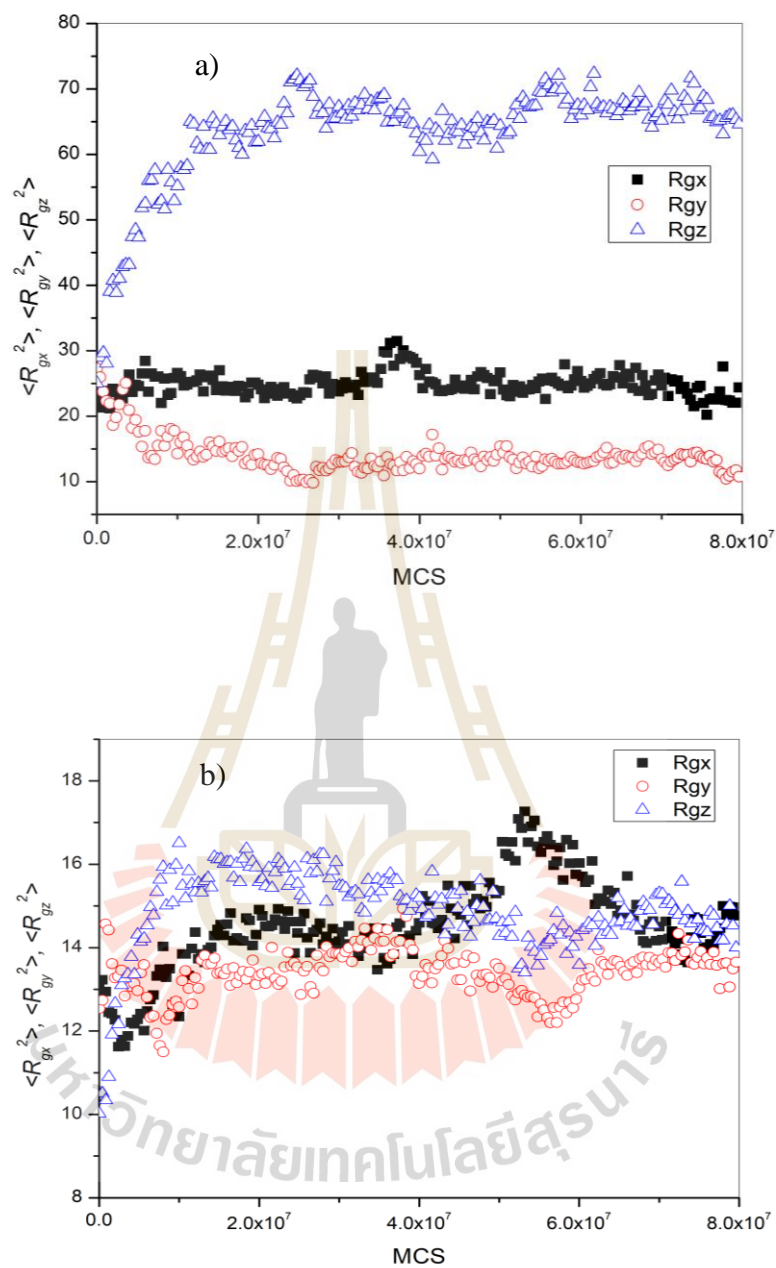
Figure 4.4.6 The component of $<R_g^2>$ along three axes of Cartesian coordinate system as a function of MCS for (a) linear-PE and (b) ring-PE.

In Figure 4.4.7, the number of consecutive bonds in the *trans* state was determined in comparison between two temperatures at the molten and crystalline states 473 K and 298 K, respectively. As expected, longer consecutive *trans* sequence is found at 298 K when the crystallization proceeds. Comparison between these two topologies at 298 K, linear chain has longer *trans* sequence (upto 25 C-C bonds) while the cyclic polymer can be at most around 16. The cyclic polymer needs to form some *gauche* conformation to maintain the ring topology and extra folding to form the ordered structure with multiple domains.
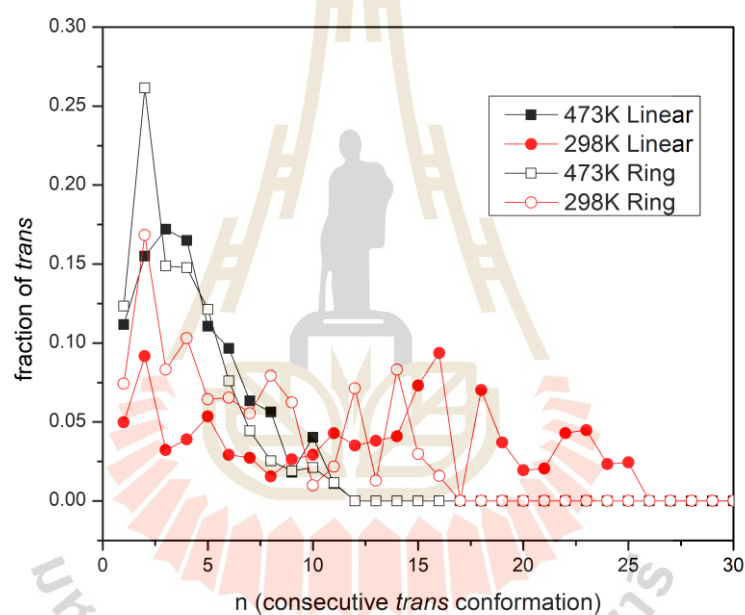
Figure 4.4.7 The fraction of *trans* state as a function of consecutive bonds for the melt and crystalline state of linear and cyclic PE.

4.4.3.4 Chain Ordering

Upon crystallization, PE chains adopt zigzag *trans* conformation. To study the growth process of structure formation, the overall orientation correlation function, S_G, can be calculated by

$$S_G = \tfrac{1}{2}[3\langle cos^2\theta\rangle - 1]$$ (4.4.6)

Here, θ is the angle between two main axes of polymer molecules, and S_G is the ensemble average for all polymer pairs. From Eq. (4.4.6), S_G = 1.0 and 0.0 when all polymers are parallel and randomly oriented, respectively.

The overall chain orientation was investigated using the global order parameter calculated from the molecular axis. From Figure 4.4.2, S_G of linear chains increases at the early stage and then reach the constant value afterward around S_G = 0.7 which is substantially larger than those of cyclic PE (S_G < 0.1). Linear chains can form much more ordered structure compared to the cyclic topology. It is noted that the lower S_G value for cyclic chains does not represent no crystallinity but it is due to different orientation from the ordered structure with multiple domains.
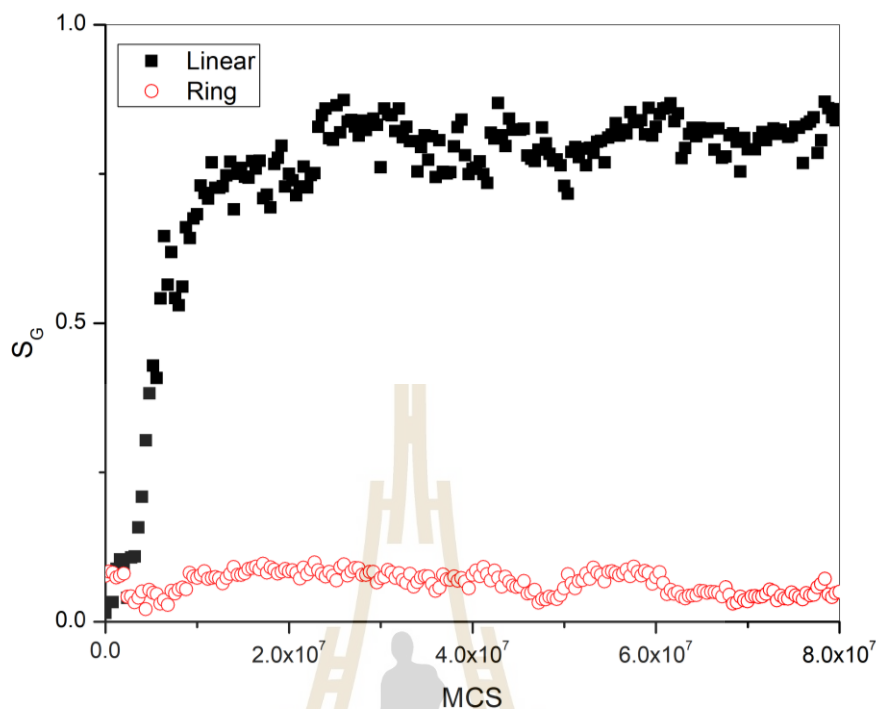
Figure 4.4.8 Evolution of the global orientational order parameter for linear and cyclic PE chain at 298 K.

Upon crystallization, PE chain has zigzag *trans* conformation and the bonds should have long distance correlation in the crystalline structure. To describe the degree of chain ordering, the intramolecular, $M_1(j)$ and $M_2(j)$, are used as defined by

$$M_1(j) = < m_i . m_{i+j} > = < \cos \theta_{i,i+j} > \qquad (4.4.7)$$

$$M_2(j) = \frac{1}{2}\left[3 < (m_i . m_{i+j})^2 > -1\right] = \frac{1}{2}[3 < cos^2\theta_{i,i+j} > -1] \qquad (4.4.8)$$

Here, $\theta_{i,i+j}$ is the angle between the *i*th and the (*i+j*)th bond in the same chain. The bond orientation correlation functions, $M_1(j)$ and $M_2(j)$, at the molten and crystalline stage for both linear and cyclic chains are presented in Figure 4.4.9. $M_1(j)$ represents the tendency for bond alignment in the parallel direction which decay gradually as the simulation proceeds. There is an upturn point at the bond n = 10, which is about the half unit of cyclic chain that the bond vector tends to orient parallel with the back folded bond from the other half. As expected, both systems have lower $M_1(j)$ in the

later crystallization stage. The second order, $M_2(j)$, is also used to represent the overall alignment of bonds along a common axis. From Figure 4.4.9(b), $M_2(j)$ exhibits the systematic change as the simulation proceeds and reach almost the constant value at the particular time. The development of a plateau in $M_2(j)$ expands roughly from $j = 3$ to $j = 14$. In general, $M_2(j)$ for cyclic chain is larger than that of linear polymer especially at 298 K. There are the peak maxima of $M_2(j)$ for cyclic chains which can be exceed the value of linear chain even at 473 K suggesting the effect of chain topology on the bond alignment. It is noted that $M_2(j)$ is not responsive to the difference between parallel and antiparallel orientations, while $M_1(j)$ is more sensitive to this difference. In general, when the crystallization take place at 298 K, the order parameter is slower decayed as polymer chains adopt more *trans* conformation. The cyclic polymer exhibits an upturn point around the half length of chain due to the topology difference.
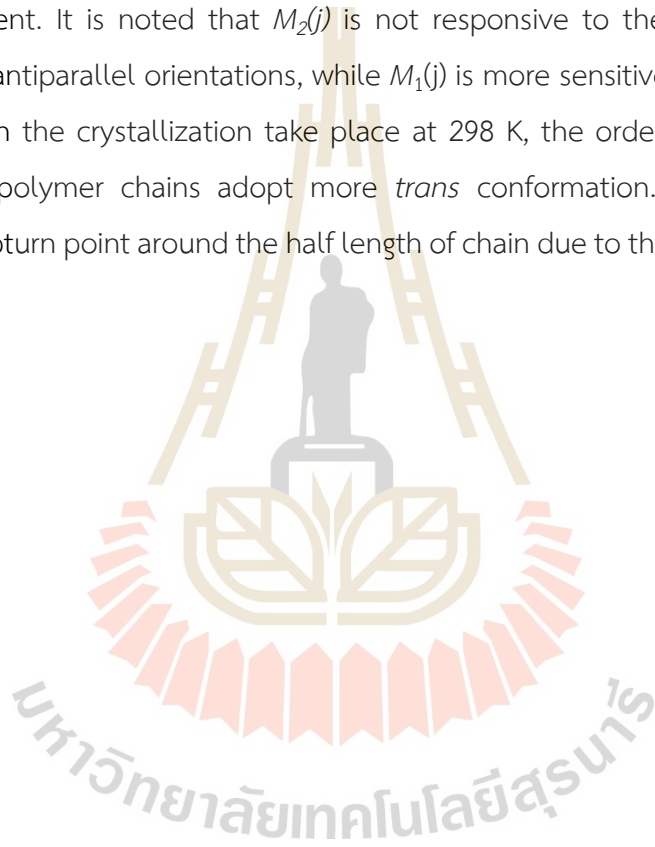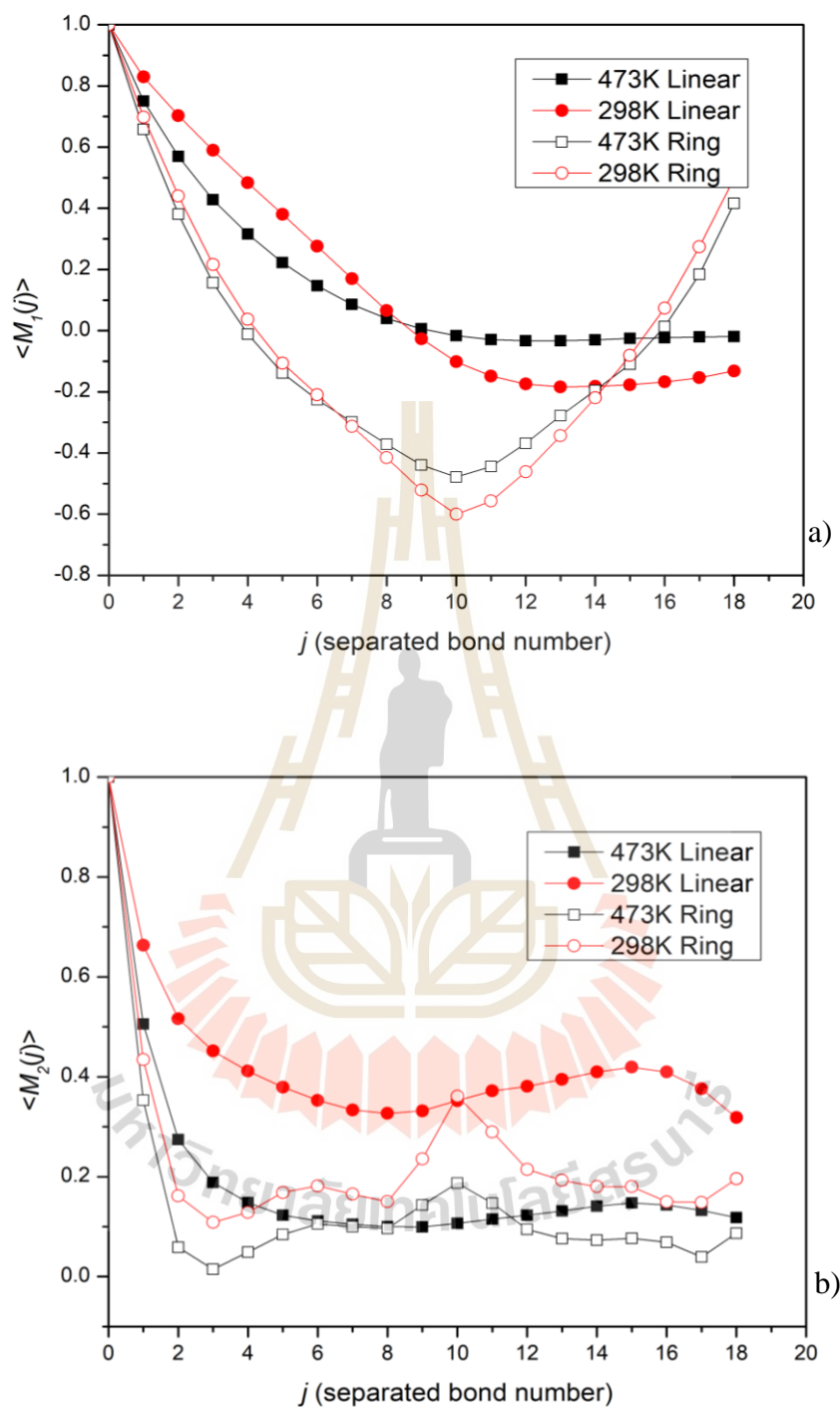
Figure 4.4.9 Intramolecular bond orientation correlation functions: (a) $M_1(j)$ and (b) $M_2(j)$, as a function of the separated bond number for linear and cyclic PE.

The intermolecular bond orientation is defined to investigate to determine how bonds from different molecules are oriented. Using similar equation to the intramolecular bond order parameter, the local (S_L) and global intermolecular orientation order parameter (S_G) can be denoted as

$$S_L(n) = \frac{1}{2}[3 < \cos^2\psi(n) > -1] \tag{4.4.9}$$

$$S_G = \frac{1}{2}[3 < \cos^2\psi > -1] \tag{4.4.10}$$

where, $\psi(n)$ in Eq. (4.4.9) is the angle between two bonds separated in the nth shell. ψ in Eq. (4.4.10) is the angle between the main axes of two chains. S_G is averaged for every pair of chains and $S_L(n)$ is averaged for all bonds located in the nth shell. Figure 4.4.10 depicts S_L for both linear and cyclic systems in comparison between the molten and crystalline stages. The first shell has small values due to high repulsive interaction of the first shell. After the maxima correlation in the second shell, S_L decays monotonically toward random orientation as a function of shell number. The largest value could be attained at n = 2 when all bond pairs (inter- and intramolecular) included in the calculation of S_L. For the bond orientation at the global scale, as presented earlier in Figure 4.4.8 for the evolution of S_G, polymers change from an isotropic disordered state ($S_G \approx 0$) toward the more ordered phase ($S_G \rightarrow 1$). As the crystallization proceed, the order parameter is monotonically increase. It is also seen that bonds at the second shell exhibit the highest correlation or parallel orientation. In contrast, the bond order parameters at higher shells are steadily decreased as a result of more random orientation for the further bonds.
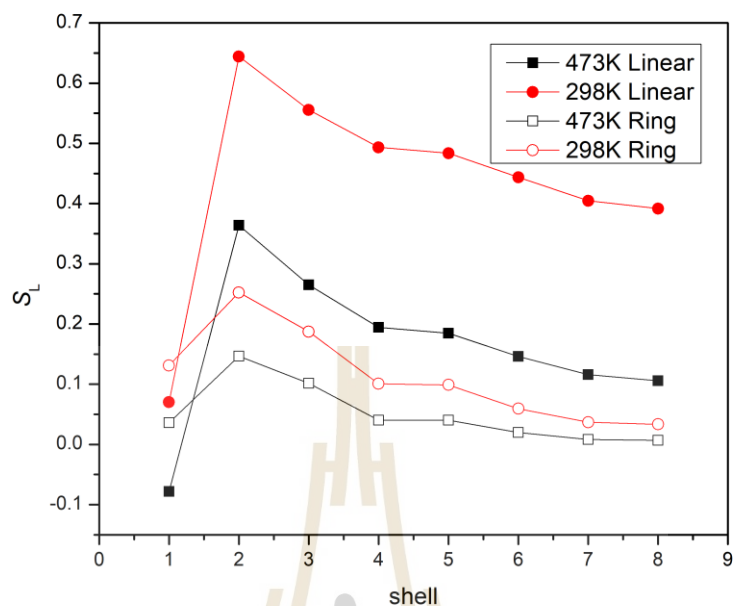
Figure 4.4.10 Local intermolecular bond orientation correlation function S_L as a function of shell number (n) for linear and ring-PE at 473 and 298 K.

4.4.3.5 Intermolecular packing

The local intermolecular packing of polymer chains can be determined from the pair correlation function (PCF) which is the probability of locating a particle A at a specified distance from another particle A. The PCF can be obtained from Eq. (4.4.11).

$$g_{AA}(i) = \frac{<n_{AA}(i)>}{(10i^2+2)V_A} \tag{4.4.11}$$

where, n_{AA} is a number occupancy of A in the ith shell from another A; V_A is a volume fraction of A. The beads on the same chain are ignored and those are separated by 1 or 2 bonds. The PCFs as a function of shell number are compared in Figure 4.4.11. The PCFs of the 2nd to 6th shells increase while those in the outer shells (7th and 8th) are slightly reduced to keep the same overall occupancy during the simulation progresses. The maximum PCF appears at the third shell as a consequence of the location of the strongest interaction in Lennard-Jones potentials and the next maximum point is at

the fifth shell. These results imply that polymer chains are packed denser in the crystalline phase as expected. PCF was also used to compare the chain packing between linear and cyclic PE system. In the melt state, the PCFs of both linear and cyclic chains are almost the same while there is a significant difference at 298K in that linear chain pack denser than those of cyclic polymer.
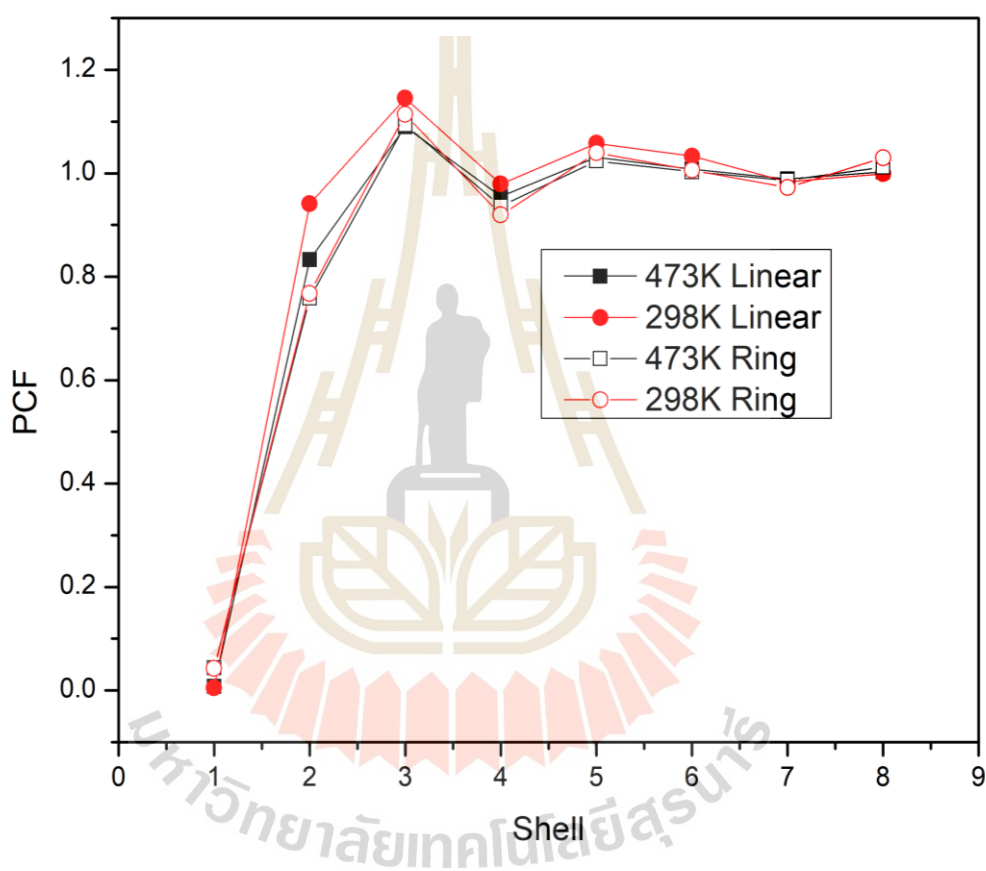
Figure 4.4.11 Pair correlation function vs shell number for comparison of linear and ring PE chains at 473 K and 298 K

4.4.3.6 Scattering structure factor

To get some properties that are related to the real experiment, the progress of the polymer crystallization can be evaluated using the spherically averaged structure factors as:

$$S(q) = \frac{1}{N_b^2}\sum_{i=1}^{N_b}\sum_{j=1}^{N_b}\frac{sin(q \cdot r_{ij})}{qr_{ij}} \qquad (4.4.12)$$

where N_b is the number of all beads, and q is $(4\pi/\lambda)sin(\theta/2)$. Figure 4.4.12(a) depicts the evolution of $S(q)$ for cyclic polymers at time t subtracted by $S(q)$ at the starting time. The intensity increases rapidly with time as the crystallization proceed while there is no significant change for the peak position. In comparison between cyclic and linear chains, the maximum intensity I_{max} is depicted in Figure 4.4.12(b). The $S(q)$ results also suggest better crystallization for linear chains. The location of q_{max} (the distance from each ordered motifs) does not change much when the regular structure forms. The fluctuation in $S(q)$ amplitude in the cyclic system is related to the instability of multiple domain crystals whereas there is always steadily increase for the crystallization of linear chains.
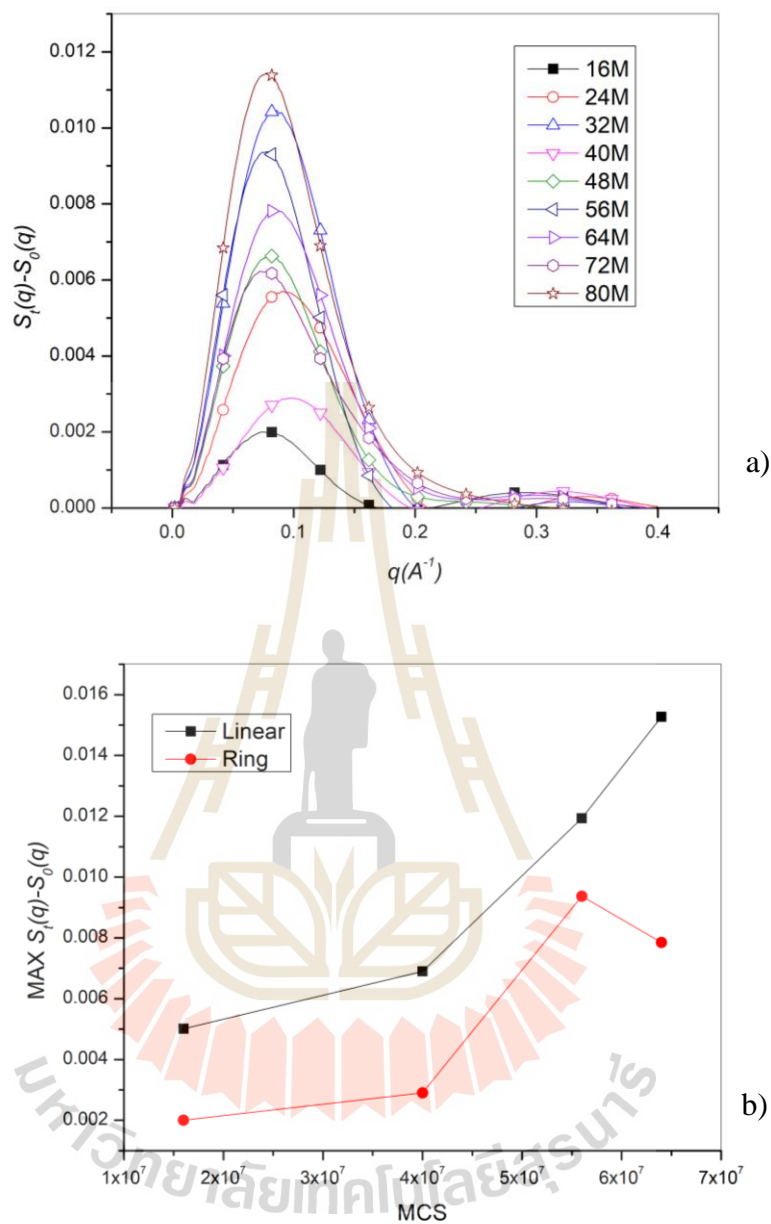
Figure 4.4.12 (a) Change in the $S_t(q)$ - $S_0(q)$ for cyclic chains (b) Maximum intensity in $S_t(q)$ - $S_0(q)$ for linear versus cyclic polymers as a function of MCS.

4.4.4 Summary

Computer simulation was employed to study the crystallization process of short polyethylene (C_{40}) model with different chain topology (linear vs cyclic). The structures at the melt state were cooled down to 298 K and the evolution of chain conformation, intermolecular ordering and scattering structure factor were determined. All these properties exhibit an ordering process as the sign of crystallization for both chains especially linear polymer. For these relatively short chains, linear polymer may prone to better crystallization process compared to the cyclic topology. It is likely that cyclic polymers may form the multiple ordered domains with different orientation.

CHAPTER V

CONCLUSION

In this thesis, molecular simulation and experimental techniques were employed to study found main parts related to the structures, dynamics, surface and crystallization characteristics of polyolefins with chemical and physical modification through copolymerization and cyclization of original polymer chains. The conclusions are as follows:

Structural and surface properties of poly(ethylene-ran-propylene) free stand thin film with different ethylene fractions were investigated using Monte Carlo simulation of a coarse-grained copolymer model on the 2nnd lattice. The relative bead densities near the mid-plane center of the films are relatively constant and significantly dropped in the surface region. The profiles become denser with sharper surface for copolymer films with larger ethylene content. The chain ends are more segregated while the middle beads are decreased in the free surface region and this observation becomes more significant for copolymer with a higher ethylene fraction. The bonds prefer to orient perpendicularly to the surface due to end bead segregation and are slightly sensitive to the ethylene fraction in the copolymer. For chain properties, the largest axis tends to orient in parallel to the film surface and the orientation become more isotropic for copolymer chain with less ethylene fraction. Chain size in normal direction becomes contraction along the direction from the film center and is decreased in the region close to the surface, while the molecular size in parallel direction component has no noticeable changed. Molecular shape in term of asphericity becomes more distorted as a function of ethylene content. The overall size of copolymer chains near the surface was also slightly changed. For chain orientation, the largest molecular axis tends to be oriented in a parallel direction to the film surface, and relatively changed toward random orientation for less ethylene content. It should be noted that the data have wide fluctuations in the bond and

chain properties in the low-density region near the surface probably due to the small number of observations.

Monte Carlo simulations of coarse-grained copolymer model were employed to investigate molecular and dynamic characteristics of ethylene propylene random copolymer (EPRC) melts. EPRC chains were consisted of the fixed fractions of ethylene monomers (P_E = 0.25, 0.50, and 0.75). The variation of comonomer sequences on EPRC can influence the conformational properties in terms of molecular size and chain rigidity, especially for low ethylene content, but with some exception in few patterns. Simulation results imply that the intrachain interaction exhibited itself in the radius of gyration (chain dimension) and in the characteristic ratio (chain stiffness) and interchain interaction, in terms of the pair correlation function, contributed to the dynamic properties of the copolymers differently subjected to the PE value and the specific monomer sequence. At low to intermediate (PE = 0.25 and 0.5), EPRC chains exhibit higher mobility so long as the chains contain block-like structure. Copolymers with long consecutive monomers of the same type is prone to express faster mobility than those with more randomly mixed comonomers. EPRC chains with low PE have higher molecular packing efficiency for the patterns close to alternating sequence, resulting in slower mobility. At high PE = 0.75, the chain dynamics are quite similar for all comonomer sequence due to large amount of ethylene beads. Nevertheless, the intramolecular interaction seems to play a more crucial role than the intermolecular packing in determining the chain mobility, especially for copolymer with long ethylene block sequence.

Non-isothermal crystallization of *isotactic* polypropylene with a small amount of ethylene defects was investigated by differential scanning calorimetry (DSC) and isothermal crystallization by synchrotron small angle X-ray scattering (SAXS). The crystallization is slowed down for *i*PP with defects. Crystallization kinetics were modeled by Avrami analysis and the results suggest that the dimension crystal growth (*n*) and the crystallization rate (*k*) tend to increase for *i*PP with defect.

For SAXS analysis, the paracrystalline model and the electron density correlation function were used to estimate the long period (*D*) and the lamellar

thickness (*L*). The *D* is increased for *i*PP with defects (from 19 to 26 nm). In general, for *i*PP with ethylene defects have higher amorphous (*La*) and *L*, but lower *L/D* ratio than pure *i*PP. Namely, the degree of crystallinity is lower for *i*PP with defects, which agrees with DSC and SAXS.

Monte Carlo simulation of coarse-grained polymer models was applied to study the crystallization process of short polyethylene (C_{40}) with different chain topology (linear vs cyclic). The structures at the melt state (473 K) were stepwise cooling and the crystallization was monitored at 298 K. The evolution of chain conformation, bond/chain orientation, molecular packing and scattering structure factor were determined. All these properties exhibit an ordering process as the signal for crystallization of linear and cyclic polymers. For these relatively short chains, linear polymer may be prone to exhibit a better crystallization process compared to the cyclic topology. It is likely that cyclic polymers may form the multiple ordered domains with different orientations.

REFERENCES
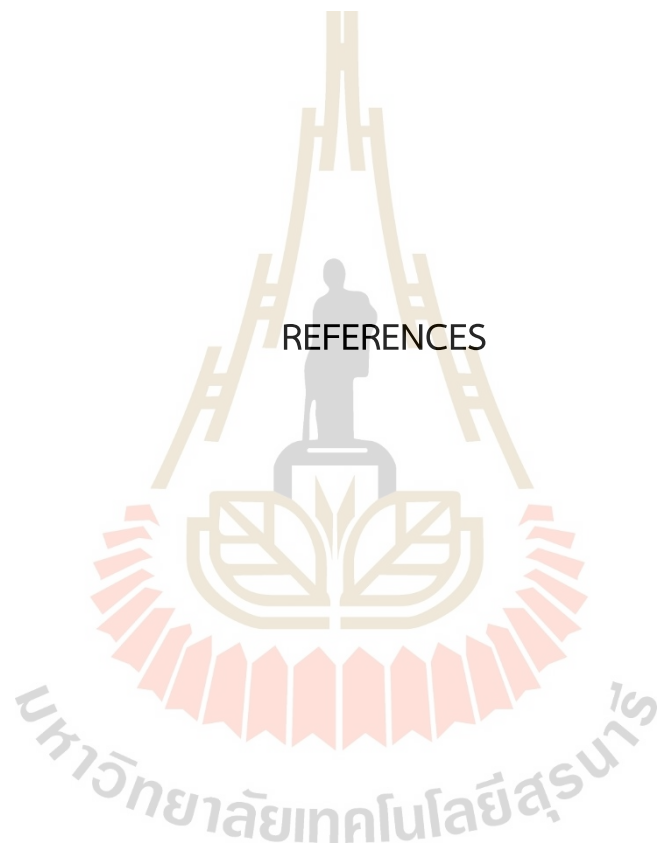
REFERENCES

Abe, A., Jernigan, R.L., and Flory, P.J. (1966). Conformational Energies of n-Alkanes and the Random Configuration of Higher Homologs Including Polymethylene. *J. Am. Chem. Soc. 88*(4); 631–639.

Akten, E.D., and Mattice, W.L. (2001). Monte Carlo Simulation of Head-to-Head, Tail-to-Tail Polypropylene and Its Mixing with Polyethylene in the Melt. *Macromolecules. 34*(10); 3389-3395.

Antoniadis, S.J., Samara, C.T., and Theodorou, D.N. (1998). Molecular Dynamics of Atactic Polypropylene Melts. *Macromolecule. 31*(22); 7944-7952.

Antoniadis, S.J., Samara, C.T., and Theodorou, D.N. (1999). Effect of Tacticity on the Molecular Dynamics of Polypropylene Melts. *Marcromolecules. 32*; 8635-8644.

Avrami, M. (1939). Kinetics of phase change. I general theory. *J Chem Phys. 7*; 1103-1112.

Avrami, M. (1940). Kinetics of phase change. II transformation-time relations for random distribution of nuclei. *J Chem Phys. 8*; 212-224.

Baschnagel, J., Binder, K., Doruker, P., Gusev, A.A., Hahn, O., Kremer, K., Mattice, W. L., Müller-Plathe, F., Murat, M., Paul, W., Santos, S., Suter, U.W., and Tries, V. (2000). Bridging the Gap Between Atomistic and Coarse-Grained Models of Polymers: Status and Perspectives. *Advance in Polymer Science. 152*; 41-156.

Busico, V., and Cipullo, R. (2001). Microstructure of polypropylene. *Progress in Polymer Science. 26*(3); 443-533.

Buzarovska, A. (2004). *Crystallization of polymers (2nd edition) Volume 2: Kinetics and mechanisms. Edited by Leo Mandelkern.* Cambridge: Cambridge University Press.

Carmesin, I., and Kremer, K. (1998). The bond fluctuation method: a new effective algorithm for the dynamics of polymers in all spatial dimensions. *Macromolecules. 21*(9); 2819–2823.

Chen, C.M., and Higgs, P. (1998). Monte-Carlo simulations of polymer crystallization in dilute solution. *The Journal of Chemical Physics, 108*; 4305-4314.

Chen, X., Kumar, S.K., and Ozisik, R. (2006). Monte Carlo simulations of the crystallization of isotactic polypropylene. *Journal of Polymer Science Part B: Polymer Physics*. *44*(24); 3453-3460.

Chen, X., Ozisik, R., Kumar, S.K., and Choi, P. (2007). Influence of stereoerrors on the formation of helices during early stage crystallization of isotactic polyproyplene. *Journal of Polymer Science*. *45*; 3349-3360.

Cho, J., and Mattice, W.L. (1997). Estimation of Long-Range Interaction in Coarse-Grained Rotational Isomeric State Polyethylene Chains on a High Coordination Lattice. *Macromolecules*. *30*(3); 637–644.

Choi, P., and Mattice, W.L. (2004). Molecular origin of demixing, prior to crystallization, of atactic polypropylene/isotactic polypropylene blends upon cooling from the melt. *The Journal of Chemical Physics*. *121*(17); 8647.

Clancy, T.C., and Mattice, W.L. (2000). Rotational isomeric state chains on a high coordination lattice: Dynamic Monte Carlo algorithm details. *Journal of Chemical Physics*. *112*(22); 10049-10055.

Clancy, T.C., and Mattice, W.L. (2001). Miscibility of poly(vinyl chloride) melts composed of mixtures of chains with differing stereochemical composition and stereochemical sequence. *Macromolecules*. *34*(18); 6482-6486.

Clancy, T.C., Pütz, M., Weinhold, J.D., Curro, J.G., and Mattice, W.L. (2000). Mixing of isotactic and syndiotactic polypropylenes in the melt. *Macromolecules*. *33*(25); 9452-9463.

Corradini, P. (2003). The discovery of isotactic polypropylene and its impact on pure and applied science. *J. Polym. Sci*. *42*(3); 391–395.

Crist, B. (1973). Small-angle x-ray scattering of semicrystalline polymers. I. Review of existing models. *J Polym Sci Part A-2 Polym Phys*. *11*(4); 635-661.

de Gennes, P. (1979). *Scaling concepts in polymer physics.* Ithaca: Cornell University Press.

Debye, P., and Bueche, A.M. (1949). Scattering by an Inhomogeneous Solid. *J. Appl. Phys*. *20*; 518-525.

Destrée, M., Lauprềtre, F., Lyulin, A., and Ryckaert, J.P. (2000). Local dynamics of isotactic and syndiotactic polypropylene in solution. *The Journal of Chemical Physics*. *112*(21); 9632.

Doruker, P., and Mattice, W.L. (1997). Reverse Mapping of Coarse-Grained Polyethylene Chains from the Second Nearest Neighbor Diamond Lattice to an Atomistic Model in Continuous Space. *Macromolecules*. *30*(18); 5520–5526.

Doruker, P., and Mattice, W.L. (1998). Simulation of Polyethylene Thin Films on a High Coordination Lattice. *Macromolecules*. *31*(4); 1418–1426.

Doruker, P., and Mattice, W.L. (1999). A second generation of mapping/reverse mapping of coarse-grained and fully atomistic models of polymer melts. *Marcromolecular*. *8*(5); 463-478.

Doruker, P., and Mattice, W.L. (1999). Mobility of the Surface and Interior of Thin Films Composed of Amorphous Polyethylene. *Macromolecules*. *32*(1); 194–198.

Doruker, P., Rapold, R.F., and Mattice, W.L. (1996). Rotational isomeric state models for polyoxyethylene and polythiaethylene on a high coordination lattice. *The Journal of Chemical Physics*. *104*; 8742.

Doucet, M., Cho, J.H., Alina, G., Bakker, J., Bouwman, W., Butler, P., Campbell, K., Gonzales, M., Heenan, R., Jackson, A., Juhas, P., King, S., Kienzle, P., Krzywon, J, Markvardsen, A., et al. *SasView version 4.2.1*. http://doi.org/10.5281/zenodo.2561236.

Everaers, R., Sukumaran, S.K., Grest, G.S., Svaneborg, C., Sivasubramanian, A., and Kremer, K., (2004). Rheology and microscopic topology of entangled polymeric liquids. *Science. 303*; 823–826.

Ezquerra, T., López-Cabarcos, E., Hsiao, B., and Baltà-Calleja, F. (1996). Precursors of crystallization via density fluctuations in stiff-chain polymers. *Physical Review E*. *54*(1); 989-992.

Feast, W.J., and Munro H.S. (1987). *Polymer Surfaces and Interfaces*. New York: Wiley.

Fixman, M. (1962). Radius of gyration of polymer chains. *J. Chem. Phys*. *36*; 306.

Flory, P.J., and Volkenstein, M. (1969). *Statistical mechanics of chain molecules.* Newyork: Wiley.

Fried, J.R. (2014). *Polymer Science and Technology (3rd Edition)*, Pearson Education Inc.

Friedman, H.L. (1964). Kinetics of thermal degradation of char-forming plastics from thermogravimetry. Application to a phenolic plastic. *J. Polym. Sci. Polym. Symp*. *6*; 183-195.

Fujiwara, S., and Sato, T. (1999). Molecular dynamics simulation of structure formation of short chain molecules. *The Journal of Chemical Physics*. *110*; 9757.

Glatter, O., and Kratky, O. (1982). *Small Angle X-ray Scattering*. London: Academic Press.

Haliloglu, T. (1998). Mapping of rotational isomeric state chains with asymmetric torsional potential energy functions on a high coordination lattice: Application to polypropylene. *The Journal of Chemical Physics. 108*; 6989.

Halverson, J.D., Lee, W.B., Grest, G.S., Grosberg, A.Y., and Kremer, K. (2011). Molecular dynamics simulation study of nonconcatenated ring polymers in a melt. I. Statics. *The Journal of Chemical Physics*. *134*(20); 204904.

Heeley, E.L., Maidens, A.V., Olmsted, P.D., Bras, W., Dolbnya, I.P., Fairclough, J.P.A. Terrill, N.J., and Ryan, A.J. (2003). Early Stages of Crystallization in Isotactic Polypropylene. *Macromolecules*. *36*; 3656–3665.

Helfand, E., and Tagami, Y. (1972). Theory of interface between immiscible polymers. *J. Chem. Phys*. *57*; 1812.

Hu, W. (2000). The melting point of chain polymers. *The Journal of Chemical Physics*. *113*(9); 3901-3908.

Hu, W., Mathot, V., Alamo, R., Gao, H., and Chen X. (2017). Crystallization of statistical copolymers. *Adv. Polym. Sci*. *276*; 1-43.

Imai, M., and Kaji, K. (2006). Polymer crystallization from the metastable melt: The formation mechanism of spherulites. *Polymer 47*(15); 5544-5554.

Imai, M., Kaji, K., and Kanaya, T. (1994). Structural Formation of Poly(ethylene terephthalate) during the Induction Period of Crystallization. 3. Evolution of Density Fluctuations to Lamellar Crystal. *Macromolecules*. *27*(24); 7103-7108.

Imai, M., Mori, K., Mizukami, T., Kaji, K., and Kanaya, T. (1992). Structural formation of poly (ethylene terephthalate) during the induction period of crystallization: 1. Ordered structure appearing before crystal nucleation. *Polymer*. *33*(21); 4451-4456.

Imai, M., Mori, K., Mizukami, T., Kaji, K., and Kanaya, T. (1992). Structural formation of poly(ethylene terephthalate) during the induction period of crystallization: 2. Kinetic analysis based on the theories of phase separation. *Polymer. 33*(21); 4457-4462.

Ivanov, D.A., Amalou, Z., and Magonov, S.N. (2001). Real-time evolution of the lamellar organization of poly(ethylene terephthalate) during crystallization from the melt: high-temperature atomic force microscopy study. *Macromolecules. 34*(26); 8944-8952.

Ivanov, D.A., Legras, R., and Jonas, A.M. (1999). Interdependencies between the evolution of amorphous and crystalline regions during isothermal cold crystallization of poly(ether-ether-ketone). *Macromolecules. 32*(5); 1582-1592.

Jernigan, R.L., and Flory, P.J. (1969). Moments of chain vectors for models of polymer chains. *J. Chem. Phys. 50*; 4178.

Jeziorny, A. (1978). Parameters characterizing the kinetics of the nonisothermal crystallization of poly(ethylene terephthalate) determined by DSC. *Polymer. 19*; 1142-1144.

Kaminsky, W., and Arndt, M. (1997). Metallocenes for polymer catalysis. *Advances in Polymer Science. 127*; 143-148.

Keller, A. (1957). A note on single crystals in polymers: Evidence for a folded chain configuration. *Philosophical Magazine. 2*(21); 1171-1175.

Kissinger, H.E. (1956). Variation of peak temperature with heating rate in differential thermal analysis. *J. Res. Nat. Inst. Stand. Technol. 57*; 217-221

Klein, J. (1986). Dynamics of Entangled Linear, Branched, and Cyclic Polymers. *Macromolecules. 19*(1); 105-118.

Koberstein, J.T., and Stein, R.S. (1983). Small-angle x-ray scattering measurements of diffuse phase-boundary thicknesses in segmented polyurethane elastomers. *J. Polym. Sci. Polym. Phys. Ed*. *21*(10); 2181-2200.

Kotelyanskii, M., and Theodorou, D.N. (2004). Simulation Methods For Polymers. *Marcel Dekker*. New York

Lee, B., Shin, T.J., Lee, S.W., Yoon, J., Kim, J., and Ree, M. (2004). Secondary crystallization behavior of poly (ethylene isophthalate-co-terephthalate): time-resolved small-angle X-ray scattering and calorimetry studies. *Macromolecules*. *37*(11); 4174-4184.

Liu, T.X., Mo, Z.S., Wang, S.E., Zhang, H.F. (1997). Nonisothermal melt and cold crystallization kinetics of poly(aryl ether ether ketone ketone). *Polym Eng Sci*. *37*; 568-575.

Luo, J., Liang, Y., Yang, J., Niu, H., Dong, J.Y., and Han, C.C. (2011). Mechanisms of nucleation and crystal growth in a nascent isotactic polypropylene/poly (ethylene-cooctene) in-reactor alloy investigated by temperature-resolved synchrotron SAXS and DSC methods. *Polymer*. *52*(20); 4590-4599.

Logotheti, G.E., and Theodorou, D.N. (2007). Segmental and Chain Dynamics of Isotactic Polypropylene Melts. *Macromolecules*. *40*(6); 2235-2245.

Madden, W.G. (1987). Monte Carlo studies of the melt–vacuum interface of a lattice polymer. *The Journal of Chemical Physics*. *87*; 1405.

Madkour, T.M., and Mark, J.E. (1997). Modeling of the crystallization of isotactic polypropylene chains. *Journal of Polymer Science*. *35*(16); 2757-2764.

Mansfield, K.F., and Theodorou, D.N. (1990). Atomistic simulation of a glassy polymer surface. *Macromolecules*. *23*; 4430-4445.

Mansfield, K.F., and Theodorou, D.N. (1991). Molecular dynamics simulation of a glassy polymer surface. *Macromolecules*. *24*(23); 6283–6294.

Mark, J.E. (1972). On the Configurational Statistics of Ethylene-Propylene Copolymers. *J. Chem. Phys*. *57*; 2541.

Martoňák, R., Paul, W., and Binder, K. (1996). Monte Carlo simulation of crystalline polyethylene. *Computer Physics Communications*. *99*(1); 2-8.

Mattice, W.L., and Clancy, T.C. (1999). Unperturbed dimensions and local stiffness of poly(vinyl chloride) with stereochemical sequences composed of repeating units. *Macromolecules*. *32*(16); 5444-5449.

Mattice, W.L., and Suter, U.W. (1994). *Conformational Theory of Large Molecules: The Rotational Isomeric State Model in Macromolecular Systems*. New York: Wiley.

Mattice, W.L., Tatek, Y.B., and Waheed, N. (2007). Variability in the Persistence Length of an Atactic Polymer Due to Quenched Randomness, As Illustrated by Atactic Polystyrene. *Macromolecules*. *40*(2); 379-383.

Mattice, W.L., and Waheed, N. (2006). An Assessment of the Role of Quenched Randomness in the Stereochemical Sequences of Atactic Vinyl Polymers. *Macromolecules*. *39*(6); 2380-2387.

McQuarrie, D.A. (1976). *Statistical Mechanics.* New York: Happer & Row.

Metropolis, N., Rosenbluth, A.W., Rosenbluth, M.N., Teller, A.H., and Teller, E. (1953). Equation of State Calculations by Fast Computing Machines. *The Journal of Chemical Physics*. *21*; 1087-1091.

Misra, S., Fleming, P.D., and Mattice, W.L. (1995). Structure and energy of thin films of poly-(1,4-*cis*-butadiene): A new atomistic approach. *J Comput.-Aided Mat Design*. *2*; 101.

Mittal, K.L. (1983). *Physicochemical Aspects of Polymer Surfaces*. Vol.1, New York: Plenum Press.

Mittal, K.L. (1983). *Physicochemical Aspects of Polymer Surfaces*. Vol.2, New York: Plenum Press.

Müller, M., and MacDowell, L.G. (2000). Interface and Surface Properties of Short Polymers in Solution: Monte Carlo Simulations and Self-Consistent Field Theory. *Macromolecules*. *33*(10); 3902–3923.

Natta, G., Pino, P., Corradini, P., Danusso, F., Mantica, E., Mazzanti, G., and Moraglio, G. (1955). Crystalline high polymers of a-olefins. *J. Am. Chem. Soc*. *77*(6); 1708–1710.

Obukhov, S.P., Rubinstein, M., and Duke, T. (1994). Dynamics of a Ring Polymer in a Gel. *Physical Review Letters*. *73*; 1263.

Olmsted, P., Poon, W., McLeish, T., Terrill, N., and Ryan, A. (1998). Spinodal-assisted crystallization in polymer melts. *Physical Review Letters*. *81*; 373-376.

Opdahl, A., Phillips, R.A., and Somorjai, G.A. (2002). Surface segregation of methyl side branches monitored by sum frequency generation (SFG) vibrational spectroscopy for a series of random poly(ethylene-co-propylene) copolymers. *J Phys Chem B. 106*; 5212.

Orwoll, R.A., and Mark, J.E. (Eds.) (1996) in *Physical Properties of Polymers Handbook*. Woodbury, New York: American Institute of Physics.

Ozawa, T. (1971). Kinetics of non-isothermal crystallization. *Polymer*. *12*; 150-158.

Ozisik, R., Meerwall, E. D., and Mattice, W. L. (2002). Comparison of the diffusion coefficients of linear and cyclic alkanes. *Polymer*. *43*; 629-635.

Pandey, A.K., Katiyar, V., Takagi, H., Shimizu, N., Igarashi, N., Sasaki, S., and Sakurai, S. (2019). Structural Evolution in Isothermal Crystallization Process of Poly(L-lactic acid) Enhanced by Silk Fibroin Nano-Disc. *Materials*. *12*; 1872.

Pérez-Camargo, R. A., Mugica, A., Zubitur, M., and Müller, A. J. (2015). Crystallization of Cyclic Polymers. *Polymer Crystallization I*. 93-132.

Pilz, I., Glatter, O., and Kratky, O. (1979). Small-angle x-ray scattering. *Methods in Enzymology*. *61*; 148-249.

Poling, B.E., Prausnitz, J.M., and O'Connell, J.P. (2002). *Properties of gases and liquids 5th*. McGraw-Hill.

Rane, S.S., Mattice, W.L., and Dhinojwala, A. (2004). Atomistic Simulation of Orientation of Methyl Groups and Methylene Bisectors, and Surface Segregation, in Freely Standing Thin Films of Atactic Poly(ethylene-co-propylene). *The Journal of Physical Chemistry*. *108*(39); 14830-14839.

Rapold, R., and Mattice, W.L. (1995). New high-coordination lattice model for rotational isomeric state polymer chains. *Journal of the Chemical Society*. *91*; 2435-2441.

Rungswang, W., Jarumaneeroj, C., and Chivatanasoontorn, V. (2015). Application of small-angle x-ray scattering (SAXS) via synchrotron radiation for Structural analysis of semi-crystalline polymer: study cases from polypropylene for industrial usage. *Suranaree J. Sci. Technol*. *22*(3); 265-276.

Rungswang, W., Jarumaneeroj, C., Petcharat, N., Soontaranon, S., and Rugmai, S. (2017). Phase-separation of heterophasic polymer in solution: A model case of impact-resistant polypropylene copolymer. *J. Appl. Polym. Sci*. *134*(28); 45069.

Ryan, A., Fairclough, J., Terrill, N., Olmsted, P., and Poon, W. (1999). A scattering study of nucleation phenomena in polymer crystallisation. *Faraday Discussions*. *112*; 13-29.

Schäler, K., Ostas, E., Schröter, K., Thurn-Albrecht, T., Binder, W. H., and Saalwächter, K. (2011). Influence of Chain Topology on Polymer Dynamics and Crystallization. Investigation of Linear and Cyclic Poly(ε-caprolactone)s by 1H Solid-State NMR Methods. *Macromolecules*. *44*(8); 2743-2754.

Soga, K., and Shiono, T. (1997). Ziegler-Natta catalysts for olefin polymerizations. *Progress in Polymer Science*. *22*(7); 1503-1546.

Solc, K., and Stockmayer, W.H. (1971). Shape of a Random-Flight Chain. *J. Chem. Phys*. *54*; 2756.

Soontaranon, S., and Rugmai, S. (2012). Small Angle X-ray Scattering at Siam Photon Laboratory. *Chinese Journal of Physics*. *50*(2); 204-210.

Stamm, M. (1992). Polymer interfaces on a molecular scale: comparison of techniques and some examples. *Adv Polymer Sci*. *100*; 357.

Stolte, I., and Androsch, R. (2014) Comparative study of the kinetics of non-isothermal melt solidification of random copolymers of butene-1 with either ethylene or propylene. *Colloid Polym Sci*. *292*(7); 1639–47.

Strobl, G.R., and Schneider, M. (1980). Direct evaluation of the electron density correlation function of partially crystalline polymers. *J. Polym. Sci., Polym. Ed*. *18*; 1343.

Su, H.H., Chen, H.L., Díaz, A., Casas, M.T., Puiggalí, J., Hoskins, J.N., Grayson, S.M., Pérez, R.A., and Müller, A.J. (2013). New insights on the crystallization and melting of cyclic PCL chains on the basis of a modified Thomson–Gibbs equation. *Polymer*. *54*; 846-859.

Suter, U.W., Pucci, S., and Pino, P. (1975). Epimerization of 2,4,6,8-tetramethylnonane and 2,4,6,8,10-pentamethylundecane, low molecular weight model compounds of polypropylene. *J. Am. Chem. Soc*. *97*; 1018–1023.

Takhulee, A., and Vao-Soongnern, V. (2014). Monte Carlo Simulation Study of the Effect of Chain Tacticity on Demixing of Polyethylene/Polypropylene Blends. *Polymer Science, Ser. A*. *56*; 936.

Takeuchi, H. (1998). Structure formation during the crystallization induction period of a short chain-molecule system: A molecular dynamics study. *Journal of Chemical Physics*. *109*(13); 5614-5621.

Terrill, N., Fairclough, P., Towns-Andrews, E., Komanschek, B., Young, R., and Ryan, A. (1998). Density fluctuations: The nucleation event in isotactic polypropylene crystallization. *Polymer*. *39*; 2381-2385.

Theodorou, D.N. (1988). Lattice models for bulk polymers at interfaces. *Macromolecules*. *21*(5); 1391-1400.

Vaĭnshteĭn, B. (1966). *Diffraction of X-rays by Chain Molecules.* New York: Elsevier Publishing Company.

Vao-soongnern, V. (2014). Effect of monomer composition on structural properties of poly(ethylene-co-propylene) nanofiber by Monte Carlo simulation. *Macromolecular Research*. *22*(5); 474–480.

Vao-soongnern, V., Doruker, P., and Mattice, W.L. (1999). Simulation of an amorphous polyethylene nanofiber on a high coordination lattice. *Macromolecular Theory and Simulations*. *9*; 1.

Vao-songnern, V., Ozisik, R., and Mattice, W.L. (2001). Monte Carlo simulation of the structures and dynamics of amorphous polyethylene nanoparticles. *Macromolecular Theory and Simulations*. *10*; 553.

Vao-Soongnern, V., Xu, G., and Mattice, W.L. (2004). Structure formation in the crystallization and annealing of tetracontane Nanoparticles. *Macromol. Theory Simul*. *13*; 539–549.

Verma, R., Marand, H., and Hsiao, B. (1996). Morphological changes during secondary crystallization and subsequent melting in poly (ether ether ketone) as studied by real time small angle X-ray scattering. *Macromolecules*. *29*(24); 7767-7775.

Vonk, C., and Kortleve, G. (1967). X-ray small-angle scattering of bulk polyethylene - II. Analyses of the scattering curve. *Kolloid-Zeitschrift & Zeitschrift für Polymere*. *220*; 19-24.

Waheed, N., Mattice, W.L., and von Meerwall, E.D. (2007). Enhanced Diffusion at Intermediate Stereochemical Composition in Polypropylene by Dynamical Monte Carlo. *Macromolecules*. *40*(5); 1504–1511.

Wang, Z.G., Hsiao, B.S., Sirota, E.B., Agarwal, P., and Srinivas, S. (2000). Probing the Early Stages of Melt Crystallization in Polypropylene by Simultaneous Small- and Wide-Angle X-ray Scattering and Laser Light Scattering. *Macromolecules*. *33*; 978–989.

Widmann A.H., Laso M., and Suter U.W. (1995). Optimized atomic Lennard-Jones 6–12 parameters for simulating pVT properties of a realistic polymethylene melt. *Journal of Chemical Physics*. *102*(14); 5761.

Wunderich, B. *Macromolecular physics*. New York: Academic Press. 1976-1980

Xia, Z., Sue, H.J., Wang, Z., Avila-Orta, C., and Hsiao, B. (2001). Determination of crystalline lamellar thickness in poly(ethylene terephthalate) using small-angle X-ray scattering and transmission electron microscopy. *Journal of Macromolecular Science*. *40*(5); 625-638.

Xu, G., Vao-soongnern, V., and Mattice, W.L. (2002). Similarities and Differences in the Rapid Crystallization Induced in n-Tetracontane by an Instantaneous Deep Quench of the Free-Standing Nanofiber and Free Standing Thin Film. *Macromol. Theory Simul. 11*; 494-500.

Yamamoto, T. (1997). Molecular dynamics simulation of polymer crystallization through chain folding. *The Journal of Chemical Physics*. *107*; 2653-2663.

Yuan, Q., Awate, S., and Misra, R.D.K. (2006). Nonisothermal crystallization behavior of polypropylene-clay nanocomposites. *Eur. Polym. J. 42*; 1994-2003.

Zhu, X., Yan, D., and Fang, Y. (2001). In Situ FTIR Spectroscopic Study of the Conformational Change of Isotactic Polypropylene during the Crystallization Process. *J. Phys. Chem. B. 105*(50); 12461-12463.
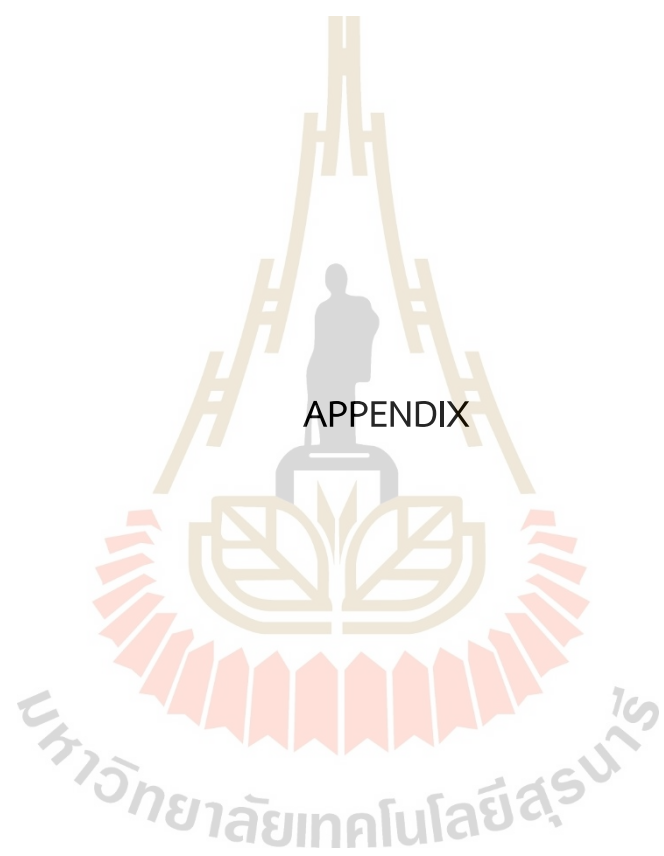
APPENDIX

SUT INTERNATIONAL VIRTUAL CONFERENCE ON SCIENCE AND
TECHNOLOGY NAKHON-RATCHASIMA, THAILAND 6TH AUGUST 2021

**Molecular simulation of the crystallization characteristics of cyclic versus linear
polyethylene models**

Supanont Jamornsuriya[1], and Visit Vao-soongnern[1]

[1]School of Chemistry, Institute of Science, Suranaree University of Technology

Nakhon Ratchasima, 30000, Thailand

Phone +66 4422 4639, Fax +66 4422 4185, *E-Mail: visit@sut.ac.th

Abstract

Abstract. The crystallization characteristics of short linear and cyclic polyethylene (PE)
models (C40) starting from the molten state at 473 K and then quenched to 298 K were
investigated using lattice Monte Carlo simulation of PE model. Intra- and interchain
interactions were based on the rotational isomeric state (RIS) model and Lennard-Jones
(LJ) potential, respectively. The simulations suggest that crystallinity can be observed
in feasible CPU time. Some properties evaluated from simulation to indicate
crystallization are the fraction of trans conformation, orientation correlation function
and evolution of the scattering structure factor. All these properties reveal an ordering

process as the sign of crystallization especially for linear chains whereas it is more difficult for cyclic polymer to form an ordered phase as shown by the evolution of intermolecular orientation correlation function, (SG). Although the trans fraction for both systems are quite high (0.85 and 0.70), SG is significantly different i.e., about 0.7 and less than 0.1 for linear and cyclic PE, respectively. By careful inspection for cyclic chain system, crystal may be able to form with multiple domains in different orientation. Nevertheless, simulation results suggest that linear chain is prone to form the ordered structure better than the cyclic polymer.

Keywords: Polyethylene; Monte Carlo simulation; Crystallization;

1. Introduction

Crystallization is significant topics in polymer science and technology [1]. There are many experimental techniques and theoretical treatment studies since the concept of chain folding was initiated many years ago [2,3]. Nevertheless, the molecular mechanism of polymer crystallization is still not well understood. For example, SAXS/WAXS methods were employed to study polymer crystallization from the melts has been reported in different polymers [4-6]. The correlation between melt density and molecular conformation [7] was used to explain this process. In recent years, cyclic polymers can be prepared and are interesting materials with new properties. To have a clear understanding of cyclic polymer crystallization should be significant for polymer science. In order to compare the crystallization characteristics between cyclic and linear polymer at the molecular level, in this work, we employ molecular simulation to

investigate the effect of polymer topology on structural formation upon cooling from the melt to crystallization temperature [8,9].

2. Method

2.1. Polyethylene model

PE model was coarse-grained to keep only every second carbon in the backbone were mapped on the *2nnd* lattice .Linear $C_{40}H_{82}$ or cyclic $C_{40}H_{40}$ are represented by 20 beads .The distance from beads i to $i+1 = 0.25$ nm .The intrachain interactions of PE chain was treated by the Rotational Isomeric State (RIS) model. The 9x9 statistical weight matrix was condensed to 3x3 dimension which contains three new parameters, a, b and c, in addition to σ and ω.

$$\mathbf{U_{PE}} = \begin{bmatrix} 1 & \sigma & \sigma \\ 1 & \sigma & \sigma\omega \\ 1 & \sigma\omega & \sigma \end{bmatrix} \rightarrow \mathbf{U_{2nnd}} = \begin{bmatrix} 1 & 4\sigma & 2\sigma\sigma(1+\omega) \\ 1 & 4a & 2b\sigma(1+\omega) \\ 1 & 4b & 2c(1+\omega) \end{bmatrix} \tag{1}$$

here $\sigma = \sigma_0 \exp(-E_\sigma/kT)$, $\omega = \omega_0 \exp(-E_\omega/kT)$ and $a = \sigma\omega^{1/8}$, $b = \sigma\omega^{1/4}$ and $c = \sigma^2\omega^{1/2}$. Interchain interactions are represented by Lennard-Jones (LJ) potential in the lattice form. The interaction parameter u_i at the ith shell can be obtained as:

$$\exp\left(-\frac{u_i}{k_B T}\right) - 1 \equiv \bar{f}_i \tag{2}$$

The LJ for PE are $\varepsilon/k_B = 185$ K and $\sigma = 4.4$ Å. Only the first three shell parameters were used to increase the speed of simulation.

2.2. Monte Carlo simulation

A single bead moves were allowed for each PE bead on *2nnd* lattice as self-avoiding random walk. Each bead was chosen randomly to move to an empty position and accepted according to the Metropolis criteria as:

$$P_{move} = min[1, P_{LR}P_{new}/P_{old}] \qquad (3)$$

where P_{LR} is the Boltzmann weights from long range interaction for each move and P_{new}/P_{old} is the of the probability ratio moving bead to a new bead site. Monte Carlo step (MCS) is defined when all the beads are moved once by average. Data analysis was obtained by an ensemble average of the 80 million MCS after equilibration. Data was recorded every 10000 MCS during this period for subsequent analysis [8,9].

3. Results & Discussion

3.1 Conformation

To determine the crystallization at the molecular level, Figure 1 shows the evolution of *trans* fraction at 298 K. PE chains have more *trans* state compared to the melts. After 20 million MCS, the fraction *trans* states reach 85% and 70% for linear and cyclic chains, respectively. As expected, the *trans* fraction of linear chains is higher. These results imply that linear chains should be able to form crystal structure better than the cyclic polymer.
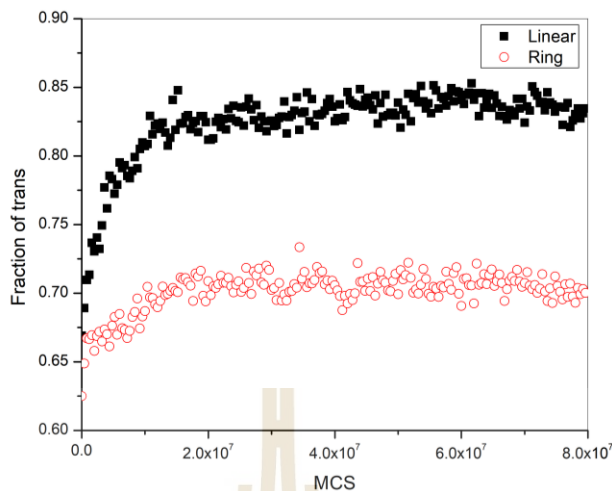
Figure 1. Evolution of *trans* fraction for linear and cyclic PE chain at 298 K.

3.2 Chain Ordering

Upon crystallization, PE chains adopt zigzag *trans* conformation. To study the growth process of structure formation, the overall orientation correlation function, S_G, was calculated by

$$S_G = \tfrac{1}{2}[3\langle cos^2\theta\rangle - 1]$$
(4)

Here, θ is the angle between two PE main axes, and S_G is ensemble averaged for all PE pairs. $S_G = 1.0$ and 0.0 when all polymers are parallel and randomly oriented, respectively.

From Figure 2, S_G for linear chains increases at the early stage and then changed to almost constant afterward to $S_G = 0.7$ which is much larger than that of cyclic chains ($S_G < 0.1$). These results suggest that linear chains can be oriented in parallel pattern better than the cyclic polymer. It should be noted that lower S_G for cyclic polymers does not mean that the cyclic chain cannot crystallize. Upon inspection of simulation

snapshot, it is likely that cyclic chains form multiple crystalline domains with different orientation and this morphology gives very low S_G value.
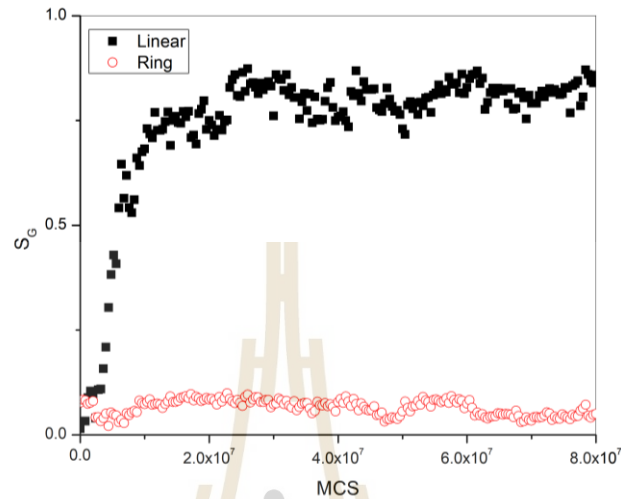

Figure 2. Evolution of intermolecular orientational order parameter for linear and cyclic PE chain at 298 K.

3.3 Scattering Structure Factor

The progress of the polymer crystal can be evaluated using the spherically averaged structure factors as:

$$S(q) = \frac{1}{N_b^2} \sum_{i=1}^{N_b} \sum_{j=1}^{N_b} \frac{sin(q \cdot r_{ij})}{q r_{ij}} \tag{5}$$

where N_b is the number of all beads, and q is $(4\pi/\lambda)sin(\theta/2)$. Figure 3a depicts the evolution of the

$S(q)$ at time t subtracted by $S(q)$ at the starting time for cyclic polymers. The intensity increases rapidly while there is no significant change in the peak position with time. In comparison of the crystallization process between cyclic and linear chains, the maximum intensity I_{max} is depicted in Figure 3b. Evolution of $S(q)$ also suggest better crystallization for linear compared to cyclic polymers because q_{max} (q at I_{max}), the

distance from each ordered motifs, does not much change when the regular structure forms.
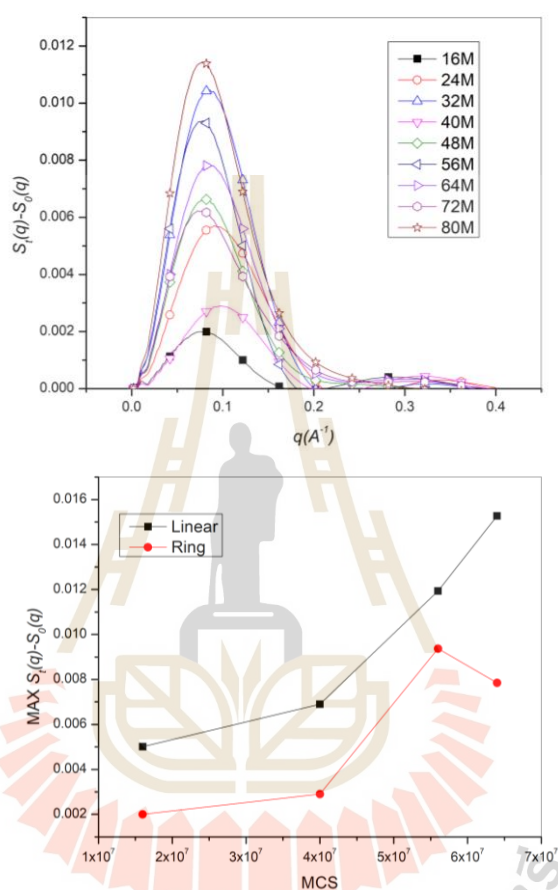

Figure 3. (a) Change in the $S_t(q) - S_0(q)$ for cyclic chains (b) Maximum intensity in $S_t(q) - S_0(q)$ for linear versus cyclic polymers as a function of MCS.

Conclusion

Computer simulation was employed to study the crystallization process of short PE (C_{40}) chains with different chain topology (linear vs cyclic). The structures at the melt state were cooled down to 298 K and the evolution of chain conformation, intermolecular ordering and scattering structure factor were determined. All these properties exhibit an ordering process as the sign of crystallization for both chains especially linear polymer. For these relatively short chains, linear polymer may prone to better crystallization process compared to the cyclic topology. It is likely that cyclic polymers may form the multiple ordered domains with different orientation.

Acknowledgments

References

[1]   Fujiwara S.; Sato, T. Molecular dynamic simulation of structure formation of short chain molecules. J Chem Phys 1999, 110: 9757-64.

[2]   Wunderich B. Macromolecular physics. New York: Academic Press, 1976-1980 .

[3]   Imai M.; Kaji K.; Kanaya T. Structure formation of poly(ethylene terephthate) during the induction period of crystallization. 3. Evolution of density fluctuations to lamellar crystal. Macromolecules 1994, 27: 7103-7108.

[4]   Ezquerra TA.; Lopez-Cabarcos E.; Hsiao BS.; Balta-Calleja FJ. Precursors of crystallization via density fluctuations in stiff-chain polymers. Phys Rev E 1996, 54: 989-992.

[5]   Ryan AJ.; Fairclough JPA.; Terrill NJ.; Olmsted PD.; Poon WCK. A scattering study of nucleation phenomena in polymer crystallization. Faraday Discuss 1999, 112: 13-29.

[6]   Terrill NJ.; Fairclough JPA.; Towns-Andrews E.; Komanschek BU.; Young RJ.; Ryan AJ. Density fluctuations: the nucleation event in isotactic polypropylene crystallization. Polymer 1998, 39: 2381-2385.

[7]   Olmsted PD.; Poon WCK.; Mcleish TCB.; Terrill NJ.; Ryan AJ. Spinodal-assisted crystallization in polymer melts. Phy Rev Lett 1998, 81: 373-376.

[8]   Visit Vao-Soongnern V.; Xu G.; Mattice WL. Structure formation in the crystallization and annealing of tetracontane Nanoparticles. Macromol. Theory Simul. 2004, 13: 539–549.

[9]   Xu G.; Vao-soongnern V.; Mattice WL. Similarities and Differences in the Rapid Crystallization Induced in n-Tetracontane by an Instantaneous Deep Quench of the Free-Standing Nanofiber and Free Standing Thin Film. Macromol. Theory Simul. 2002, 11: 494-500.

Preferred type of talk (Oral, Poster): **Oral**

Preferred conference session: **Physical and Life science**

CURRICULUM VITAE

Supanont Jamornsuriya was born on June 3, 1994 in Chonburi, Thailand. His current address is in Nakhon Ratchasima. He received scholarship in "The Development and Promotion of Science and Technology Talented Project, DPST" when he starts his undergraduate at Suranaree University of Technology. He obtained Bachelor's Degree in Chemistry from School of Chemistry, Institute of Science at Suranaree University of Technology (SUT) with first class honor in 2017. He is skillful on molecular simulation and modeling (techniques (Monte Carlo (MC) and Molecular Dynamic (MD)) of polymeric material. He had been awarded for excellence in poster presentation in Asian Workshop on Polymer Processing 2015 (AWPP2015), National University of Singapore. He continued the Master's degree in Chemistry at School of Chemistry, Institute of Science at Suranaree University of Technology. Also, he experienced in using synchrotron SAXS/WAXD to study the crystallization of polymer. He presented poster in topic "Molecular Simulation for Molecular and Surface Properties of Random Poly(ethylene-Co- Propylene) Copolymer Free-Standing Thin Film" in the virtual conference named National Graduate Research Polymer Conference 2021, (NGRPC2021) at Virginia Tech, USA. He also awarded in best presentation for oral presenting "Molecular simulation of the crystallization characteristics of cyclic versus linear polyethylene models" in SUT International Virtual Conference on Science and Technology (IVCST2021), Nakhon Ratchasima, Thailand. He also done oral presentation on "Molecular Simulation of crystallization process of poly(ethylene) with different topology: linear vs ring" in 70th Symposium on Macromolecule, Society of Polymer Science, Japan (SPSJ) virtual conference. He published "Molecular simulation of structural and surface properties of Poly(ethylene-ran-propylene) thin films" in the Journal of Polymer Research as a co-author during his Master's degree.